



ORNL/TM-6412

3 4456 0551446 8

## Chemical and Physical Considerations of the Use of Nuclear Fuel Spikants for Deterrence

J. E. Selle

OAK RIDGE NATIONAL LABORATORY

CENTRAL RESEARCH LIBRARY

CIRCULATION SECTION

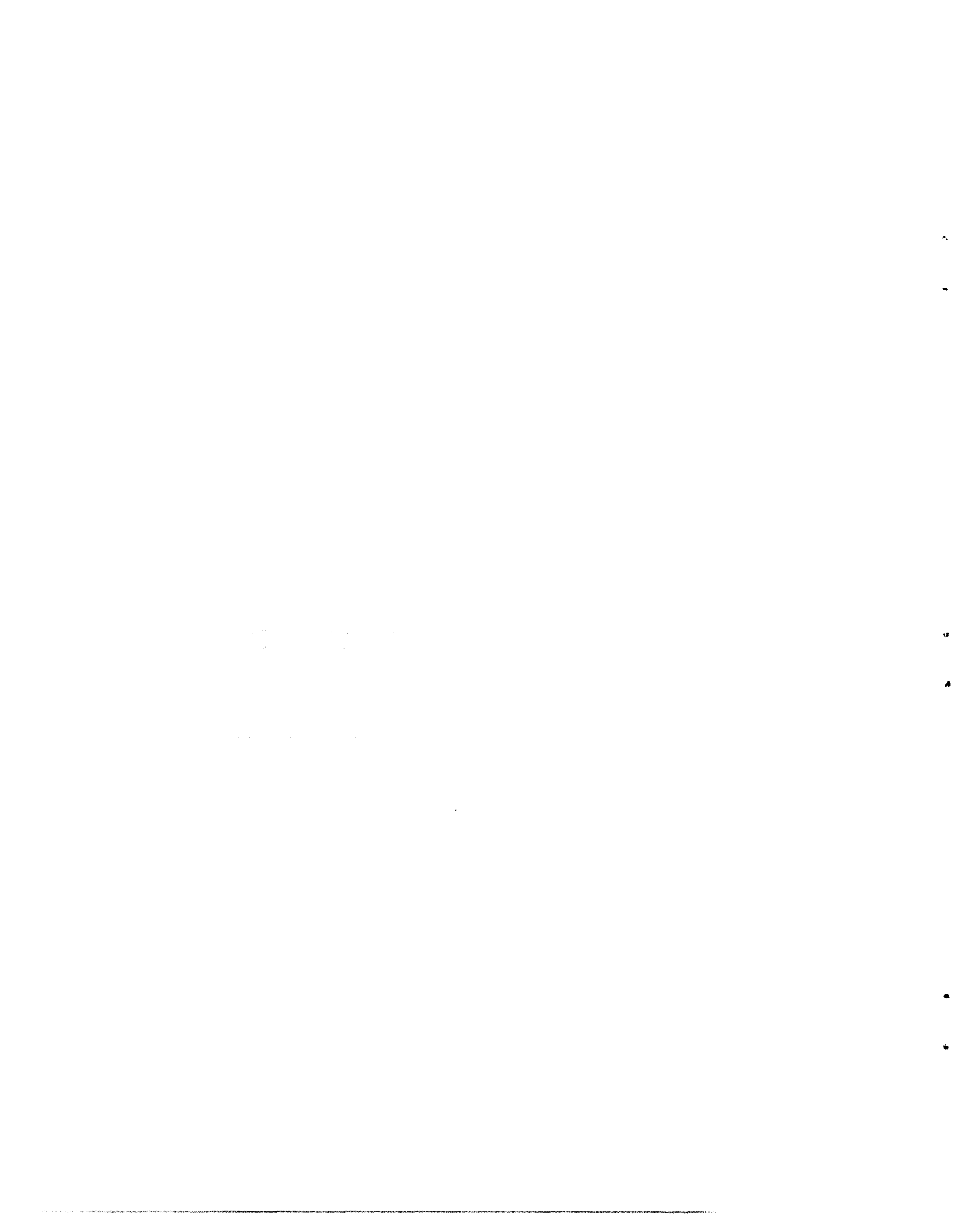
4500N ROOM 175

### **LIBRARY LOAN COPY**

DO NOT TRANSFER TO ANOTHER PERSON

If you wish someone else to see this  
report, send in name with report and  
the library will arrange a loan.

OAK RIDGE NATIONAL LABORATORY  
OPERATED BY UNION CARBIDE CORPORATION • FOR THE DEPARTMENT OF ENERGY



ORNL/TM-6412  
Distribution Categories  
UC-77, UC-79-b,  
-c, -d, -e, UC-83

Contract No. W-7405-eng-26

METALS AND CERAMICS DIVISION

HTGR FUEL RECYCLE DEVELOPMENT PROGRAM (198a OH045)

Studies and Analyses — Task 100

CHEMICAL AND PHYSICAL CONSIDERATIONS OF THE  
USE OF NUCLEAR FUEL SPIKANTS FOR DETERRENCE

J. E. Selle

Date Published: October 1978

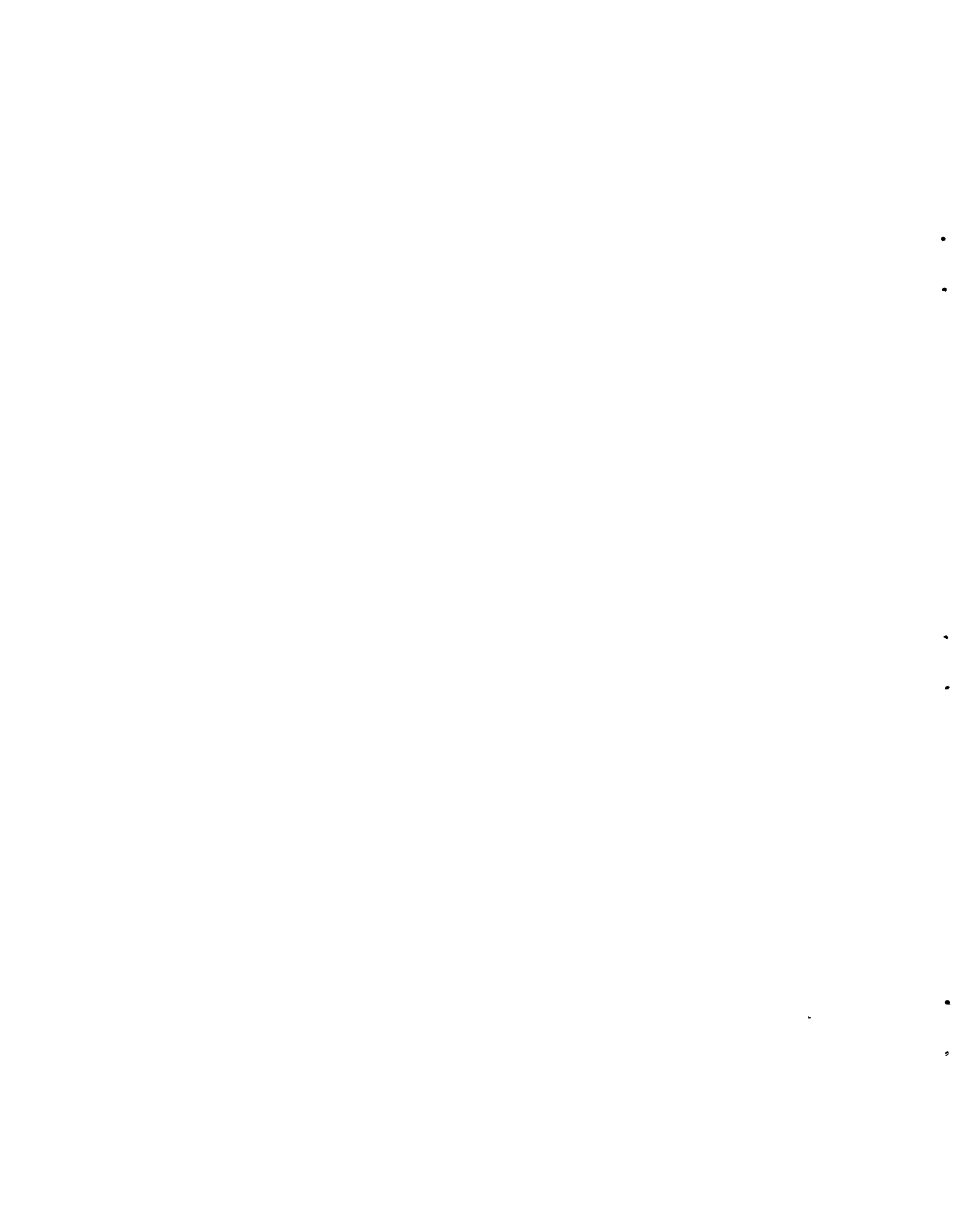
**NOTICE** This document contains information of a preliminary nature.  
It is subject to revision or correction and therefore does not represent a  
final report.

OAK RIDGE NATIONAL LABORATORY  
Oak Ridge, Tennessee 37830  
operated by  
UNION CARBIDE CORPORATION  
for the  
DEPARTMENT OF ENERGY

OAK RIDGE NATIONAL LABORATORY LIBRARIES

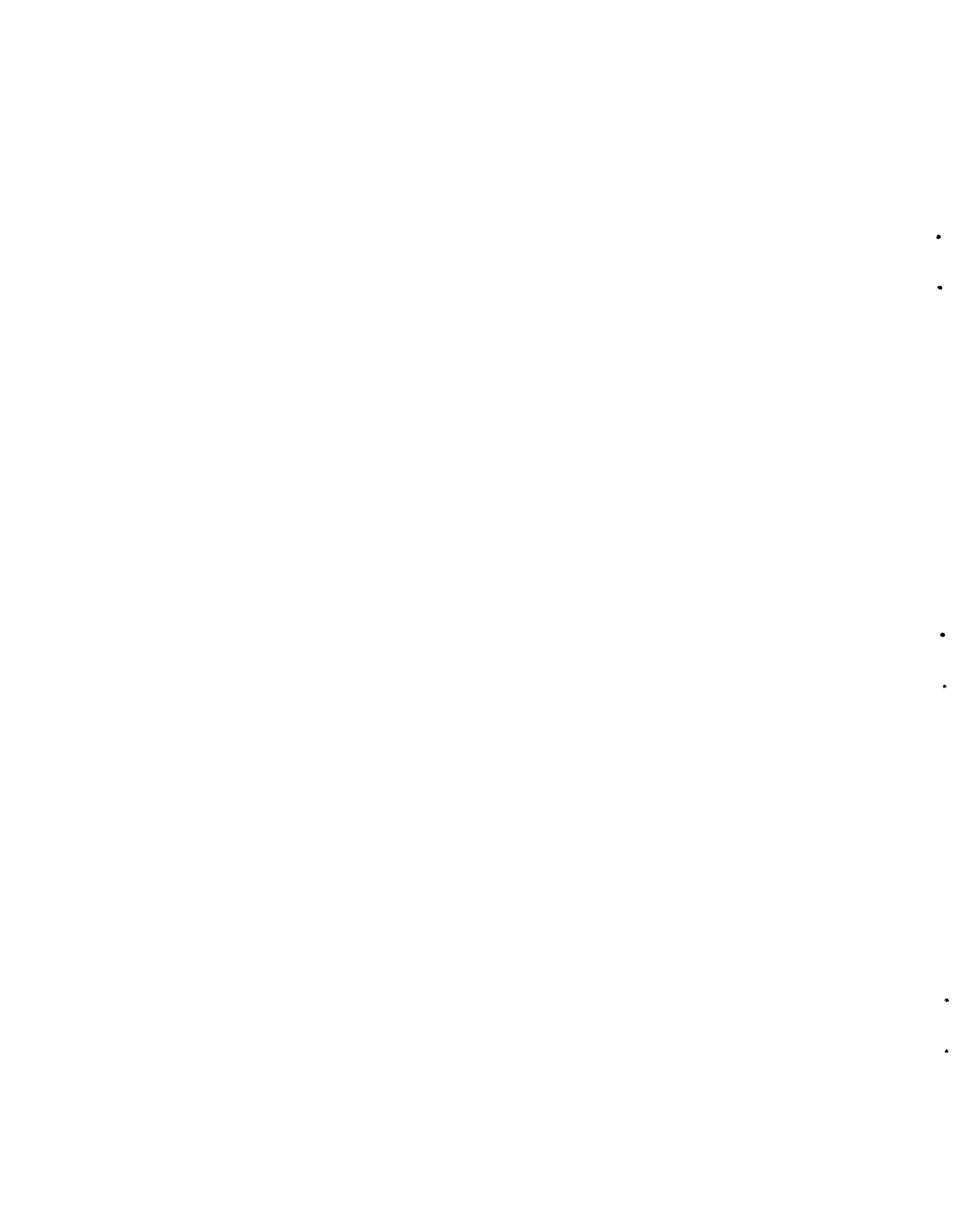


3 4456 0551446 8



## CONTENTS

ABSTRACT . . . . .	1
INTRODUCTION . . . . .	1
SPIKANT CANDIDATE SELECTION . . . . .	3
THERMODYNAMICS . . . . .	5
PHASE RELATIONSHIPS — SUMMARY . . . . .	11
ANALYSIS . . . . .	13
Characteristics of Spikants in the Fuel . . . . .	13
Dose Rates Available from Fission Products . . . . .	15
SUGGESTIONS FOR FURTHER WORK . . . . .	17
ACKNOWLEDGMENTS . . . . .	20
REFERENCES . . . . .	21
APPENDIX A — PHASE RELATIONSHIPS . . . . .	25
APPENDIX B — FISSION PRODUCT INTERACTIONS . . . . .	69
APPENDIX C — CALCULATION OF THE FUEL SPIKANT CONCENTRATION REQUIRED FOR A DOSE RATE OF 27,000 R/H . . . . .	89



CHEMICAL AND PHYSICAL CONSIDERATIONS OF THE USE  
OF NUCLEAR FUEL SPIKANTS FOR DETERRENCE

J. E. Selle

ABSTRACT

One proposed method of inhibiting the diversion of nuclear fuel for clandestine purposes is to add to the fuel a highly gamma-active material of such intensity that remote handling equipment is necessary in all stages of handling and reprocessing. This is called spiking for deterrence. The present work sought to identify candidate spikants and identify potential materials problems that might occur as the result of incorporation of these spikants with the fuel.

We identified potential spikants and did a thermodynamic analysis to determine their chemical and physical states. Phase relationships between spikants (and their decay products) and the fuel constituents were surveyed. According to criteria defined in this report,  $^{60}\text{Co}$ ,  $^{106}\text{Ru}$ , and  $^{144}\text{Ce}$  appear to have the greatest potential as spikants. Cerium should be present as the oxide, soluble in the fuel, while cobalt and ruthenium should be present in the metallic state with very low solubility in the fuel.

Experimental work on the distribution of fission products and their interactions with cladding was also surveyed to provide information on the distribution of spikants in the fuel and describe the probable effects of spikants on the fuel. Cobalt, ruthenium, and cerium should not present any problems due to reaction with stainless steel cladding.

Suggestions for further work are also presented.

---

INTRODUCTION

A number of schemes have been proposed to prevent diversion of nuclear fuel for clandestine purposes. One of these schemes involves the use of a spikant in the fuel to provide a gamma flux of sufficient intensity to induce death after a very short exposure time. This concept has been given a great deal of attention recently, and many methods have been proposed to incorporate these spikants into either the fuel or the shipping cask.<sup>1,2</sup> The advantages and disadvantages of the various

methods have been the subject of detailed analyses and have been discussed by Taylor et al.<sup>2</sup>

Some disadvantages to this method were presented,<sup>1,2</sup> and these are summarized as follows:

1. Spikants are chemically separable.
2. Cost to industry is greatly increased.
3. Radiation hazards to workers are increased.
4. Public hazards from sabotage are increased.
5. It causes considerable interference with nondestructive assay.
6. Bomb production is not prevented.
7. The spikant provides divertors with material for radiation dispersal weapons.
8. The public could react unfavorably to making dangerous material even more dangerous.
9. Changed physical and chemical properties will likely require new fuel research and development.

We shall not delve into the relative merits or demerits of these disadvantages. Rather, our purpose is to examine the various radioactive nuclides with regard to their suitability for use as spikants and attempt to evaluate their effect on fuel fabrication processes and fuel performance. That is, we examine their probable chemical state, physical state, and subsequent state in the fuel and the possible consequences. Even though we are considering primarily the spikants, the decay products of these spikants must also be considered, since these will build up within the system.

Various potential fuels are considered. A considerable amount of prior work has been directed at uranium and uranium-plutonium fuels, and accumulated literature on these fuels is discussed. Recently, however, thorium-based fuels have achieved a credible level of importance, so that an attempt has been made to address the use of spikants in thorium-based fuels.

The procedure has been to examine the literature to extract information relative to the potential effects of spikants on the thermodynamic properties, phase relationships, and radiation effects. With this

information the principles established by prior work can be extended to the use of spikants in present and potential reactor fuels.

Details of the phase relationships between fuel constituents, spikants, and decay products, and fuel-spikant and fuel-decay product systems are presented in Appendix A, while a summary of the information is included in the main body of the report. Details on fission product interactions are presented in Appendix B. This detail is provided in appendices in order to give the reader a more complete background, if desired, and to present the logic used to evaluate the effects of potential spikants.

#### SPIKANT CANDIDATE SELECTION

Selection of candidates for spiking nuclear fuel is a somewhat subjective process involving the application of rather arbitrary limits to the nuclear properties of candidate radionuclides. In order to select the candidates, nuclides were subjected to the following criteria:

1. Half-Life: An absolute minimum of two months was applied. Nuclides with half-lives between two and three months were considered only if they had very high-energy gamma rays ( $E_{\gamma} > 1000$  keV) of high intensity.

2. Other: No nuclide was considered that did not satisfy two or more of the following criteria:

- a. half life from about 8 months to about 50 years
- b. gamma ray energy,  $E_{\gamma}$ ,  $\geq 1000$  keV
- c. gamma ray intensity,  $I_{\gamma}$ ,  $\geq 25\%$  for all energies  $E_{\gamma} \geq 1000$  keV
- d. can be produced by  $(n,\gamma)$  reaction using a nuclide with a natural abundance  $> 10\%$ , with a cross section greater than  $10^{-28} \text{ m}^2$  (1 b), or is a fission product with a significant yield ( $\geq 0.1\%$ ).

3. Alternate Production Methods: Production methods requiring charged particles or  $(n,2n)$  reactions were eliminated on the basis of cost or inefficiency of production.

Nuclides selected on the basis of these criteria are given in Table 1. Primary candidates satisfy at least three requirements under criterion 2 above, while the secondary candidates satisfy at least two

Table 1. Spikant Candidates

Nuclide	Half-Life	Decay Product	Concentration for 27,000 R/h after 2 years (ppm)	Production Method <sup>a</sup>	Probable Form in Oxide Fuels	Remarks
<u>Primary Candidates</u>						
<sup>46</sup> Sc	83.9 d	<sup>46</sup> Ti	374	<sup>45</sup> Sc(100%)(n,γ) σ = 23 b	Sc <sub>2</sub> O <sub>3</sub> TiO	
<sup>60</sup> Co	5.26 y	<sup>60</sup> Ni	30	<sup>59</sup> Co(100%)(n,γ) σ = 37 b	Co metal Ni metal	
<sup>65</sup> Zn	245 d	<sup>65</sup> Cu	108	<sup>64</sup> Zn(48.9%)(n,γ) σ = 0.46 b	Zn vapor Cu metal	Low σ(n,γ); Low bp -- (Zn)
<sup>106</sup> Ru	367 d	<sup>106</sup> Pd	343	Fission Product	Ru metal Pd metal	
<sup>110m</sup> Ag	253 d	<sup>110</sup> Cd	37	<sup>109</sup> Ag(48.6%)(n,γ)	Ag metal Cd vapor	Low I; Low bp -- (Cd)
<sup>124</sup> Sb	60 d	<sup>124</sup> Te	8800	<sup>123</sup> Sb(42.8%)(n,γ) σ = 3.3 b	Sb vapor Te vapor	Short half-life; Low bp -- (Sb, Te)
<sup>144</sup> Ce	284 d	<sup>144</sup> Nd	4220	Fission Product	CeO <sub>2</sub> Nd <sub>2</sub> O <sub>3</sub>	Low I
<sup>194</sup> Os	60 y	<sup>194</sup> Pt	8400	<sup>192</sup> Os(41%)(n,γ) σ = 1 b <sup>192</sup> Os(31h)(n,γ) σ = 200 b	Os metal Pt metal	Low I
<u>Secondary Candidates</u>						
<sup>95</sup> Zr	65 d	<sup>95</sup> Mo	5900	Fission Product	ZrO <sub>2</sub> Mo metal	Short half-life; Low E
<sup>121m</sup> Te	154 d	<sup>121</sup> Sb	445	<sup>120</sup> Te(0.089%)(n,γ) σ = 2 b	Te vapor Sb vapor	Low I; Poor production method; Low bp -- (Te, Sb)
<sup>125</sup> Sb	2.7 y	<sup>125</sup> Te	220	<sup>124</sup> Sn(5.94%)(n,γ) σ = 0.1 b	Sb vapor Te vapor	Low E; Low σ(n,γ); Low bp -- (Sb, Te)
<sup>134</sup> Cs	2.05 y	<sup>134</sup> Ba	57	<sup>133</sup> Cs(100%)(n,γ) σ = 30 b	Cs vapor Ba vapor	Low I; Liquid; Low bp -- (Cs, Ba)
<sup>137</sup> Cs	30 y	<sup>137</sup> Ba	1250	Fission Product	Cs vapor Ba vapor	Low E; Liquid; Low bp -- (Cs, Ba)
<sup>152</sup> Eu	14 y	<sup>152</sup> Sm	497	<sup>151</sup> Eu(47.8%)(n,γ) σ = 5300 b	Eu <sub>2</sub> O <sub>3</sub> Sm <sub>2</sub> O <sub>3</sub>	High cross section; <sup>152</sup> Eu (σ = 6000 b)
<sup>154</sup> Eu	7.8 y	<sup>154</sup> Gd	226	<sup>153</sup> Eu(52.2%)(n,γ) σ = 480 b	Eu <sub>2</sub> O <sub>3</sub> Gd <sub>2</sub> O <sub>3</sub>	High cross section; <sup>154</sup> Eu (σ = 1500 b)
<sup>182</sup> Ta	115.1 d	<sup>182</sup> W	800	<sup>181</sup> Ta(100%)(n,γ) σ = 21 b	Ta <sub>2</sub> O <sub>5</sub> W metal	Short half-life; High cross section; <sup>182</sup> Ta (σ = 17,000 b)

<sup>a</sup>The percentages in parentheses are the natural abundances. 1 b =  $10^{-28}$  m<sup>2</sup>.

requirements under criterion 2. Nuclides were included on these lists on the basis of neutronic characteristics only without consideration of any other physical properties such as melting point, boiling point, or thermodynamic properties.

Included in this table is the concentration of the nuclide required to produce 27,000 R/h two years after incorporation into the fuel. The dose rate of 27,000 R/h is that amount of radiation required to induce a 50% probability of death after 1 min of exposure. This is the so-called  $LD_{50}$  criterion. A detailed description of the method used to make these calculations is given in Appendix C. For lower dose rates, the concentration of the radionuclide will decrease proportionally. These values are for the radionuclide only and do not include other isotopes of the same element. Therefore, actual elemental concentration will be higher by a factor of 5 to 25. This point will be discussed in a later section.

#### THERMODYNAMICS

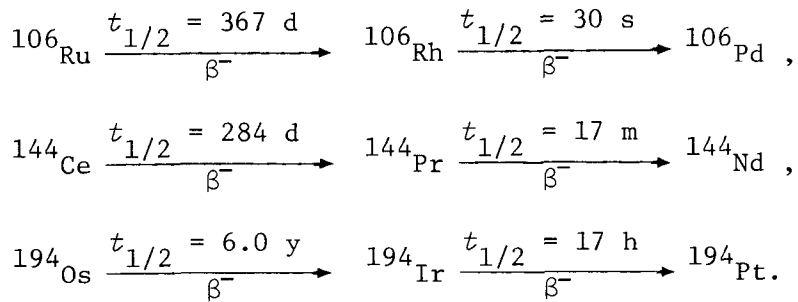
In determining the usefulness of a potential spikant for oxide fuels a number of factors must be considered. Among these are

1. thermodynamics of oxide formation,
2. melting and boiling points of the oxides,
3. melting and boiling points of the pure element,
4. phase relationships between the fuel matrix, fuel container, and both the spikant and its decay product.

Thermodynamics allows one to determine whether a given element will be oxidized under the conditions existing in the system. Once it is determined whether the element will exist as an oxide or uncombined, the melting and boiling points of the species involved become important. Melting or vaporization of the species can cause its redistribution within the system, thereby introducing complications such as high concentration at cooler portions of the fuel pin, chemical interaction with the cladding, or alteration of the properties of the fuel. If an element is present as the oxide, the solubility of this oxide in the fuel

becomes important. If the spikant or its decay product is insoluble in the fuel, complications might arise from uneven dispersal of the spikant in the fuel or alteration of the properties of the fuel by secondary phase precipitation.

Data<sup>3</sup> for the free energy of formation for the oxides of the various potential spikants are summarized in Fig. 1. In this figure, the free energy of formation,  $\Delta G_f$ , of the various oxides (per mole of O<sub>2</sub>) is plotted as a function of temperature to compare their relative stabilities. Superimposed on this figure are data for the oxygen potential of various uranium-plutonium fuels. The oxygen potentials for all single-phase oxides (10–30% Pu) can be expressed<sup>4</sup> as functions of oxidation state and temperature and fuels with the same oxidation state have the same oxygen potential. Oxidation states can be related<sup>5</sup> to the oxide-to-metal (O/M) ratio and to Pu/(U + Pu) ratios, as shown in Table 2. By the use of this table it is possible to convert from average oxidation state to O/M ratio for fuels with plutonium contents between 10 and 30% Pu. Oxides of rhodium (Rh<sub>2</sub>O<sub>3</sub>), praeseodymium (Pr<sub>2</sub>O<sub>3</sub>), and iridium (Ir<sub>2</sub>O<sub>3</sub>) are included in Fig. 1 because these elements would be present as transients by virtue of the spikants <sup>106</sup>Ru, <sup>144</sup>Ce, and <sup>194</sup>Os with the following decay schemes:



while rhodium, praeseodymium, and iridium should be present in small amounts, they are included in this report to provide a complete analysis of all possible constituents in fuel-spikant systems.

In the presence of (U,Pu)<sub>0.2-x</sub>, the compounds TiO, Sc<sub>2</sub>O<sub>3</sub>, Ce<sub>2</sub>O<sub>3</sub>, CeO<sub>2</sub>, Pr<sub>2</sub>O<sub>3</sub>, Nd<sub>2</sub>O<sub>3</sub>, and ThO<sub>2</sub> are stable, while all the other oxides are unstable. For (U,Pu)<sub>0.20</sub>, ZnO is stable below about 1300 K, while above this temperature zinc is present in the elemental (vaporized) form. As

ORNL-DWG 78-10387

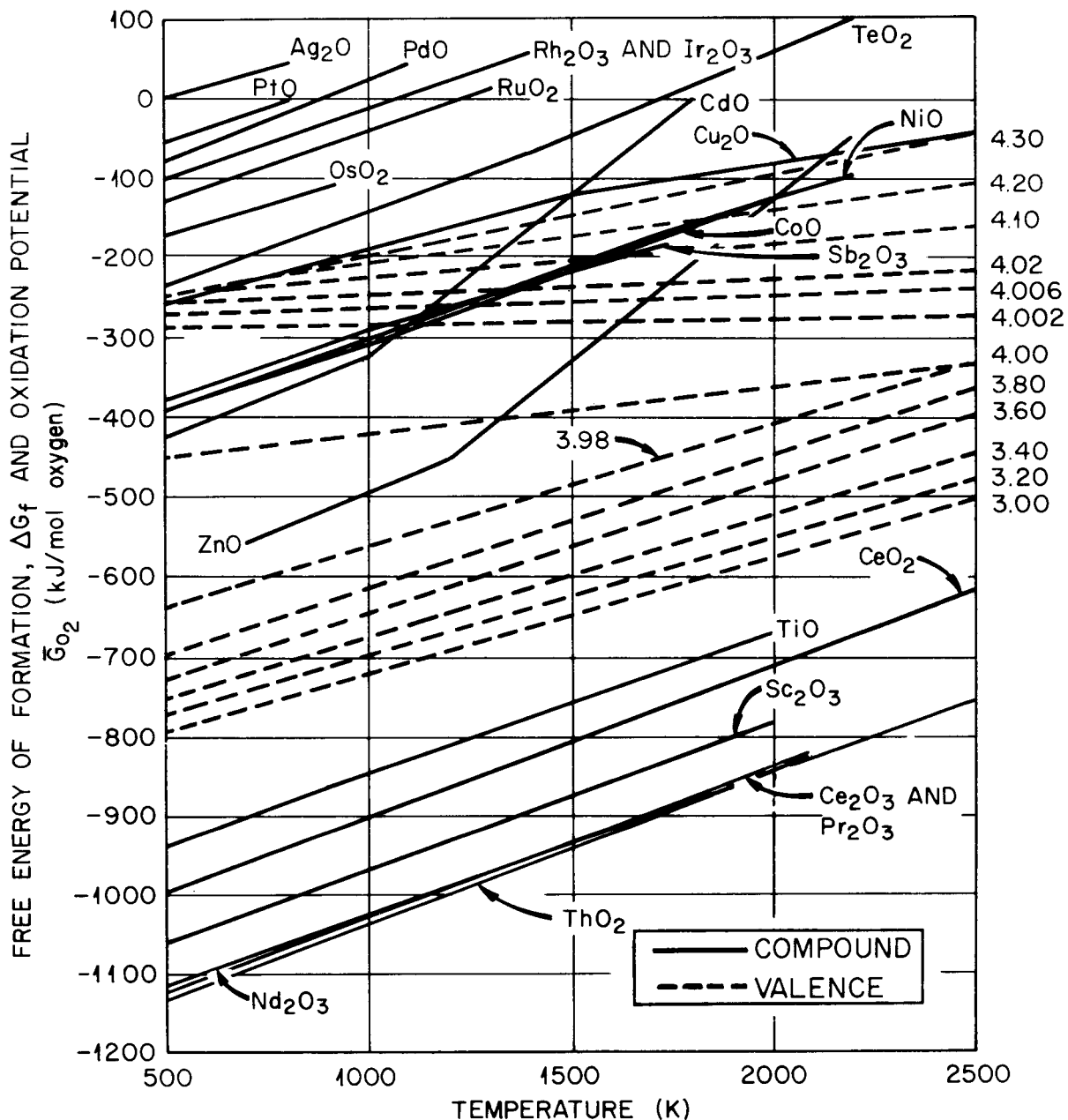


Fig. 1. Thermodynamic Data for Fuels and Potential Spikants and Decay Products. Based on A. Glassner, ANL-5750 (October 1965).

Table 2. Oxygen-to-Metal Ratios for  $(U, Pu)O_{2+x}$  as a Function of Plutonium Content and Metal Oxidation States

Valence	U	Pu	Oxygen-to-Metal Ratio <sup>a</sup> for Given Metal Ratio $Pu/(U + Pu)$				
			0.10	0.15	0.20	0.25	0.30
4.30	4.000	2.135	2.128	2.120	2.113	2.105	
4.20	4.000	2.090	2.085	2.080	2.075	2.070	
4.10	4.000	2.045	2.043	2.040	2.038	2.035	
4.02	4.000	2.009	2.009	2.008	2.008	2.007	
4.006	4.000	2.003	2.003	2.002	2.002	2.002	
4.002	4.000	2.001	2.001	2.001	2.001	2.001	
4.000	4.000	2.000	2.000	2.000	2.000	2.000	
4.000	3.98	1.999	1.999	1.998	1.998	1.997	
4.000	3.80	1.990	1.985	1.980	1.975	1.970	
4.000	3.60	1.980	1.970	1.960	1.950	1.940	
4.000	3.40	1.970	1.955	1.940	1.925	1.910	
4.000	3.20	1.960	1.940	1.920	1.900	1.880	
4.000	3.00	1.950	1.925	1.900	1.875	1.850	

<sup>a</sup>The oxygen-to-metal ratio is calculated as half the average metal oxidation number.

the cation valence of the fuel increases, CoO, NiO, Sb<sub>2</sub>O<sub>3</sub>, and CdO can become stable below about 1100 K for a valence of 4.002. As the fuel valence increases, the temperature of stability also increases. Thus, as uranium and plutonium are fissioned and oxygen is released from the fuel the O/M ratio will increase, and certain oxides can become stable at lower temperatures. However, the temperature range of stability does not extend to high enough temperatures to be useful for stabilizing volatile elements such as zinc and antimony.

Melting and boiling point data for the elements under consideration and their oxides are summarized in Tables 3 and 4, respectively. Also given in Table 3 is the probable form of each spikant and its decay

Table 3. Melting and Boiling Points and Probable Form of Various Radionuclides and Their Decay Products<sup>a</sup>

Element	Melting Point (°C)	Boiling Point (°C)	Probable Form <sup>b</sup>
<u>Radionuclides</u>			
Sc	1539	2730	Sc <sub>2</sub> O <sub>3</sub>
Co	1495	2900	Metal
Zn	420	906	Metal
Ru	2500	4900	Metal
Rh	1966	4500	Metal
Ag	961	2210	Metal
Sb	630	1380	Metal
Ce	804	3470	CeO <sub>2</sub>
Pr	919	3020	Pr <sub>2</sub> O <sub>3</sub>
Os	~2700	~4900	Metal
Ir	2454	5500	Metal
<u>Decay Products</u>			
Ti	1668	3260	TiO
Ni	1435	2730	Metal
Cu	1083	2593	Metal
Pd	1552	3980	Metal
Cd	321	795	Vapor
Te	450	990	Vapor
Nd	1019	3180	Nd <sub>2</sub> O <sub>3</sub>
Pt	1769	4530	Metal

<sup>a</sup>Based on *Metals Handbook*, vol. 1, American Society for Metals, Metals Park, Ohio, 1961.

<sup>b</sup>Assumes fuel composition of U,Pu O<sub>1.998</sub> or less oxygen.

Table 4. Melting and Boiling Point Data for Oxides<sup>a</sup>

Oxide	Melting Point (°C)	Boiling Point (°C)
Sc <sub>2</sub> O <sub>3</sub>	(2227)	
CoO	1805	(2627)
ZnO	1975	
RuO <sub>2</sub>	dec. 1127	
RuO <sub>4</sub>	27	dec.
Rh <sub>2</sub> O <sub>3</sub>	dec. 1115	
Ag <sub>2</sub> O	dec. 187	
Sb <sub>2</sub> O <sub>3</sub>	655	1425
Ce <sub>2</sub> O <sub>3</sub>	1687	(3227)
CeO <sub>2</sub>	2727	
Pr <sub>2</sub> O <sub>3</sub>	(1927)	
PrO <sub>2</sub>	dec. 427	
OsO <sub>2</sub>	dec. 650	
Ir <sub>2</sub> O <sub>3</sub>	(1177)	(1977)
TiO	dec. 1737	
Ti <sub>2</sub> O <sub>3</sub>	2127	3027
Ti <sub>3</sub> O <sub>5</sub>	(2177)	(3327)
NiO	1957	dec.
Cu <sub>2</sub> O	1230	dec.
PdO	dec. 877	
CdO	dec.	
TeO <sub>2</sub>	733	dec.
Nd <sub>2</sub> O <sub>3</sub>	2272	
Pt + O	dec. 507	
Pt + O <sub>2</sub>	450	dec. 477

<sup>a</sup>Values in parentheses are estimates. dec. = decomposes. Based on A. Glassner, ANL-5150 (October 1965).

product, based on the information given in Fig. 1. Solid or liquid metals are, in general, undesirable because they may cause problems because of redistribution and difficulty in incorporating them uniformly into the fuel. Thus, oxides provide the greatest potential for this application, even in the small amounts required. However, the oxides should be either solid or in solid solution to be of any value. Liquid or vapor species can also provide a distribution problem.

#### PHASE RELATIONSHIPS — SUMMARY

The chemical properties of a fuel for the most part depend upon its oxygen potential. The oxygen potential determines the reactivity of the fuel with the cladding. The oxygen potential is a function of location within the fuel pin because of the temperature gradient within the fuel and also is a function of the type and quantity of fission products generated during irradiation. These complications result in a dynamic and complex system, which is not completely understood. Suffice it to say that the oxygen potential varies according to location (temperature) within the pin and time of irradiation (amount of burnup).

Phase relationships for the Pu-O, U-O, and U-Pu-O systems are given in Appendix A. Large deviations from stoichiometry occur in the single-phase field in both the Pu-O and the U-O systems. However, deviations from stoichiometric  $\text{M}_\text{O}_2$  as the single phase occur in opposite directions, namely,  $\text{PuO}_{2-x}$  and  $\text{UO}_{2+x}$ . Crystallographically, the deviations from stoichiometry are accommodated by means of defect structures. A wide range of solid solution exists between  $\text{UO}_{2+x}$  and  $\text{PuO}_{2-x}$ .

The Th-O and the Th-U-O systems are also shown in Appendix A. Slight substoichiometry is possible in  $\text{ThO}_2$  at very high temperatures ( $>1500^\circ\text{C}$ ). Substoichiometry has not been reported in the ternary Th-U-O system. Stoichiometric  $\text{ThO}_2$  and  $\text{UO}_2$  show a continuous solid solution system. Deviations from stoichiometry are toward hyperstoichiometric compositions  $\text{M}_\text{O}_{2+x}$ . Thus, one would expect higher oxygen potentials in thorium-uranium fuels than in pure  $\text{ThO}_2$  or  $\text{PuO}_{2-x}$ -bearing fuels.

Complete solubility exists between stoichiometric  $\text{PuO}_2$  and  $\text{ThO}_2$ . No data were found on the  $\text{PuO}_{2-x}\text{-ThO}_2$  system.

Table 5 summarizes the phase relationships for the various spikants and decay products with  $\text{PuO}_2$ ,  $\text{ThO}_2$ , and  $\text{UO}_2$ . More complete data are presented in Appendix A. It is apparent that the  $\text{ThO}_2$  and  $\text{UO}_2$  phase relationships with the various additives are analogous. Therefore, behavior applicable to  $\text{UO}_2$ -based fuels will probably be applicable to  $\text{ThO}_2$ -based fuels.

Extensive solubility is found between the fuel constituents and the rare earth oxides  $\text{CeO}_2$ ,  $\text{PrO}_x$  and  $\text{Nd}_2\text{O}_3$ . No solubility data were reported for cobalt, nickel, ruthenium, or their oxides.

Table 5. Summary of Phase Relationships Between Potential Spikants with Decay Products and Fuel Components

Spikant or Decay Product	Relationships in Specific Fuel Components		
	$\text{PuO}_2$	$\text{ThO}_2$	$\text{UO}_2$
$\text{Sc}_2\text{O}_3$	0.5 mol % (1100°C) 2.4 mol % (1550°C)	0.4 mol % (1200°C) 0.9 mol % (1750°C)	Some solubility in $\text{UO}_{2.0}$ Considerable solubility in $\text{UO}_{2+x}$ ; fluorite compound $\text{ScUO}_4$
$\text{CeO}_2$	Soluble in all proportions	Soluble in all proportions	Soluble in all proportions
$\text{PrO}_x$		Complete solubility	
$\text{CoO}$			$\text{CoU}_2\text{O}_6$ formed
$\text{TiO}_2$		Compound formed	Compounds formed; some solubility possible
$\text{Nd}_2\text{O}_3$		~35 mol % (1400°C) <40 mol % (2200°C)	Extensive solubility
$\text{NiO}$			Compounds formed — no solubility data reported
$\text{RuO}_2$			

## ANALYSIS

Characteristics of Spikants in the Fuel

Using the knowledge gained from prior studies of the distribution of fission products in nuclear fuels, presented in Appendix B, we have a basis for identifying the ultimate distribution of spikants and their decay products. From Table 1, spikants that would be present as the oxide are  $^{46}\text{Sc}$  and  $^{144}\text{Ce(Pr)}$ . The decay products of these nuclides are titanium and neodymium, respectively, which would also be present as oxides. Cerium and neodymium should be soluble in the fuel and thus indistinguishable from the fuel matrix. Scandium and titanium may not be completely soluble and may appear as second-phase oxides in the fuel matrix.

The potential spikant  $^{65}\text{Zn}$  would volatilize at temperatures above 906°C and migrate to colder portions of the element. At temperatures between 420 and 906°C zinc is in the liquid state and has been shown<sup>6</sup> to be very corrosive. This makes zinc undesirable as a spikant. Decay products cadmium and tellurium vaporize at 765 and 990°C, respectively, and would also migrate to the cooler portions of the fuel pin, where severe corrosion problems would arise. Thus, the spikants  $^{110m}\text{Ag}$  and  $^{124}\text{Sb}$  are also considered to be undesirable. Antimony itself is volatile above 1380°C.

The remaining spikants  $^{60}\text{Co}$ ,  $^{106}\text{Ru}$ , and  $^{194}\text{Os}$  would also be present in the elemental form and would form a second phase in the grain boundaries of the columnar grain region or in the central void. In later stages of burnup these elements would form a homogeneous alloy with fission products such as rhodium, palladium, and molybdenum. The decay products nickel, palladium, and platinum would behave similarly.

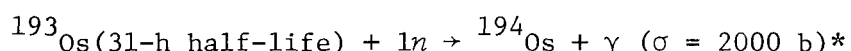
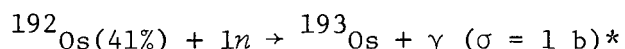
This analysis is summarized in Table 6, which lists the potential problems of the various decay schemes. Thus,  $^{65}\text{Zn}$ ,  $^{110m}\text{Ag}$ , and  $^{124}\text{Sb}$  can be eliminated from further consideration on the basis that volatility, migration, and subsequent condensation of corrosive elements could present severe corrosion problems. Of the remaining candidates, the

Table 6. Summary Analysis of Primary Spikant Candidates

Nuclide	Decay Product	Probable Form	Potential Problems
Sc		Oxide	Short half-life
	Ti	Oxide	
Co		Metal	Volatile
	Ni	Metal	
Zn		Metal	Volatile
	Cu	Metal	
Ru(Rh)		Metal	Volatile
	Pd	Metal	
Ag		Metal	Volatile
	Cd	Metal	
Sb		Metal	Volatile, short half-life
	Te	Metal	
Ce(Pr)		Oxide	Low-intensity gammas
	Nd	Oxide	
Os(Ir)		Metal	Volatile
	Pt	Metal	

half-life of  $^{46}\text{Sc}$  is rather short (83.9 days), which makes its value as a spikant somewhat questionable.

The intensity of the gamma radiation provided by  $^{194}\text{Os}$  is quite low, and for this reason 8400 ppm of the nuclide are required to provide the stipulated radiation level. Production of this nuclide can occur by the following reactions:




---

\*1 b =  $1 \times 10^{-28} \text{ m}^2$ .

The efficiency of these reactions for producing  $^{194}\text{Os}$  can be expected to be low since two ( $n,\gamma$ ) reactions are required, which not only raises the cost but results in a low nuclide concentration. Even if the  $^{194}\text{Os}$  concentration in the gamma source would be as high as 10%, the total osmium content of the fuel matrix would be at least 8%, which is considered excessive. For this reason,  $^{194}\text{Os}$  can be eliminated from further consideration for the stipulated radiation level.

Consideration of these factors narrows the list of primary candidates to  $^{60}\text{Co}$ ,  $^{106}\text{Ru}$ , and  $^{144}\text{Ce}$ . Of these, only cerium would be present as the oxide, soluble in the fuel. Cobalt and ruthenium would be present in the elemental form, as separate phase metallic particles dispersed in the fuel matrix. Cerium and ruthenium have the advantage that they are present as fission products in spent fuel, so that it would not be necessary to set up a separate facility to produce the nuclides by irradiation. However, reprocessing schemes would have to be altered to separate the cerium and ruthenium from other fission products.

#### Dose Rates Available from Fission Products

The nuclide concentrations required to produce 27,000 R/h after two years, given in Table 1, assume that the isotope is 100% pure. In reality this is never the case since other isotopes of the same element are present and decrease the isotopic concentration of the spikant. Figures 2 and 3 summarize the isotopic concentrations of the fission products  $^{106}\text{Ru}$  and  $^{144}\text{Ce}$ , respectively, from previously unspiked fuel as a function of time since removal from the reactor for four different reactor systems. These concentrations were obtained with the ORIGEN code under the conditions summarized in Table 7. One year after removal from the reactor, none of the systems indicate isotopic concentrations of either  $^{106}\text{Ru}$  or  $^{144}\text{Ce}$  greater than 7%. Two years after removal from the reactor the isotopic concentrations are less than 3%. For a PWR, this means that to satisfy the criterion of 27,000 R/h two years after fuel refabrication (total of 4 years since removal from reactor), the

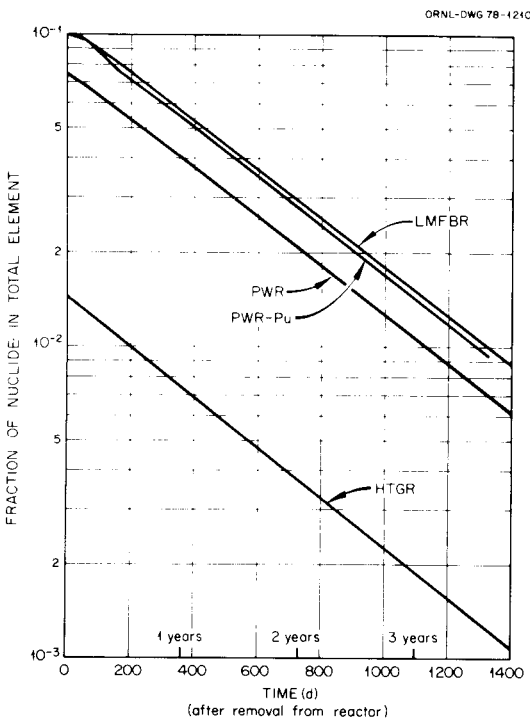


Fig. 2. Fraction of  $^{106}\text{Ru}$  in Total Element as a Function of Time After Removal from the Reactor.

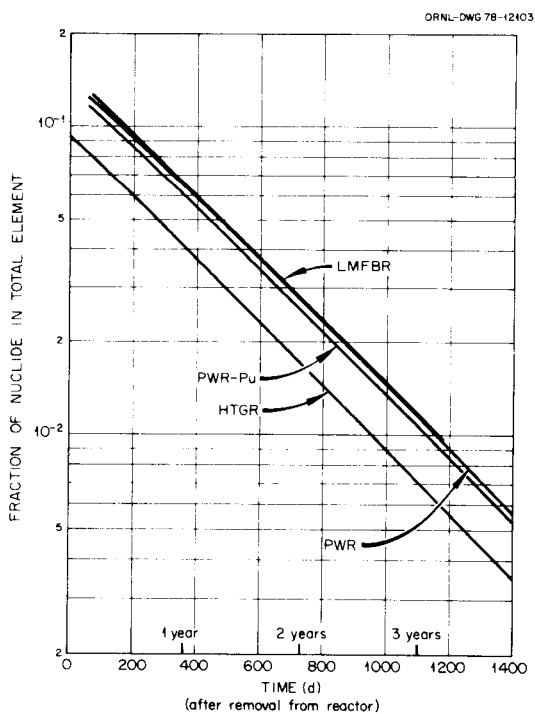


Fig. 3. Fraction of  $^{144}\text{Ce}$  in Total Element as a Function of Time After Removal from the Reactor.

Table 7. Conditions Used for ORIGEN Calculation of Fission Product Concentrations

Reactor	Flux (n/m <sup>2</sup> s)	Power (MW/Mg)	Burnup (MW/Mg)
PWR-U	$3.89 \times 10^{17}$	37.50	33,000
PWR-Pu	$2.06 \times 10^{17}$	37.50	33,000
HTGR	$8.04 \times 10^{17}$	64.57	94,271
LMFBR	$2.49 \times 10^{19}$	49.28	37,118

cerium concentration would have to be 15.6% and the ruthenium concentration about 1.7%. Neither of these values is attainable from fission products for the stipulated radiation level.

Radiation levels attainable as a function of time after removal from the reactor are summarized in Fig. 4. This figure assumes that 100% of each fission product is processed with the fuel (100% recovery of either  $^{106}\text{Ru}$  or  $^{144}\text{Ce}$ ).

Presumably one could add spikants produced in another reactor. Data pertaining to commercially obtainable gamma sources is summarized in Table 8. These values will obviously change with time but are presented as representative of commercially available sources. The nuclides  $^{106}\text{Ru}$  and  $^{144}\text{Ce}$  are fission products, and their isotopic concentrations should be similar to those presented in Fig. 3. For  $^{106}\text{Ru}$ , this is the case. However, for  $^{144}\text{Ce}$  the isotopic concentration appears to be high. This value was calculated by assuming that all the activity comes from  $^{144}\text{Ce}$ . However, since other rare earths are carried along with cerium, their decay probably contributes to the total activity, which results in the rather high apparent isotopic concentration.

#### SUGGESTIONS FOR FURTHER WORK

An analysis of the phase diagrams surveyed in this report suggests a number of areas where further work is required to help clarify the effects of spikants on the fuel. Most of the systems discussed have

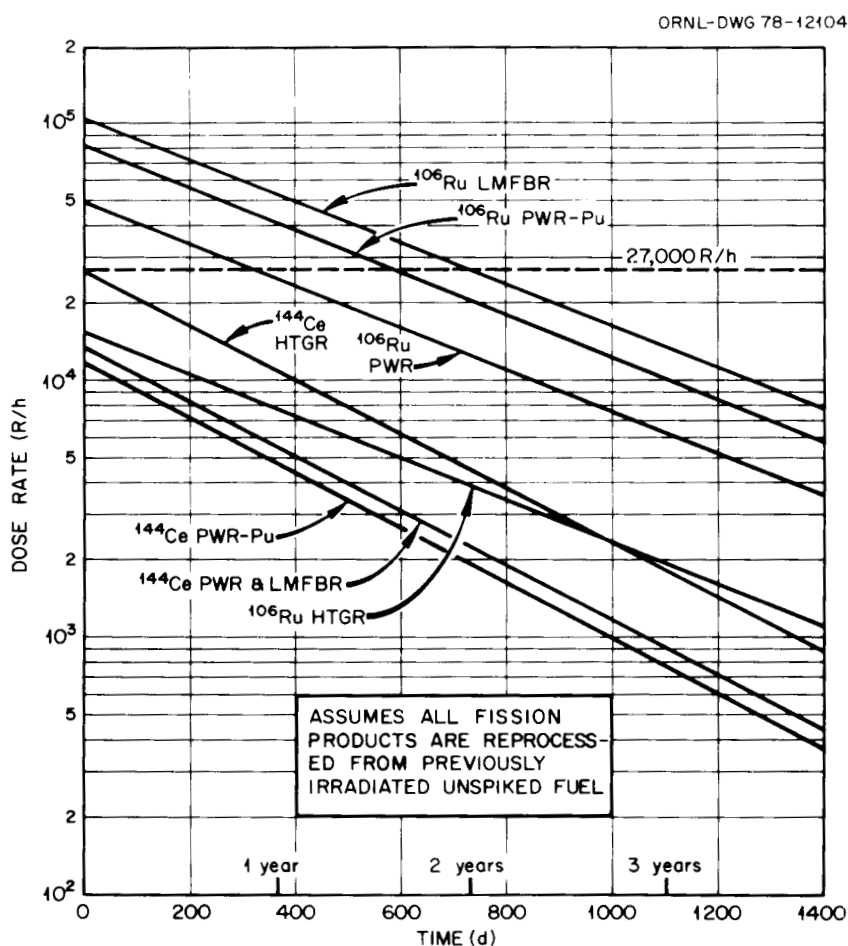


Fig. 4. Available Dose Rate as a Function of Time After Removal from the Reactor.

Table 8. Commercially Available Gamma Sources<sup>a</sup>

Sources Available	Activity, Ci/g		Isotope in Source (%)
	Based on Source	Based on Isotope	
<sup>60</sup> Co	300	1132.6	26.49
<sup>106</sup> Ru	85	3356.4	2.53
<sup>144</sup> Ce	450	3192.8	14.09

<sup>a</sup>Private communication, E. Lamb and ORNL-Isotope Sales.

<sup>b</sup>Assumes all activity comes from nuclide.

regions of uncertainty, which require more work to complete the system or to resolve conflicts between two or more investigators. However, resolution of these questions would have only secondary impact on the properties of the fuel or on the use of spikants. Therefore, the following discussion will refer only to severe deficiencies in the data.

Information available on the  $\text{PuO}_2\text{-ThO}_2$  system is sparse. Data on the liquidus and solidus temperatures are lacking. These data should be developed for both high and low oxygen pressures. There appears to be a need for studying the phase relationships under various oxygen pressures because of the tendency for  $\text{PuO}_2$  to become substoichiometric at low oxygen pressures. Chemical potential data as a function of stoichiometry are also lacking.

Since it appears desirable for fuel to be substoichiometric it would be desirable to investigate the substoichiometric region of the  $\text{ThO}_2\text{-UO}_2$  system and establish boundaries for the single-phase region  $(\text{U},\text{Th})\text{O}_{2-x}$ . Data on the Ce-U-O and Ce-Th-O system suggest that cerium would enlarge the single-phase field  $(\text{Ce},\text{U},\text{Th})\text{O}_{2-x}$ . Therefore, this should be investigated further. Information on the  $\text{CeO}_{1.5}\text{-CeO}_2\text{-ThO}_2$  system is somewhat limited, but it would be very desirable to accurately locate the position of the miscibility gap (see Fig. A22) in this system.

Very little work has been done on the Ce-Pu-O system, and it is desirable that liquidus and solidus temperatures be determined for the  $\text{CeO}_2\text{-PuO}_2\text{-PuO}_{2-x}$  system. In addition, the system  $\text{CeO}_{1.5}\text{-CeO}_2\text{-PuO}_2$  should be determined to establish the boundaries for the single-phase region  $(\text{Ce},\text{Pu})\text{O}_{2-x}$ .

In keeping with the concept of desirability of substoichiometric fuel it is necessary to establish the conditions of existence of the compound "ThO" and investigate the feasibility of stabilizing either this phase or substoichiometric  $\text{ThO}_2$ . Carbon and nitrogen have been suggested as possible stabilizers for ThO, and it appears that trivalent rare earths may promote  $(\text{RE},\text{Th})\text{O}_{2-x}$ .

Although future reactor fuels could contain plutonium, thorium, and uranium, no information appears to be available on the Pu-Th-U-O system.

Therefore, it is necessary that work be conducted on this system at high and low oxygen pressures in order that oxygen limits can be placed on the stability of the single-phase region  $(\text{Pu}, \text{Th}, \text{U})\text{O}_{2+x}$ . Following this, the effects of cerium on this system should be established. Although it is expected that the solubility of cobalt and ruthenium in fuel constituents will be low, it is important that the exact limits be determined not only for these spikants, but for their decay products nickel and palladium as well.

It has been reported that cerium and neodymium increase the oxygen potential of  $\text{UO}_2$ .<sup>8</sup> In view of this potential for altering the thermodynamic properties of fuel by small additions of a rare earth, complete characterization of the fuel requires that the effect of spikants on the oxidation potential of the fuel be determined. Changes in the oxygen potential of the fuel can have considerable effect on the fuel-cladding reactions.

Development efforts are needed to determine the influence of spikants on reprocessing and refabrication processes and equipment. For example, the influence of potential spikants on fuel sinterability is important. The physical form and distribution of the spikant, and the resulting influence on fuel properties must be determined.

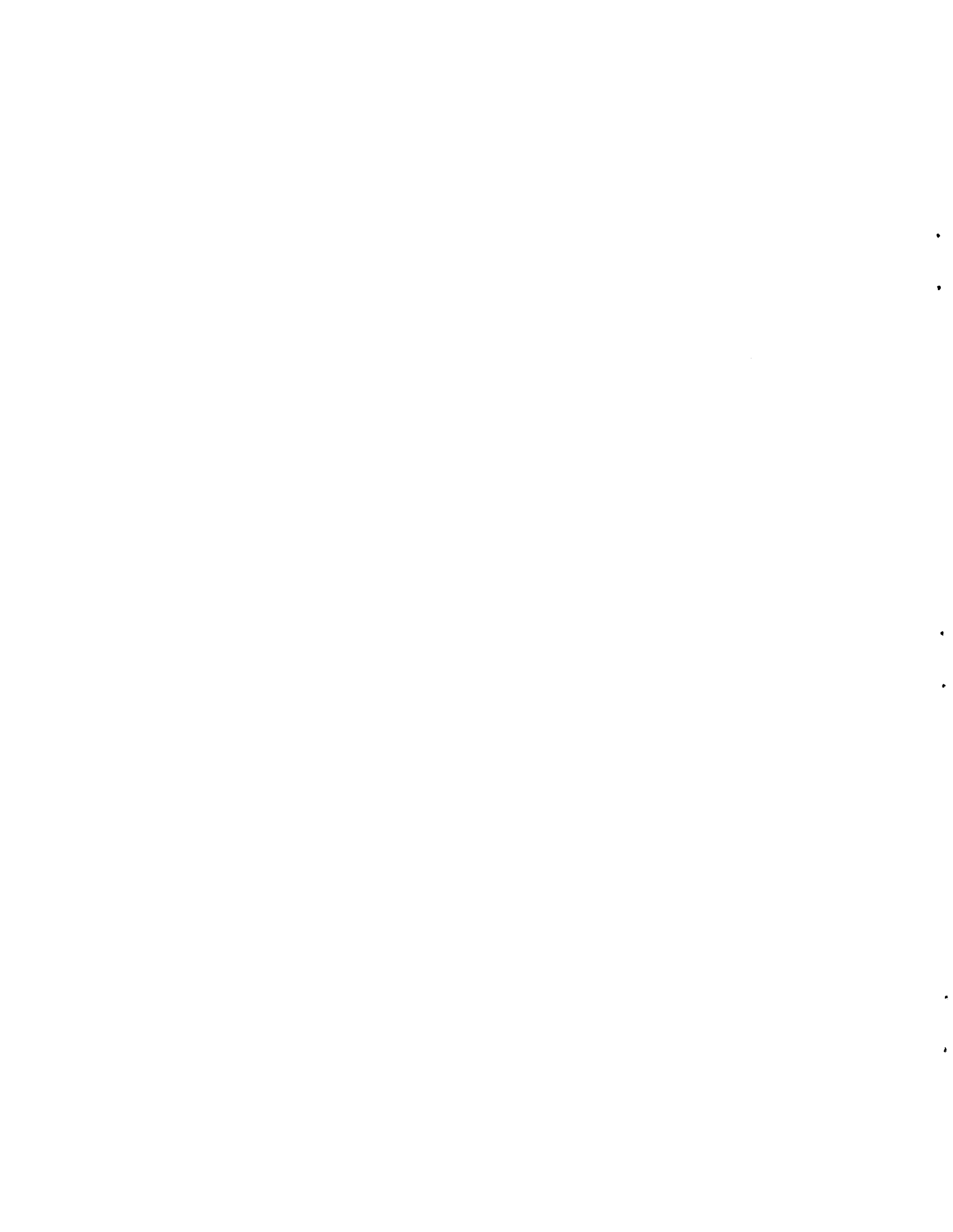
Ultimately, fuel-spikant combinations will have to undergo extensive irradiation proof testing. These tests should be done with several potential spikants at different concentrations and over a range of fuel O/M ratios. Among the important determinations to be made by these tests are: fuel-cladding chemical and mechanical interactions and fuel and spikant redistribution as a result of thermal gradients and mechanical forces.

#### ACKNOWLEDGMENTS

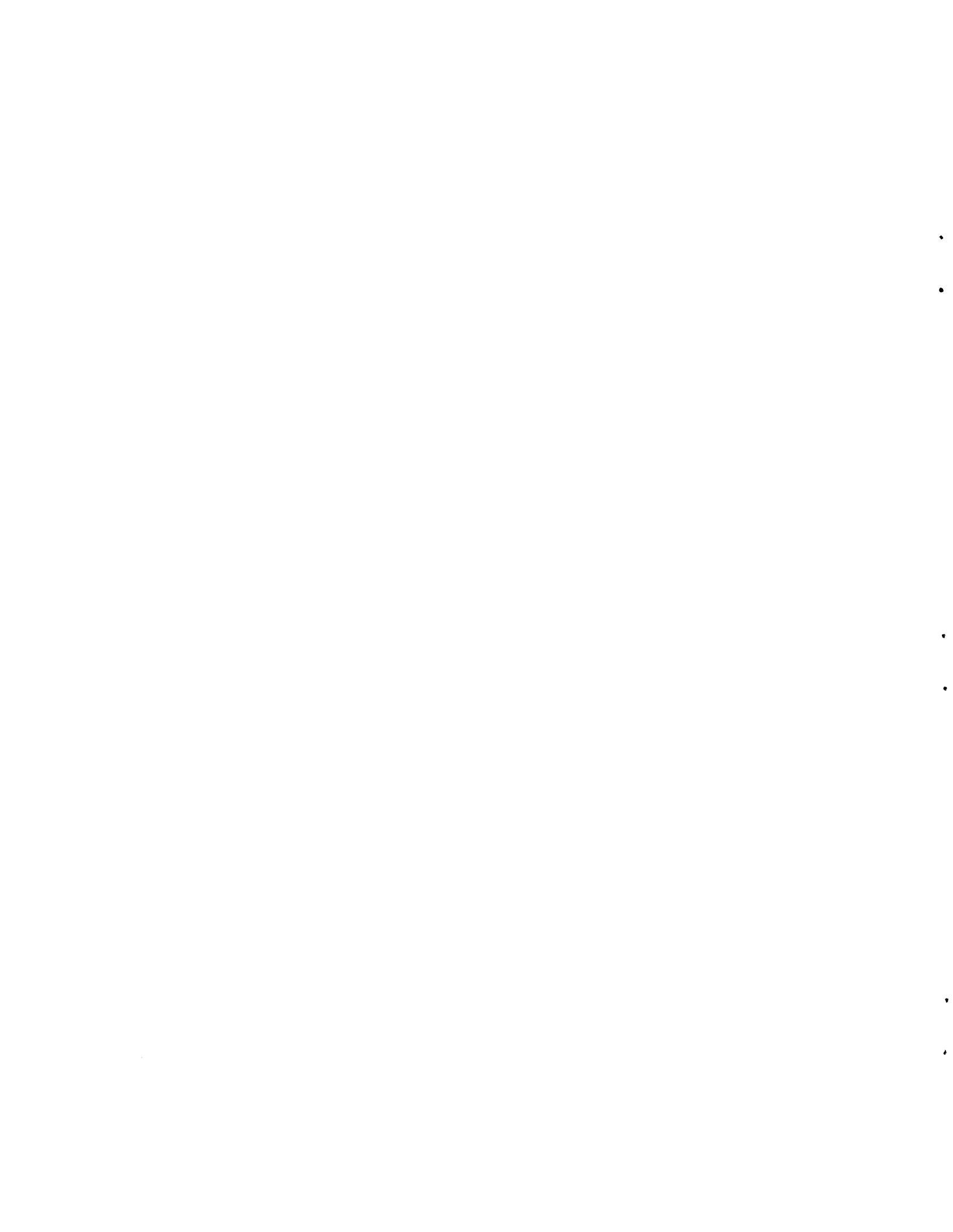
The author would like to express his appreciation to P. Angelini for the dose rate calculations, T. M. Besmann and J. I. Federer for review of the manuscript, W. J. Lackey and A. R. Olsen for helpful comments and discussions and to S. Peterson for editing and L. J. Renfro for typing the manuscript.

## REFERENCES

1. E. V. Weinstock, *The Spiking of Special Nuclear Materials as a Safeguards Measure*, Vol. 1, Nuclear Regulatory Commission Report, submitted in fulfillment of NRC Task 75-1 (Sept. 19, 1975).
2. T. B. Taylor, "Modification of Strategic Special Nuclear Materials to Deter Their Theft or Unauthorized Use," Vol. 2 of *The Spiking of Special Nuclear Materials as a Safeguards Measure*, Nuclear Regulatory Commission Report IRT-378-R (Nov. 6, 1975).
3. A. Glassner, *The Thermochemical Properties of the Oxides, Fluorides, and Chlorides to 2500°K*, ANL-5750 (October 1965).
4. T. L. Markin, "Thermodynamic Data for Uranium and Uranium/Plutonium Oxides Applied to Fuel Preparation Problems," pp. 43-49 in *Preparation of Nuclear Fuels, Nuclear Engineering -- Part XVIII, Chem. Eng. Progr. Symp. Ser. 80*, American Institute of Chemical Engineers, New York, 1967.
5. K. E. Spear, A. R. Olsen, and J. M. Leitnaker, *Thermodynamic Applications to (U,Pu)O<sub>2+x</sub> Fuel Systems*, ORNL/TM-2494, (April, 1969).
6. R. N. Lyon, *Liquid-Metals Handbook*, USAEC-Department of the Navy, Document NAVEXOS, (Rev.) (June 1952), p. 733.
7. C. W. Kee, A. G. Croff, and J. O. Blomeke, *Updated Projections of Radioactive Wastes to be Generated by the U. S. Nuclear Power Industry*, ORNL/TM-5427 (December 1976).
8. M. Tetenbaum, "High Temperature Vaporization Behavior of Hypostoichiometric U-Pu-O and U-Nd-O Solid Solutions," *Thermodynamics of Nuclear Materials 1974*, Vol. I, International Atomic Energy Agency, Vienna, 1975, pp. 305-16.



**APPENDIX A**  
**PHASE RELATIONSHIPS**



## PHASE RELATIONSHIPS

## Fuel Constituents

Pu-O System

The phase diagram for this system is not well established. Two versions<sup>1-4</sup> are given in Figs. A1 and A2. Melting points for this system are poorly defined because of the tendency for changes in stoichiometry at elevated temperature. Most of the conflicts in this system have centered in the region around Pu<sub>01.61</sub>. This phase appears to be closely related to the cubic Pu<sub>01.52</sub> structure. However, above 650°C there is evidence to suggest that this phase is merely the lower limit of the substoichiometric Pu<sub>02</sub> (Pu<sub>02-x</sub>) phase. Extensive metallographic and x-ray analyses by Blank et al.,<sup>3,4</sup> have produced the diagram given in Fig. A2. In this diagram, the existence of Pu<sub>01.6</sub> as a separate phase is proposed.

The presence of a miscibility gap in the Pu<sub>02-x</sub> region below 650°C has been verified by several workers,<sup>2,5</sup> and the primary disagreement has centered around the lower composition limit of the gap. Figure A1 reflects the data of Gardner et al.,<sup>2</sup> who used x-ray diffraction to establish the lower limit of this gap at about Pu<sub>01.61</sub>. Earlier work by Chikalla et al.,<sup>5</sup> using thermal expansion and electrical resistivity measurements, set the monotectoid limit at Pu<sub>01.70</sub>. The presence of Pu<sub>01.61</sub> has not been detected below 300°C.

It appears that there are at least three compounds in this system: hexagonal Pu<sub>2</sub>O<sub>3</sub> (Pu<sub>01.5</sub>); cubic Pu<sub>01.52</sub>; and cubic Pu<sub>02-x</sub>, where  $0 < x < 0.39$  and the temperature is above 300°C. Crystal structure data are summarized in Table A1. Included in this table are data<sup>4</sup> on the phase of Fig. A2 having an O/M ratio of 1.62 to 1.69 and a bcc structure. A fifth compound PuO has been suggested by several workers, but recent works<sup>6,7</sup> suggest that phases identified as PuO are probably Pu(C,O).

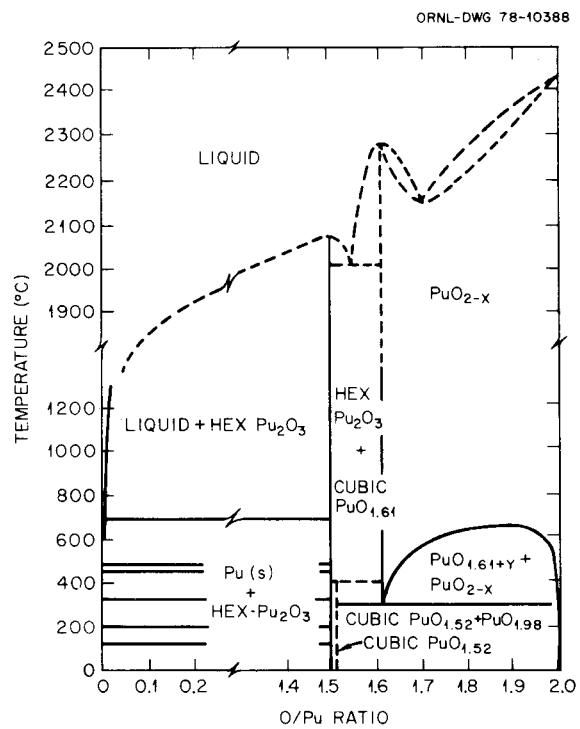


Fig. A1. Tentative Plutonium-Oxygen Phase Diagram. Based on Rand et al.<sup>1</sup>

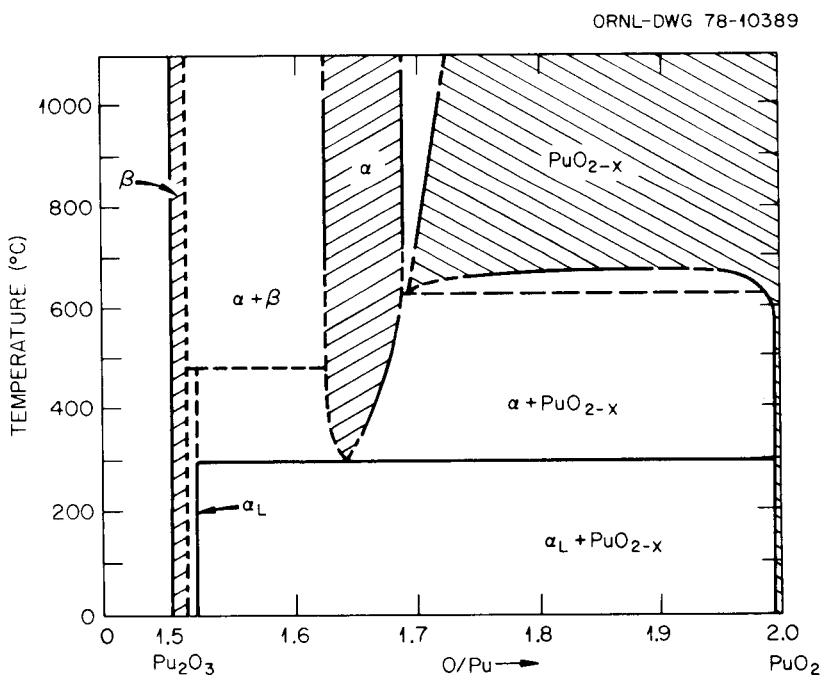


Fig. A2. Phase Diagram of the Plutonium-Oxygen System:  $\text{PuO}_{2-x}$ , fcc Structure;  $x\text{PuO}_{1.62+x}$ , bcc Structure;  $\beta\text{Pu}_2\text{O}_3$ , Hexagonal Structure. Based on Blank and Co-workers.<sup>3,4</sup>

Table A1. Crystal Structure Data for the Pu-O System

Phase	Composition	Crystal Structure	Space Group	$D_x$ (g/cm <sup>3</sup> )	Type	Cell Parameter (nm)
$\beta$ -Pu <sub>2</sub> O <sub>3</sub>	PuO <sub>1.5</sub>	Hexagonal	<i>P</i> 3 <i>m</i> <i>L</i>	11.47	Type A Rare Earth La <sub>2</sub> O <sub>3</sub> type	$a = 0.3841 \pm 0.0006$ $c = 0.5958 \pm 0.0005$
Cubic PuO <sub>1.5</sub>	PuO <sub>1.52</sub>	Body-centered cubic	<i>I</i> $\alpha$ 3	10.2	C Form Rare Earth Sesquioxides	$a = 1.1047, 1.1050$
	PuO <sub>2</sub>	Face-centered cubic	<i>F</i> $\bar{m}$ 3 <i>m</i>	11.46	CaF <sub>2</sub>	$a = 0.5396 \pm 0.0003$
$\alpha$	PuO <sub>1.62-1.69</sub>	Body-centered cubic C type				$a = 1.095 - 1.101 \pm 0.002$

Th-O System

The only complete determination of the thorium-oxygen system is that given by Benz,<sup>8</sup> shown in Fig. A3. The diagram is presented as the Th-ThO<sub>2</sub> binary system since there is no oxide of thorium higher than ThO<sub>2</sub>.

This diagram is at variance with earlier works,<sup>9-12</sup> which indicate the existence of two oxides of thorium, ThO and ThO<sub>2</sub>. Crystal structure data are summarized in Table A2. Thermodynamic data for both these compounds have also been published,<sup>13</sup> although there is no indication in the experimental work of Benz<sup>8</sup> of the existence of ThO. Brewer<sup>14</sup> states that all of the elements from thorium to americium are known to have an MO oxide with the NaCl structure. More recently, Eyring<sup>15</sup> states that ThO probably only exists when stabilized by substantial nitrogen or carbon impurity. This point needs to be resolved.

U-O System

The most reasonable diagram for this system is given in Fig. A4. The liquidus and solidus portion of the diagram from an O/U ratio of 1.45 to 2.25 was determined by Latta and Fryxell.<sup>16</sup> Edwards and Martin<sup>17</sup> established the existence of a miscibility gap by metallographic

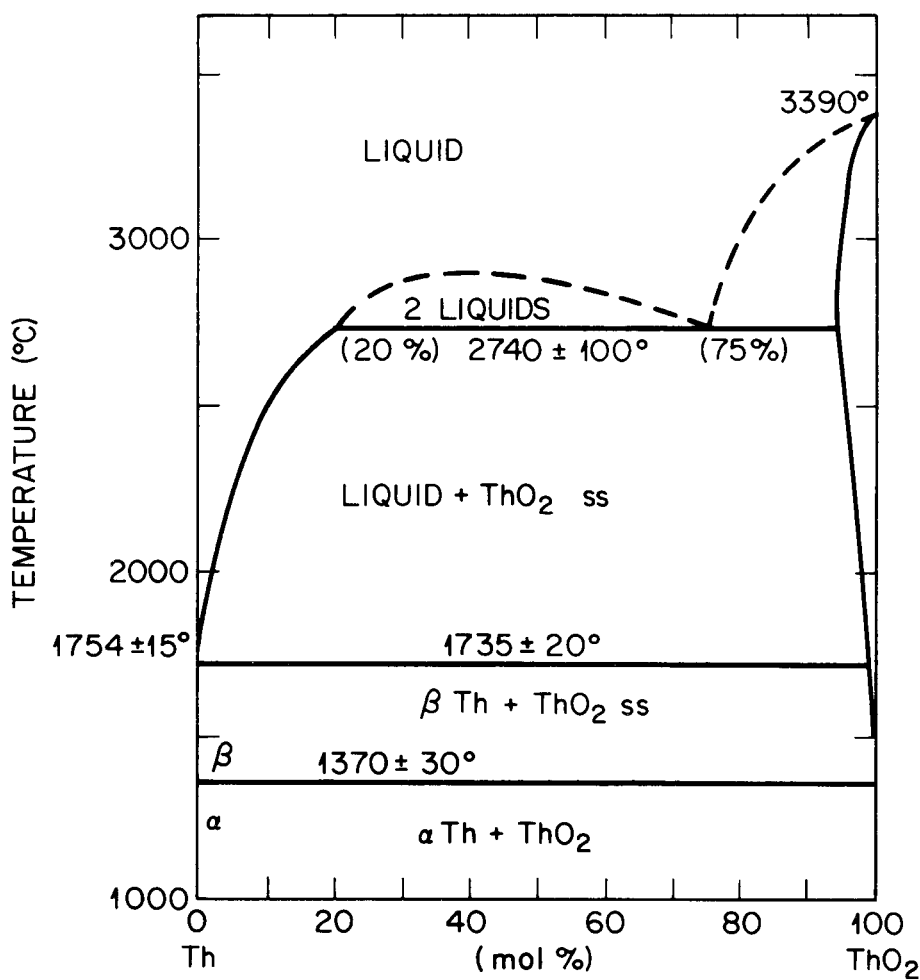


Fig. A3. System Th-ThO<sub>2</sub>. Based on Benz.<sup>8</sup>

Table A2. Crystal Structure Data for the Th-O System

Composition	Crystal Structure <sup>a</sup>	$a$ , Cell Parameter (nm)	Reference	Remarks
ThO	c	0.520	9	Fluorite type
ThO	fcc	0.525	10	NaCl type
ThO <sub>2</sub>	fcc	0.5973	11	Isotopic with CaF <sub>2</sub> (fluorite)
ThO <sub>2</sub>		0.5997	12	

<sup>a</sup>c = cubic; fcc = face-centered cubic.

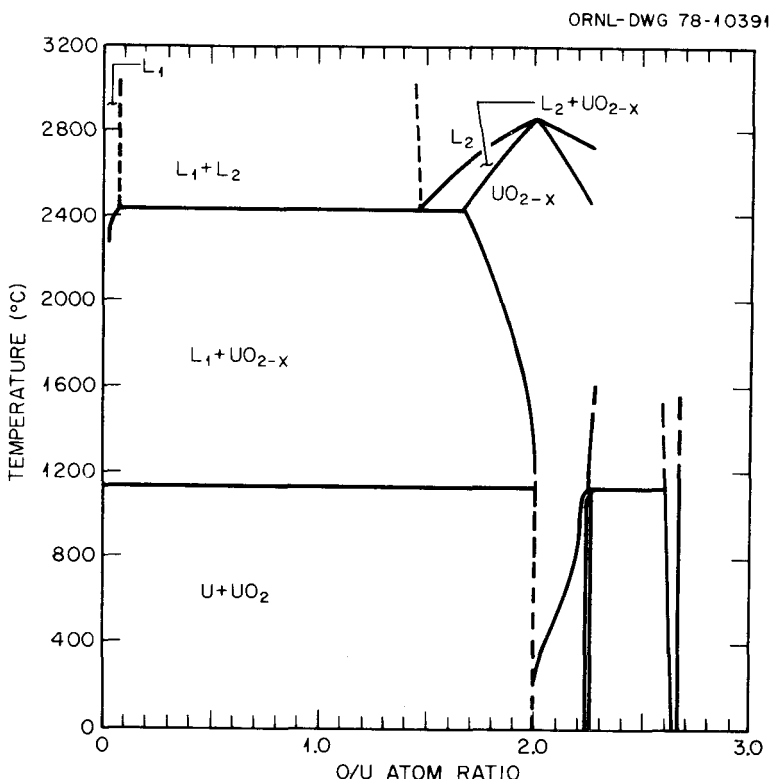


Fig. A4. The Uranium-Oxygen System.

examination of arc-melted alloys, and the monotectic composition was established at an O/U ratio of  $1.30 \pm 0.10$  ( $65 \pm 5$  mol % UO<sub>2</sub>). This was subsequently modified by Latta and Fryxell to O/U of 1.46. Edwards and Martin established the location of the solvus line between O/U ratios of 1.66 and 2.00.

The region between UO<sub>2</sub> and UO<sub>3</sub> has received considerable attention, although the issue is still very much confused. A number of configurations have been proposed for this region,<sup>18-22</sup> and all of them agree that:

1. UO<sub>2</sub> shows a wide range of deviation from stoichiometry to UO<sub>2+x</sub>;
2. the compound U<sub>4</sub>O<sub>9</sub> forms by a peritectoid reaction at about 1125°C;
3. the compound U<sub>3</sub>O<sub>8</sub> is stable over a range of oxygen contents.

Figure A4 was drawn after we considered these points.

Two papers have considered the peritectoid reaction for U<sub>4</sub>O<sub>9</sub> in detail. Experiments conducted by Roberts and Walter<sup>18</sup> led them to conclude the configuration given in Fig. A4 pertains. Kotlar, Gerdanian, and Dode<sup>19</sup> produced similar results.

Hoekstra, Siegel, and Gallagher<sup>20</sup> have summarized the crystal data on the uranium oxides, and these are given in Table A3. A total of 16 separate phases has been identified among the nine oxides, although many of these are no doubt metastable phases. These nine oxides have been included in a diagram proposed by Hoekstra et al.,<sup>20</sup> which is adapted in Fig. A5. No justification for this configuration is given, and this diagram is probably speculative, at best. While the essential features of Fig. A4 are present, the various polymorphs of  $\text{UO}_3$  and  $\text{U}_3\text{O}_8$  are not indicated. The diagram of Fig. A5 is probably incomplete, because of lack of data for the higher oxides.

A second alternative for this region is suggested by Rand and Roberts<sup>21</sup> and given in Fig. A6. Except that it does not extend beyond an O/U ratio of about 2.67 ( $\text{U}_3\text{O}_8$ ). Some of the confusion involving this portion of the diagram results from the apparent inability to determine whether compounds such as  $\text{U}_8\text{O}_{21}$  are really separate compounds, or merely the lower limit of stability of  $\text{U}_3\text{O}_{8-y}$ . More recent work by Kozhina and Shiryaeva<sup>22</sup> shows that several phases are not stable during repeated cycling and are thus considered to be metastable. These include  $\beta$ - $\text{U}_3\text{O}_8$ , hexagonal  $\text{U}_2\text{O}_5$ , and tetragonal oxides, presumably  $\text{U}_{16}\text{O}_{37}$  and  $\alpha$ - $\text{U}_3\text{O}_7$ .

#### Pu-Th-O System

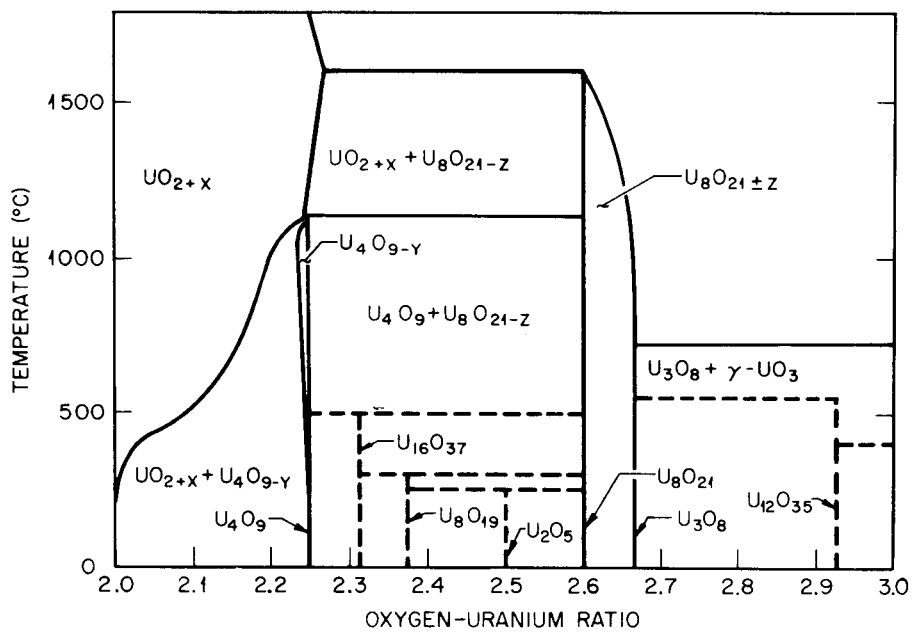
Limited melting point data, measured under a helium atmosphere, indicate a constant melting point up to about 25 wt %  $\text{ThO}_2$ , then a steady rise in melting point with increasing  $\text{ThO}_2$  content.<sup>23</sup> This is shown in Fig. A7. Lattice parameter data show a linear relationship with  $\text{ThO}_2$  content, indicating complete solid solubility across the diagram.<sup>23,24</sup> With  $\text{PuO}_2$ -rich pellets, traces of  $\alpha$ - and  $\beta$ - $\text{Pu}_2\text{O}_3$  were found, suggesting a stoichiometry shift.<sup>23</sup> In view of the instability of  $\text{PuO}_2$  at high temperature (high  $P_{\text{O}_2}$  over  $\text{PuO}_2$ ) this shift is not surprising and may be responsible for the nonidealized curve of Fig. A7.

Table A3. Crystallographic Data on Uranium Oxides<sup>a</sup>

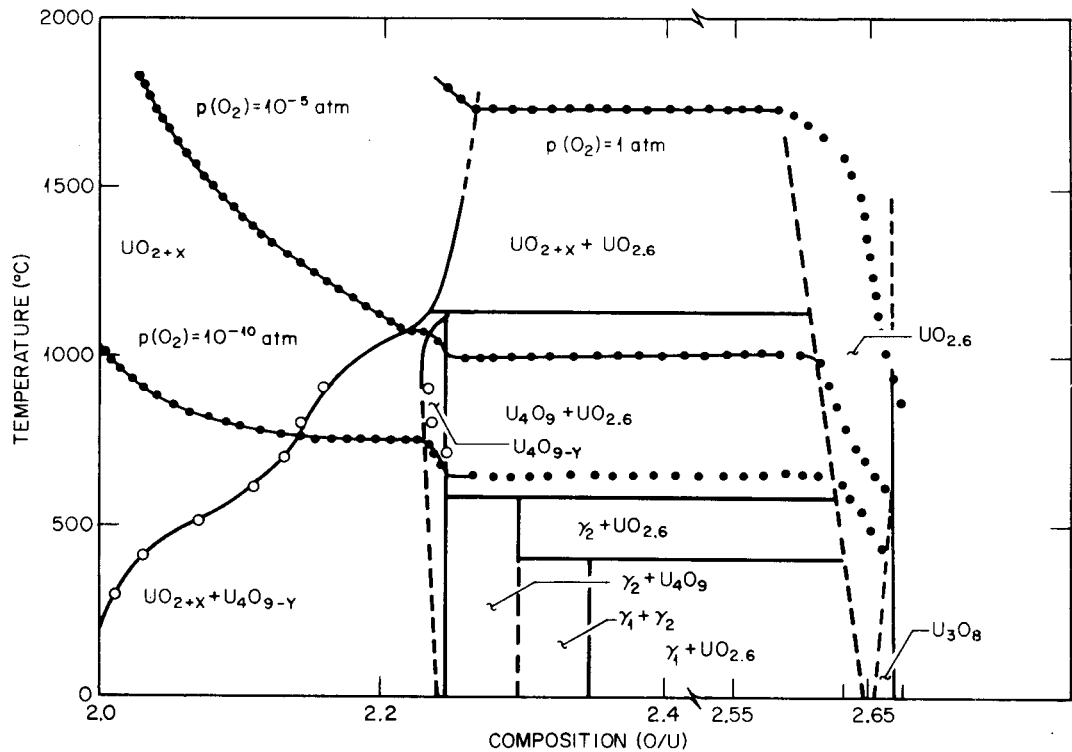
Compound	Symmetry	Lattice Parameters, nm			$\beta$ , Cell Angle (deg)	Z	Density (Mg/m <sup>3</sup> )
		$a$	$b$	$c$			
UO <sub>2</sub>	Cubic	0.54704				4	10.97
U <sub>4</sub> O <sub>9</sub>	Cubic	0.54411				64	11.31
U <sub>16</sub> O <sub>37</sub>	Tetragonal	0.541		0.549 <sup>b</sup>			11.37
$\alpha$ -U <sub>3</sub> O <sub>7</sub> (?)	Tetragonal	0.546		0.540 <sup>b</sup>			11.35
U <sub>8</sub> O <sub>19</sub>	Monoclinic	0.5378	0.5559	0.5378	90.29		11.42
U <sub>2</sub> O <sub>5</sub> (?)	Hexagonal	0.3885		0.4082 <sup>b</sup>			8.65
U <sub>8</sub> O <sub>21</sub>	Orthorhombic	0.6751	0.3176	0.8286		4	8.37
$\alpha$ -U <sub>3</sub> O <sub>8</sub>	Orthorhombic	0.6716	1.1981	0.4144		2	8.43
$\beta$ -U <sub>3</sub> O <sub>8</sub>	Orthorhombic	0.705	1.142	0.829		4	8.38
U <sub>12</sub> O <sub>35</sub>	Orthorhombic	0.691	0.392	0.416 <sup>b</sup>			8.41
$\alpha$ -UO <sub>3</sub>	Hexagonal	0.3971		0.417		1	8.34
$\beta$ -UO <sub>3</sub>	Monoclinic	1.034	1.433	0.391	99.03	4	8.30
$\gamma$ -UO <sub>3</sub>	Orthorhombic	0.971	0.977	1.992		32	8.02
$\delta$ -UO <sub>3</sub>	Cubic	0.416				1	6.67
$\epsilon$ -UO <sub>3</sub>	Triclinic	0.4002	0.3841	0.4165	90.55 <sup>c</sup>	1	8.73
$\zeta$ -UO <sub>3</sub>	Orthorhombic	0.7511	0.5466	0.5224		4	8.86

<sup>a</sup>Based on Hoekstra et al.<sup>20</sup><sup>b</sup>Cell parameters of this phase refer to the pseudo-cell.<sup>c</sup> $\alpha = 98.28^\circ$ ,  $\gamma = 120.47^\circ$ .

ORNL-DWG 78-10392

Fig. A5. Phase Diagram —  $\text{UO}_2\text{-UO}_3$ . Based on Hoekstra et al.<sup>20</sup>

ORNL-DWG 78-10393

Fig. A6. Portion of Uranium-Oxygen Phase Diagram (Dotted lines represent oxygen isotherms). Based on Rand and Roberts.<sup>21</sup>

ORNL-DWG 78-10394

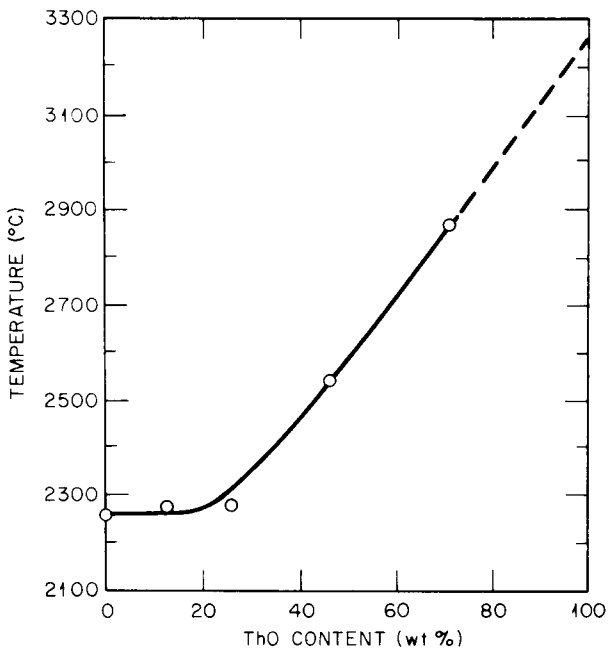


Fig. A7. Melting Point of  $(\text{Th},\text{Pu})\text{O}_2$  Solid Solution. Based on Freshly and Mattys.<sup>23</sup>

#### Pu-U-O System

Work on the  $\text{PuO}_2-\text{UO}_2$  system by a number of workers shows that these two stoichiometric compounds form a continuous series of solid solutions.<sup>25-27</sup> Melting point studies show a continuously decreasing liquidus with increasing  $\text{PuO}_2$  content, with no maximum or minimum, as shown in Fig. A8. X-ray diffraction studies show a linear change of lattice parameter with composition, with only the fcc fluorite phase present.

Deviations from stoichiometric  $(\text{U},\text{Pu})\text{O}_2$  occur relatively easily and tend toward hypostoichiometry  $[(\text{U},\text{Pu})\text{O}_{2-x}]$  when the plutonium content is high and toward hyperstoichiometry  $[(\text{U},\text{Pu})\text{O}_{2+x}]$  when the plutonium content is low. Available information on the Pu-U-O system is summarized in Figs. A9 and A10. Figure A9 is essentially that of Markin and Street.<sup>26</sup> The results of Sari, Benedict, and Blank<sup>28</sup> are similar to this, with only minor differences in the extent of the fcc  $\text{MO}_{2.0}$  + fcc  $\text{MO}_{2-x}$  phase field. This field extends to a  $\text{Pu}/(\text{U} + \text{Pu})$  ratio of about

ORNL-DWG 78-10395

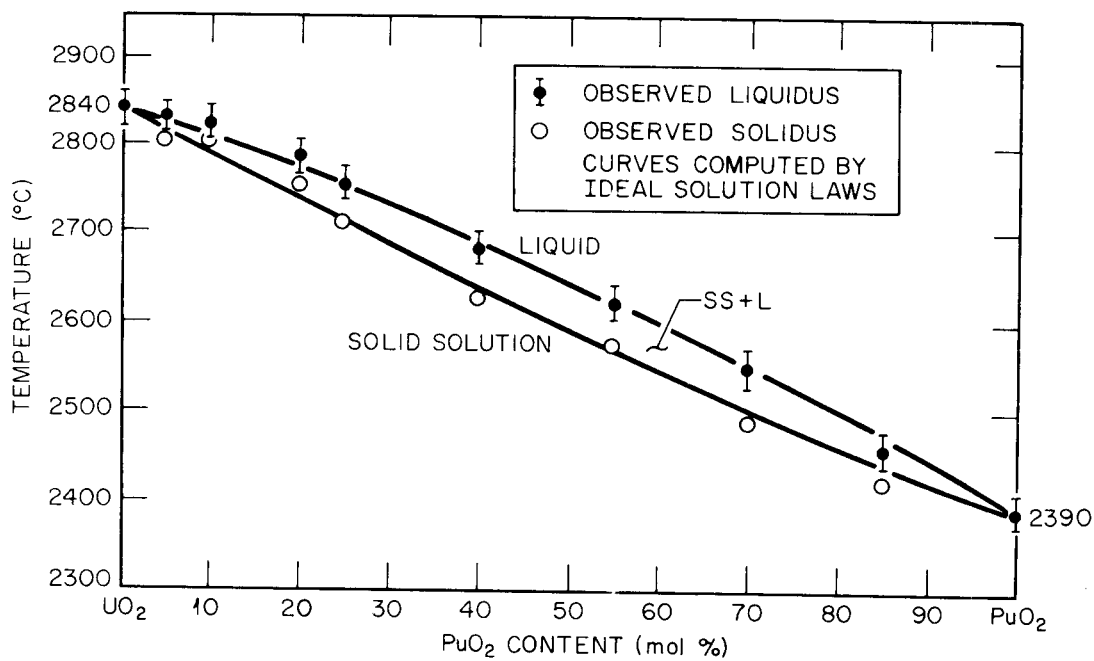


Fig. A8. Solid-liquid Phase Diagram for the  $\text{UO}_2$ - $\text{PuO}_2$  System.  
Based on Lyon and Baily.<sup>25</sup>

ORNL-DWG 78-10396

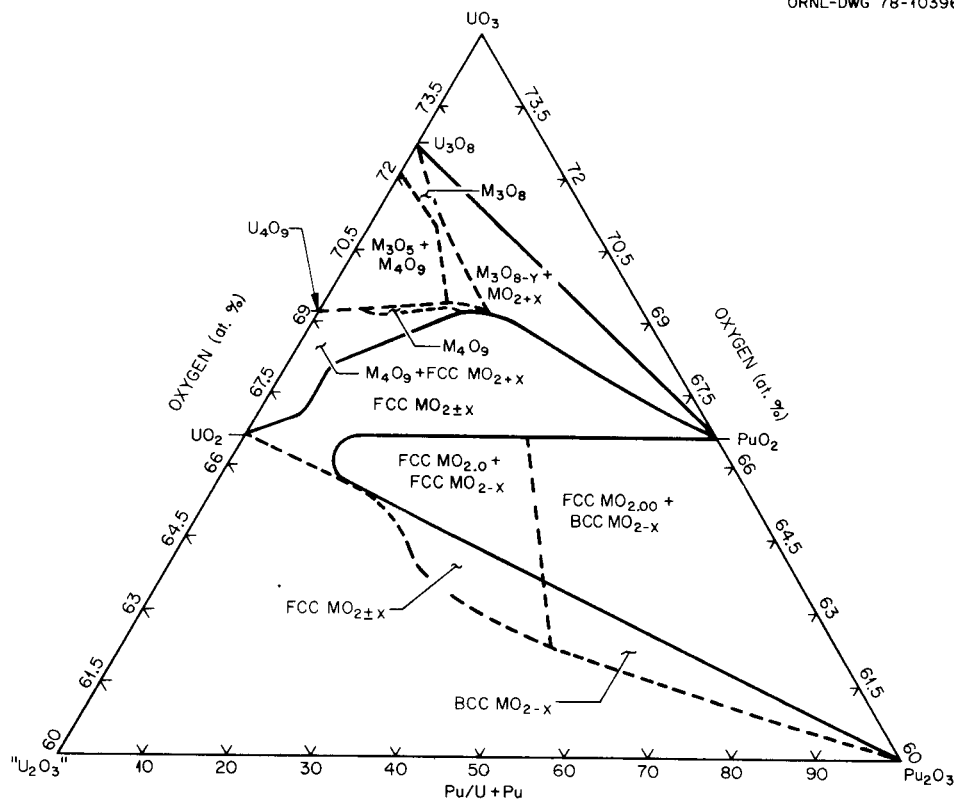


Fig. A9. The  $\text{UO}_3$ - $\text{U}_2\text{O}_3$ - $\text{Pu}_2\text{O}_3$  System at Room Temperature.

ORNL-DWG 78-10397

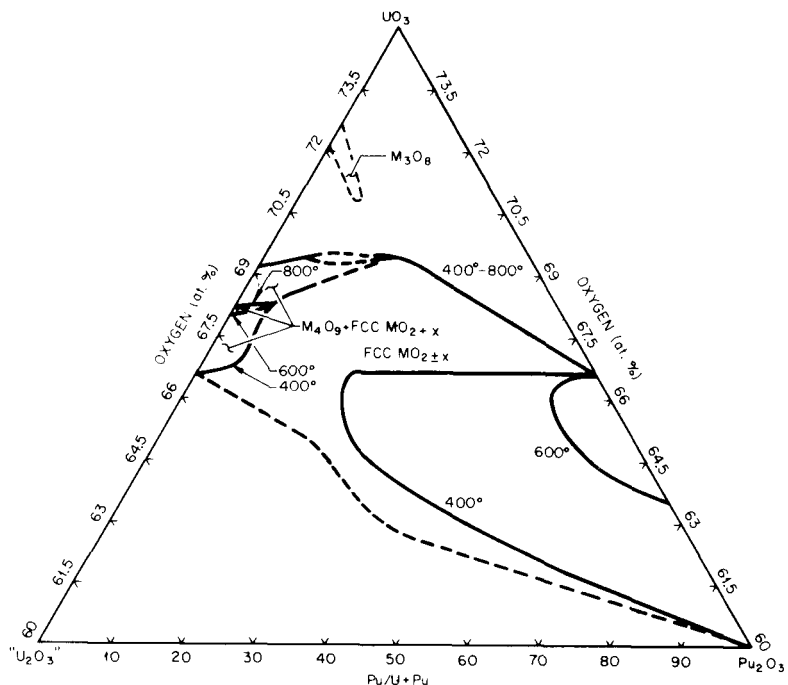


Fig. A10. The  $\text{UO}_3\text{-U}_2\text{O}_3\text{-Pu}_2\text{O}_3$  System at 400, 600, and 800°C.

0.35 in the results of Markin and Street,<sup>26</sup> compared to about 0.17 indicated by Sari et al.<sup>28</sup> Koizumi and Nakamuri<sup>29</sup> also suggest that this field extends to a  $\text{Pu}/(\text{U} + \text{Pu})$  ratio of about 0.20.

Nakayama<sup>30</sup> worked out the relationships between  $\text{U}_3\text{O}_7$  and  $\text{PuO}_2$ , and his results on solubility limits, two-phase fields, etc. agree very well with Fig. A9. Figure A10 shows the diagram of Markin and Street at 400, 600, and 800°C. The single-phase field becomes increasingly large as the temperature increases, resulting in a large single-phase field covering a wide range of stoichiometry and  $\text{Pu}/\text{U}$  compositions. This shrinking two-phase field is shown more clearly in Fig. A11,<sup>28</sup> which gives differential thermal analysis results at different  $\text{Pu}/(\text{U} + \text{Pu})$  ratios. As the  $\text{Pu}/(\text{U} + \text{Pu})$  ratio decreases, the two-phase field also decreases.

From the viewpoint of fast breeder reactor fuel fabrication these observations show that for stoichiometric  $(\text{U}, \text{Pu})\text{O}_2$  only one phase, fcc  $\text{MO}_{2.0}$ , exists. However, for substoichiometric material there are conditions under which two phases exist. The likelihood that two phases

ORNL-DWG 78-10398

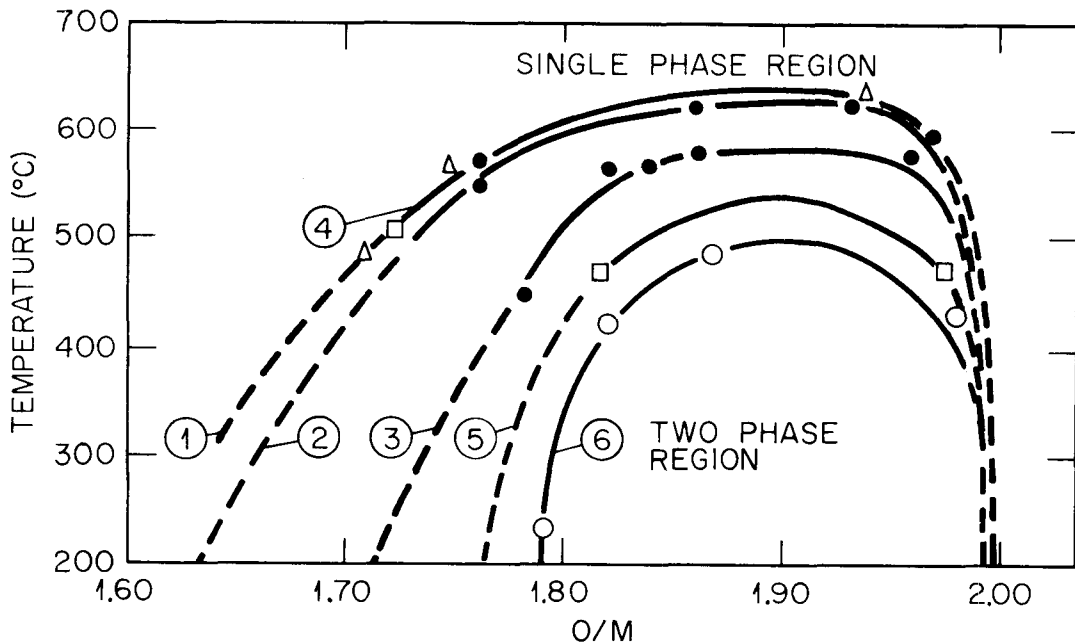


Fig. All. Limits of the Two-Phase Region Determined by DTA.  
 $\text{Pu}/(\text{U} + \text{Pu})$  ratios are (1) 1, (2) 0.95, (3) 0.8, (4) 0.58, (5) 0.58,  
(6) 0.42. Adapted from Sari et al.<sup>28</sup>

exist increases with increasing plutonium content, decreasing oxygen content, and decreasing temperature. The quantity of any second phase would increase with decreasing oxygen content. For light water reactor fuels the plutonium content is sufficiently low that only one phase will be present under equilibrium conditions.

Several investigations<sup>31,32</sup> suggest the presence of a rhombohedral phase  $\text{M}_7\text{O}_{12}$  for  $\text{Pu}/(\text{U} + \text{Pu})$  ratios of 0.64 to 0.84 at an O/M of about 1.85. More work is necessary to establish the extent of stability of this phase.

#### Th-U-O System

Lattice parameter measurements in mixtures of  $\text{ThO}_2$  and  $\text{UO}_2$  show a continuous, single-phase fluorite structure, indicating a continuous solid solution system.<sup>33-36</sup> This is not unexpected since both  $\text{ThO}_2$  and  $\text{UO}_2$  have the fluorite structure with lattice parameters of

approximately 0.5596 and 0.5470 nm, respectively, which is a 2.3% difference. Melting point measurements<sup>35-37</sup> indicate that a minimum exists in the liquidus at about 5 mol % ThO<sub>2</sub>. The diagram is given in Fig. A12.

Deviations from stoichiometric Mo<sub>2</sub> in this system are toward hyperstoichiometric oxygen compositions (Mo<sub>2+x</sub>). Several investigations have reported on the UO<sub>2</sub>-ThO<sub>2</sub>-UO<sub>3</sub> system.<sup>38-41</sup> Data presented by Paul<sup>38</sup> and Paul and Keller<sup>39</sup> at 600 and 1100°C and 1250-1550°C are given in Figs. A13 and A14. The data of Cohen and Berman<sup>40</sup> and Friedman and Thoma<sup>41</sup> are in substantial agreement with these figures, with only minor differences in exact location of boundary lines. The single-phase fluorite structure is stable over a wide range of oxygen concentrations and Th/(U + Th) ratios.

Rachev and co-workers<sup>42</sup> suggested a new compound, U<sub>2</sub>Th<sub>2</sub>O<sub>9</sub>, but Paul,<sup>38</sup> and Paul and Keller<sup>39</sup> conclude that this composition is merely the limit of solubility of tetravalent thorium in U<sub>4</sub>O<sub>9</sub> with superlattice lines.

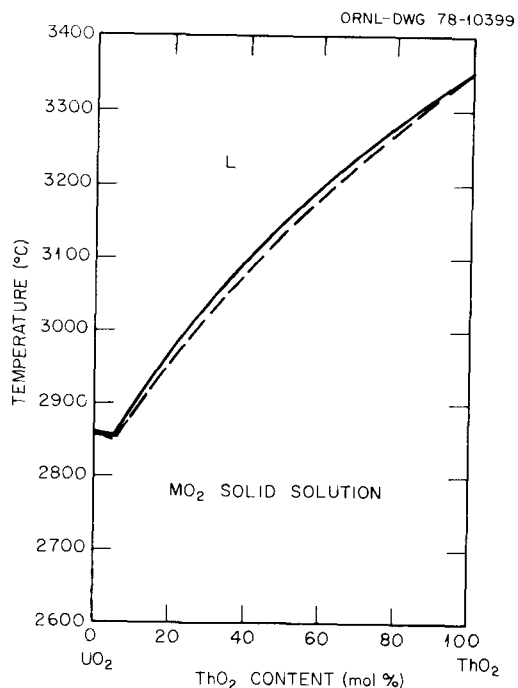
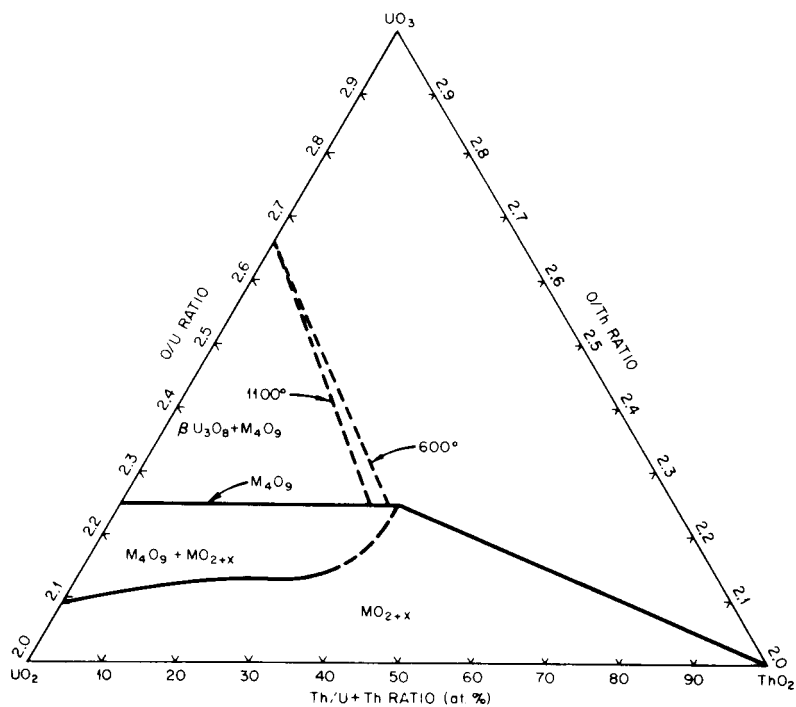
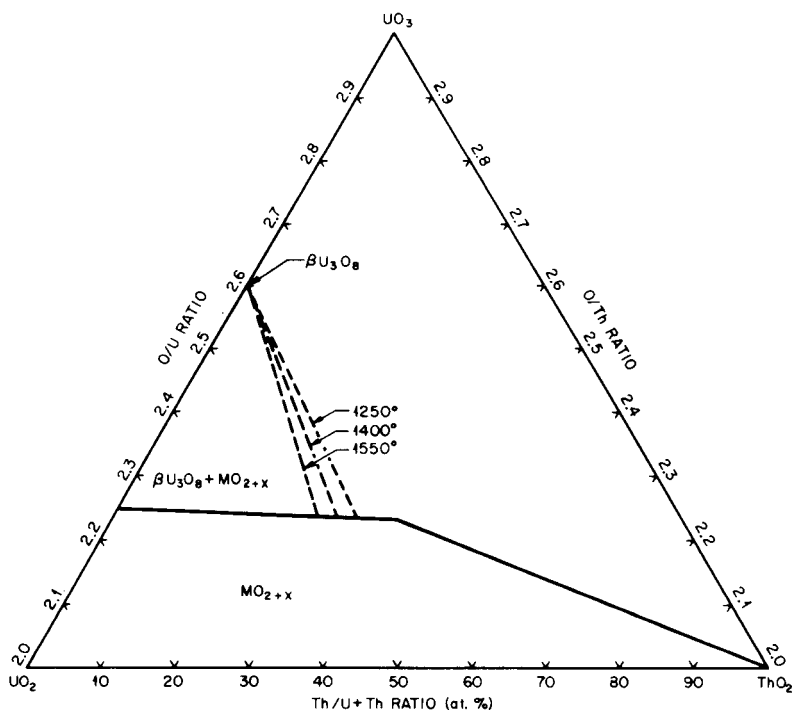


Fig. A12. The ThO<sub>2</sub>-UO<sub>2</sub> System.

ORNL-DWG 78-10400

Fig. A13. The  $\text{ThO}_2\text{-}\text{UO}_2\text{-}\text{UO}_3$  System at 600 to 1100°C.

ORNL-DWG 78-10401

Fig. A14. The  $\text{ThO}_2\text{-}\text{UO}_2\text{-}\text{UO}_3$  System at 1250 to 1550°C.

Work by Lynch<sup>43</sup> suggests that above 1250°C complete solid solubility exists between ThO<sub>2</sub> and U<sub>3</sub>O<sub>8</sub>, with partial solid solubility at 1000°C. In another work Braun et al.<sup>44</sup> found continuous solid solubility for the systems U<sub>0.5</sub>Th<sub>0.5</sub>O<sub>2.25</sub>-ThO<sub>2</sub> and UO<sub>2.25</sub>-ThO<sub>2</sub>.

#### Pu-Th-U-O System

No data are available in the literature on this system. If only the ternary system between dioxides, PuO<sub>2</sub>-ThO<sub>2</sub>-UO<sub>2</sub>, is considered, one would expect complete solid solubility in all proportions since all three dioxides have the fluorite structure, and all three binary systems are solid solution type diagrams. Reeve<sup>55</sup> has speculated that in the presence of excess oxygen PuO<sub>2</sub> and particularly ThO<sub>2</sub> would be effective in stabilizing UO<sub>2</sub> against oxidation to U<sub>3</sub>O<sub>8</sub>.

#### Spikants and Decay Products

#### Ce-O System

Phase relationships for this system below about 1169°C are largely the result of work by Bevan and Kordis.<sup>46</sup> The CeO<sub>2</sub>-Ce<sub>2</sub>O<sub>3</sub> phase diagram given in Fig. A15 is based primarily on that work, although it has been modified slightly to reflect the work of others.<sup>47-50</sup> Seven phases have been identified in this system. The intermediate compounds, in general, correspond to the relationship Ce<sub>n</sub>O<sub>2n-2</sub> where n = 6, 7, 9, 10, and 11. Available crystal structure data on these compounds are summarized in Table A4.

Neutron diffraction studies were used to identify the exact composition of the compounds Ce<sub>7</sub>O<sub>12</sub> (Ce<sub>0.714</sub>), Ce<sub>9</sub>O<sub>16</sub> (Ce<sub>0.778</sub>), Ce<sub>10</sub>O<sub>18</sub>(Ce<sub>0.80</sub>), and Ce<sub>11</sub>O<sub>20</sub>(Ce<sub>0.818</sub>).<sup>47,48</sup> This latter compound is considered to be an ordered modification of the defect fluorite (CeO<sub>2-x</sub>) phase.<sup>49</sup> The phase at Ce<sub>0.67</sub>(Ce<sub>6</sub>O<sub>10</sub>) is considered to be the type CCe<sub>2</sub>O<sub>3</sub> phase and is not stable below 600°C. Work by Ray, Nowick, and Cox,<sup>48</sup> using x-ray and neutron diffraction techniques, indicates that the structure of Ce<sub>9</sub>O<sub>16</sub>, Ce<sub>10</sub>O<sub>18</sub>, and Ce<sub>11</sub>O<sub>20</sub> cannot be indexed with

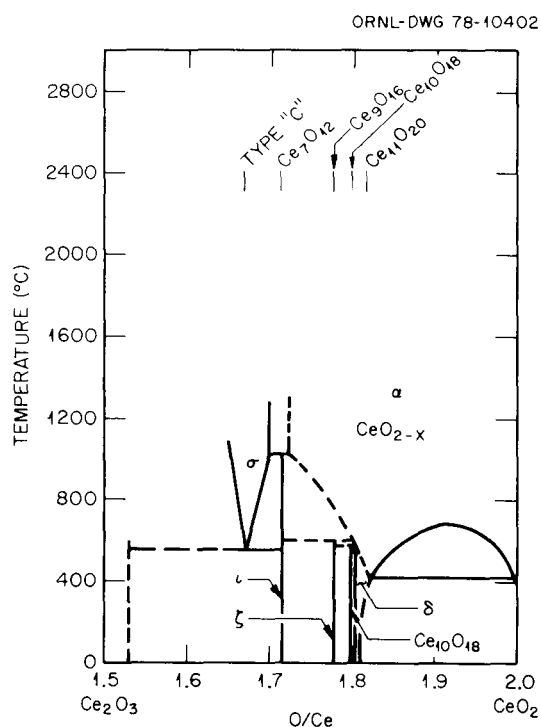


Fig. A15. The  $\text{CeO}_2\text{-}\text{Ce}_2\text{O}_3$  System.

Table A4. Crystallographic Data for the  $\text{CeO}_2\text{-}\text{Ce}_2\text{O}_3$  System

Phase	System	Structure Type	Lattice Parameter, nm		$c/a$	M	Space Group
			$a$	$c$			
$\text{CeO}_2$	cubic	$\text{CaF}_2 (c_1)$	0.5409			4	$Fm\bar{3}m$
$\delta \text{ Ce}_{11}\text{O}_{20}$ ( $\text{CeO}_{1.818}$ )							
$\epsilon \text{ Ce}_{10}\text{O}_{18}$ ( $\text{CeO}_{1.80}$ )							
$\xi \text{ Ce}_9\text{O}_{16}$ ( $\text{CeO}_{1.778}$ )							
$\eta = \text{Ce}_7\text{O}_{12}$ ( $\text{CeO}_{1.714}$ )	rhombohedral hexagonal cell		1.037	0.967	0.932		$\bar{R}\bar{3}$
$\text{Ce}_2\text{O}_3$ ( $\text{CeO}_{1.67}$ )	hexagonal	$(D5_2)$ Type A	0.388	0.606	1.561	1	$P\bar{3}m\bar{l}$
		$C_{\text{Mn}_2\text{O}_3}$ Type	1.111				

rhombohedral cells based on  $\langle 111 \rangle$  vacancy strings as had been suggested by other workers, but structures of lower symmetry (monoclinic or triclinic) are indicated. In view of this, the structures of these compounds are unknown at this point. Bevan<sup>49</sup> has defined the limit of stability of Ce<sub>2</sub>O<sub>3</sub> as CeO<sub>1.53</sub>.

The region above 1169°C is still very much in doubt. Bevan and Kordis<sup>46</sup> claim a two-phase region between CeO<sub>1.70</sub> and CeO<sub>1.72</sub> above the decomposition temperature ( $\sim$ 1023°C) of Ce<sub>7</sub>O<sub>12</sub> (CeO<sub>1.714</sub>). Panlener et al.<sup>51</sup> agree that the compound is not present between 1300 and 1500°C but do not comment on the possibility of a two-phase region in this part of the diagram. Brauer and Gingerich,<sup>52</sup> however, indicate a continuous series of solid solutions between CeO<sub>2.0</sub> and CeO<sub>1.65</sub>. Hyde and Eyring<sup>53</sup> also suggest this possibility. Rather strong arguments are presented for the existence of two phases in this region. In view of this, several alternatives are possible for the high-temperature portion of this system, and the diagram given in Fig. A16 is not unreasonable. Obviously more work is required on this system.

The compound CeO is known. Brewer<sup>14</sup> states that the third-group elements (including the lanthanides) have stable MO gases, but it seems probable that the MO solids are unstable at low temperatures and disproportionate into M and M<sub>2</sub>O<sub>3</sub>. Very few references to CeO were found, and these were thermodynamic data at high temperature for the vaporized species.<sup>54</sup> More recently, Eyring<sup>55</sup> states that solid CeO probably exists only when stabilized by substantial nitrogen or carbon impurities.

#### Nd-O System

A tentative phase diagram<sup>56</sup> of the Nd-O system<sup>67</sup> is shown in Fig. A17 and pertinent crystal structure data are given in Table A5. There appears to be no deviation from stoichiometry in Nd<sub>2</sub>O<sub>3</sub>. In addition to the compounds NdO and Nd<sub>2</sub>O<sub>3</sub>, a third compound, Nd<sub>6</sub>O<sub>11</sub>, has been found and identified<sup>57</sup> as cubic with a lattice parameter  $a = 1.107 \pm 0.003$  nm. These same workers also claim that NdO<sub>2</sub> is obtained by oxidizing neodymium vapor. Both these compounds need to be confirmed. According to Shunk,<sup>58</sup> there is some question on the stability of the

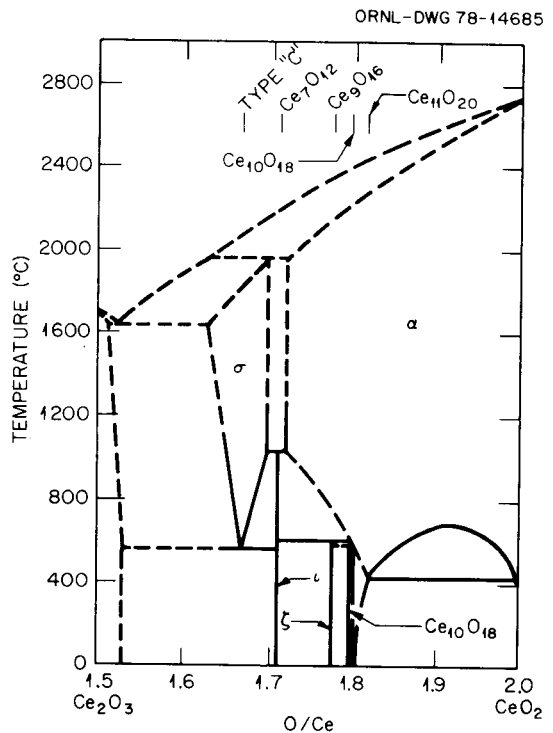


Fig. A16. Alternative  $\text{CeO}_2$ - $\text{Ce}_2\text{O}_3$  System, Including High-Temperature Region.

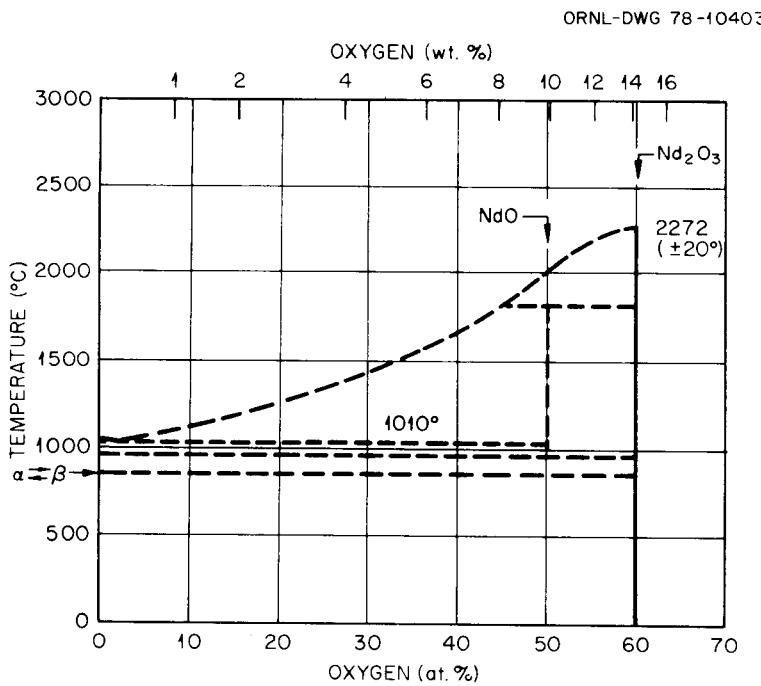


Fig. A17. Tentative Phase Diagram of the Nd-O System. Based on Love.  
56

Table A5. Crystallographic Data for the Nd-O and Pr-O Systems

Phase	System	Structure Type	Lattice Parameters, nm	
			$\alpha$	$c$
$\text{Nd}_2\text{O}_3$ (A type)	Hexagonal	$\text{La}_2\text{O}_3$	0.383	0.5999
$\text{Nd}_2\text{O}_3$ (C type)	bcc	$\text{Mn}_2\text{O}_3$	1.107	
$\text{NdO}$	fcc	$\text{NaCl}$	0.5068	
$\text{Pr}_2\text{O}_3$ (A type)	Hexagonal		0.385	0.600
$\text{Pr}_2\text{O}_3$ (C type)	bcc	$\text{Mn}_2\text{O}_3$	1.1152	
$\text{Pr}_5\text{O}_8$ ( $\sigma$ )	bcc	$\text{Mn}_2\text{O}_3$	1.1070	
$\text{Pr}_{11}\text{O}_{22}$ ( $\text{Pr}_{12}\text{O}_{22}$ )	Cubic		0.5462	
$\text{PrO}_2$	fcc	$\text{CaF}_2$	0.53938	

C-form of  $\text{Nd}_2\text{O}_3$ . Several workers claim that the A-form is the only stable form. More work on this is apparently needed.

#### Pr-O System

A number of compounds exist in this system. The diagram<sup>59</sup> is given in Fig. A18 and is quite similar to the Ce-O system, although less work has been done on structural identification of compounds. Table A5 summarizes available structural data. The intermediate compounds presented in Fig. A18 follow the generalized homologous series  $\text{Pr}_n\text{O}_{2n-2}$ , where  $n = 5, 7, 9, 10, 11, 12$ . Hyde and Eyring<sup>53</sup> state that the structures of analogous compounds in the Ce-O and Pr-O systems are probably equivalent and that the analogs of the same composition are isostructural.

#### Sc-O System

The phase diagram for the scandium-oxygen system<sup>60</sup> is given in Fig. A19. The compound  $\text{Sc}_2\text{O}_3$  has a bcc structure of the  $\text{Mn}_2\text{O}_3$  type with a lattice parameter<sup>61-63</sup> in the range  $\alpha = 0.9845 \pm 0.0002$  nm.

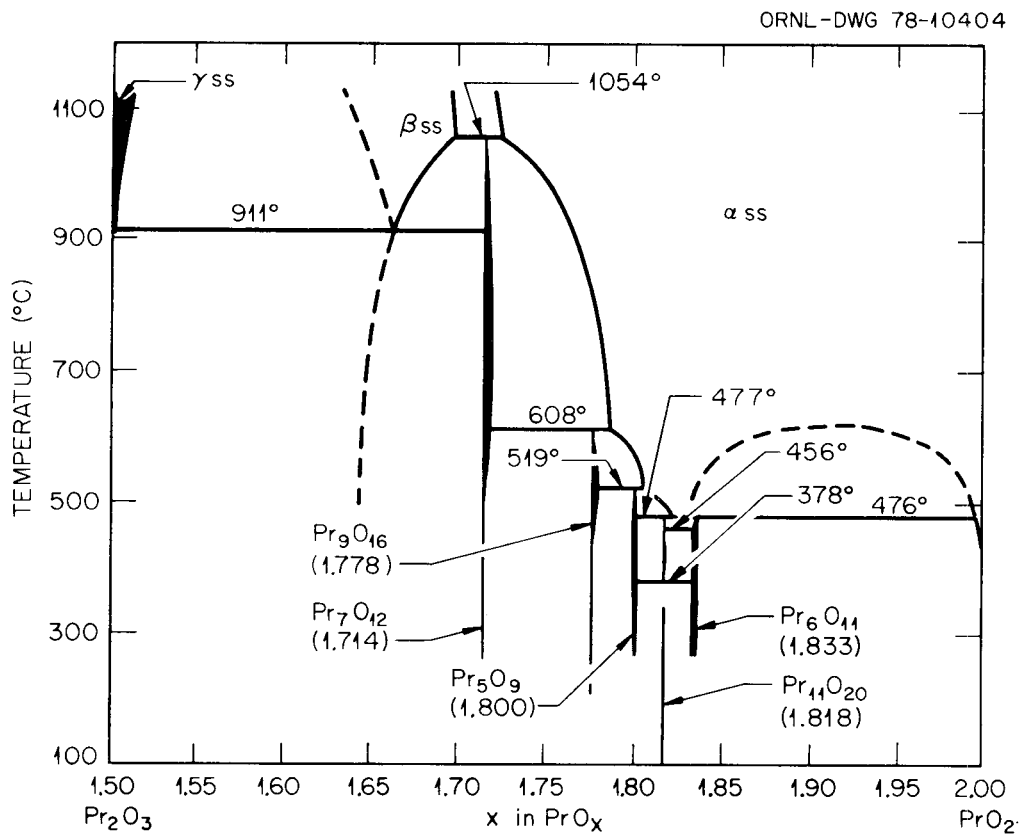


Fig. A18. The Pr-O System. Adapted from Hyde et al.<sup>59</sup>

There appears to be considerable range of solubility of oxygen in the two allotropes of scandium but none in the compound Sc<sub>2</sub>O<sub>3</sub>. Although Fig. A19 shows a melting point for Sc<sub>2</sub>O<sub>3</sub> of 2300°C, Toropov and Vasileva<sup>64</sup> determined it to be 2470 ± 50°C.

#### Ti-O System

This system is quite complicated, with a large number of intermediate compounds. A reasonably complete diagram<sup>65</sup> is given in Fig. A20, which presents information of most importance to fuels work. Stable compounds such as TiO<sub>2</sub> and Ti<sub>2</sub>O<sub>3</sub>, which are the most likely forms of titanium in fuels, show a range of oxygen concentrations. A number of compounds are shown between O/Ti ratios of 1.7 and 2.0, corresponding to the homologous series Ti<sub>n</sub>O<sub>2n-1</sub>. Most of the compounds in this system, with the exception of those in the homologous

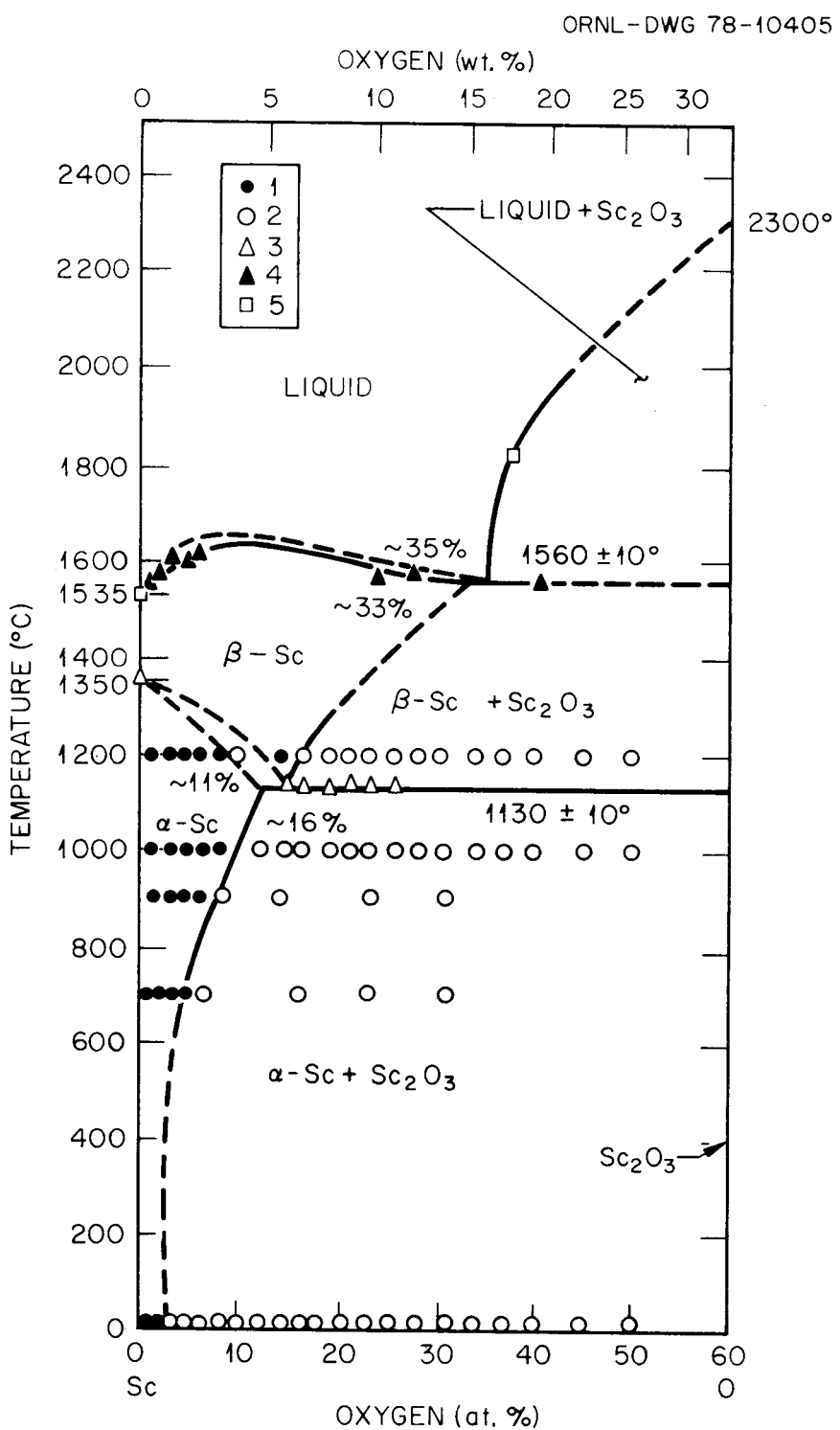


Fig. A19. The Scandium-Oxygen Phase Diagram. (1) Single-phase alloys; (2) two-phase alloys; (3) differential thermal analysis; (4) dropping thermal analysis; (5) temperature of complete melting of the sample. Based on Kuprashvili et al.<sup>60</sup>

ORNL-DWG 78-10406

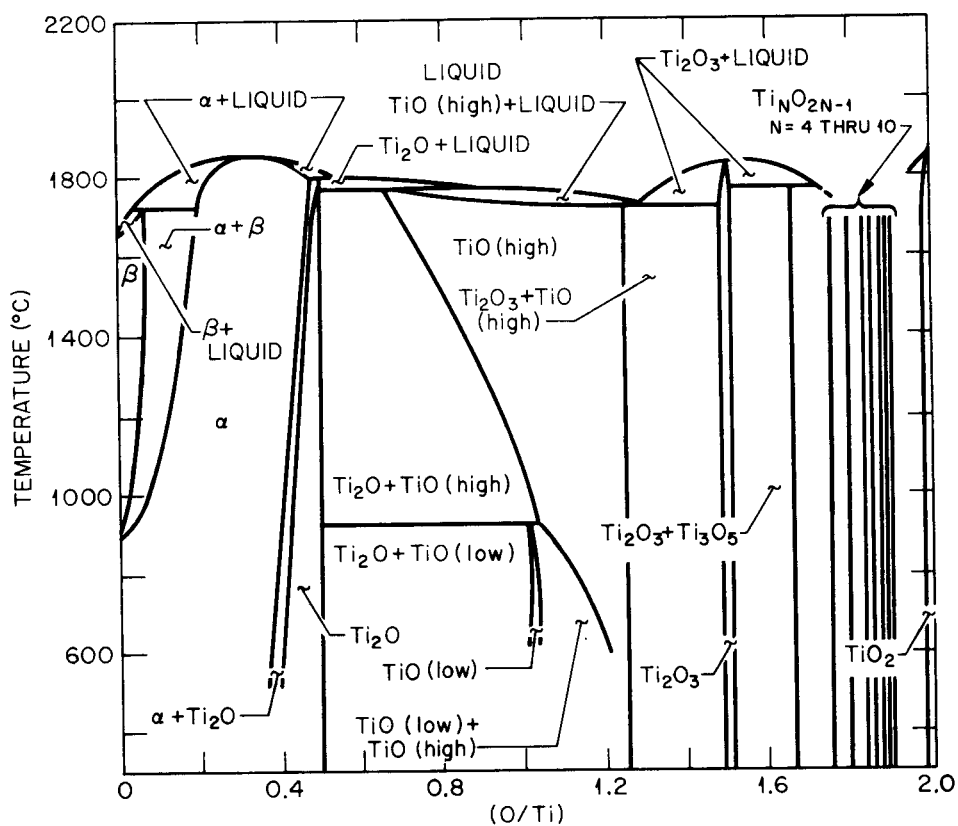


Fig. A20. The Ti-TiO<sub>2</sub> System Adapted from Wahlbeck and Gilles.<sup>65</sup>

series, show a range of solubility of oxygen. Available crystallographic data for the various compounds are summarized in Table A6.

#### Fuel-Spikant and Fuel-Decay-Product Systems

##### Ce-Pu-O System

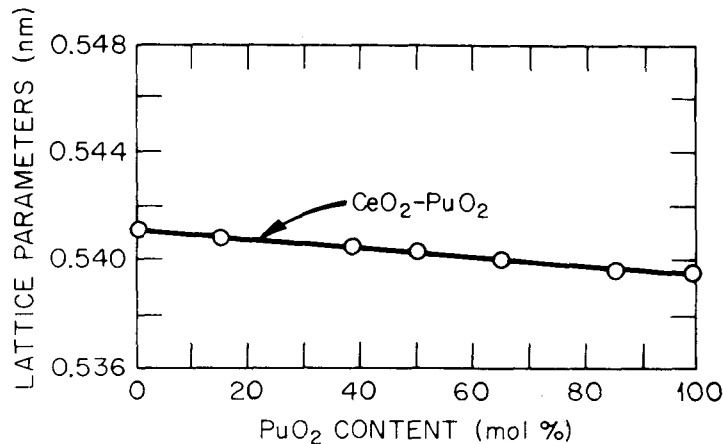
The only information found for this system is that of Mulford and Ellinger,<sup>24</sup> who found a linear relationship between lattice parameter and mole percent PuO<sub>2</sub>, indicating complete solid solubility between CeO<sub>2</sub> and PuO<sub>2</sub>. The x-ray data are given in Fig. A21. No melting point data were found.

Table A6. Crystallographic Data for the Ti-O System

Phase	System and Structure Type	Lattice Parameter, nm			Atoms/Unit Cell	Space Group
		a	b	c		
Ti <sub>3</sub> O	Hexagonal	0.51411		0.95334	16	P <sub>3</sub> 1c
Ti <sub>2</sub> O	Hexagonal	0.29593		0.48454	3	P <sub>3</sub> m <sub>1</sub>
TiO <sub>2</sub> (Anatase)	BC Tetragonal, C5	0.3777		0.9501		
(Brookite)	Orthorhombic	0.925	0.546	0.516		Pbc <sub>a</sub>
(Rutile)	Tetragonal	0.45937		0.29581		
δ	Tetragonal or Hexagonal	0.320		0.512		
Ti <sub>2</sub> O <sub>3</sub>	Rhombohedral	0.542 <sup>a</sup>				R3c
	Hexagonal parameters	0.5148		1.3636		
Ti <sub>3</sub> O <sub>5</sub>	Monoclinic (low temp.)	0.9752 <sup>b</sup>	0.38020	0.9449		
	(high temp.)	0.982 <sup>c</sup>	0.378	0.997		
TiO	fcc, NaCl(B1)	0.4174				

<sup>a</sup> $\alpha$  = 56.9°.<sup>b</sup> $\beta$  = 91.547°.<sup>c</sup> $\gamma$  = 91.0°.

ORNL-DWG 78-10408

Fig. A21. Lattice Parameter vs Mole % PuO<sub>2</sub> for the CeO<sub>2</sub>-PuO<sub>2</sub> System.<sup>34</sup>Ce-Th-O System

The CeO<sub>2</sub>-ThO<sub>2</sub> system is characterized by complete solid solubility at all compositions.<sup>66-68</sup> This is not unexpected, since the crystal structures of the two compounds are identical and the lattice parameters are similar.

For the  $\text{ThO}_2\text{-CeO}_2\text{-Ce}_2\text{O}_3$  system, conflicting reports were found. Hoch and Yoon<sup>66</sup> produced the diagram given in Fig. A22, in which a large two-phase region is shown. In the  $\text{ThO}_2\text{-CeO}_{1.5}$  system the fluorite phase extends to approximately 45 mol %  $\text{CeO}_{1.5}$ . The two phases present in the miscibility gap are a fluorite phase based on  $\text{ThO}_2$  in equilibrium with a fluorite phase based on  $\text{CeO}_2$ . On the other hand, Whitfield et al.<sup>68</sup> found that reduction of  $(\text{Th},\text{Ce})\text{O}_2$  at 700–1400°C gave a single phase  $(\text{Th},\text{Ce})\text{O}_{2-x}$  with the fluorite structure when  $x$  was less than 0.25. When  $x$  was greater than 0.25, they found extra lines, which were indexed in terms of a bcc structure.

#### Ce-U-O System

Several investigations<sup>69–71</sup> have reported that  $\text{CeO}_2$  and  $\text{UO}_2$  form a continuous series of solid solution. X-ray diffraction data indicate an approximately linear relationship between lattice parameter and composition. Deviations from linearity are rationalized in terms of deviation from stoichiometry toward an O/M ratio greater than 2.0.

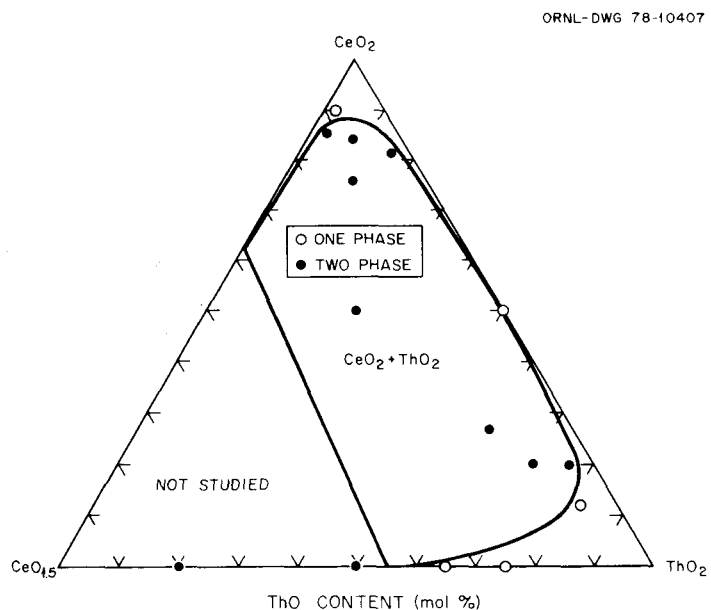


Fig. A22. Isothermal Section of the  $\text{CeO}_2\text{-ThO}_2\text{-CeO}_{1.5}$  System at 1200°C, According to Hoch and Yoon.<sup>66</sup>

Between  $\text{CeO}_2$  and  $\text{U}_3\text{O}_8$ , the fluorite structure is retained between 55 and 100 mol %  $\text{CeO}_2$ . Below 55 mol %  $\text{CeO}_2$  a two-phase structure and  $\text{U}_3\text{O}_8$  was observed. Later work<sup>38</sup> shows the solubility of  $\text{CeO}_2$  in  $\beta\text{-U}_3\text{O}_8$  to be below detectable limits. This work also indicated increasing stability of the fluorite-phase field with increasing temperature, as shown in Fig. A23.

Portions of the system between  $\text{UO}_2 + \text{U}_3\text{O}_8$  and  $\text{CeO}_2 + \text{Ce}_2\text{O}_3$  are given in Figs. A24 and A25. The diagram presented by Hoch and Furman<sup>72</sup> for 900°C is given in Fig. A24. A large single-phase field in which the fluorite phase  $\text{MO}_{2+x}$  is stable is found at 900°C. This single phase is found with both hypo- and hyperstoichiometric  $\text{MO}_2$  compositions. Other workers<sup>71,72</sup> are in general agreement with this construction. Markin et al.<sup>71</sup> presented a diagram for room temperature, 200, 400, and 600°C. They suggest that the solution of  $\text{CeO}_2$  extends the single-phase field towards hyperstoichiometric  $\text{MO}_{2+x}$  as the temperature increases. There is apparently some solubility of cerium in  $\text{U}_4\text{O}_9$ . The diagrams at 200, 400, and 600°C are given in Fig. A25. The figure is in general agreement with Fig. A24 in that both show a large single-phase field in which the fluorite phase is stable. Hoch and Furman<sup>72</sup> do not consider the compound  $\text{U}_4\text{O}_9$ , while Markin et al. do not indicate the

ORNL-DWG 78-10409

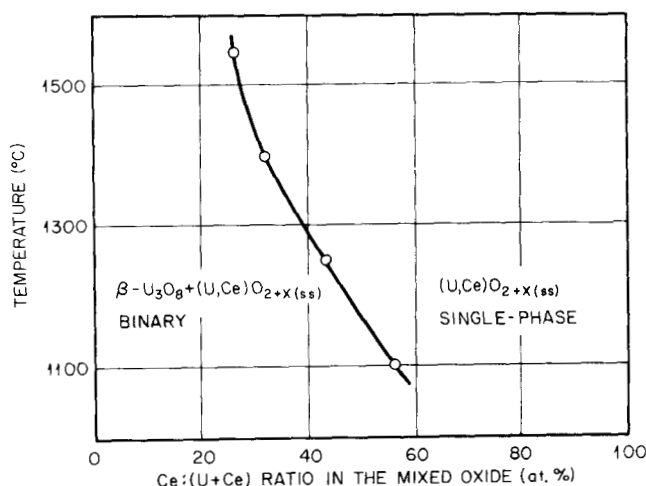


Fig. A23. Phase Diagram of the Quasibinary System  $\text{CeO}_2\text{-UO}_2 +$  (1 atm  $\text{O}_2$ ).<sup>84</sup>

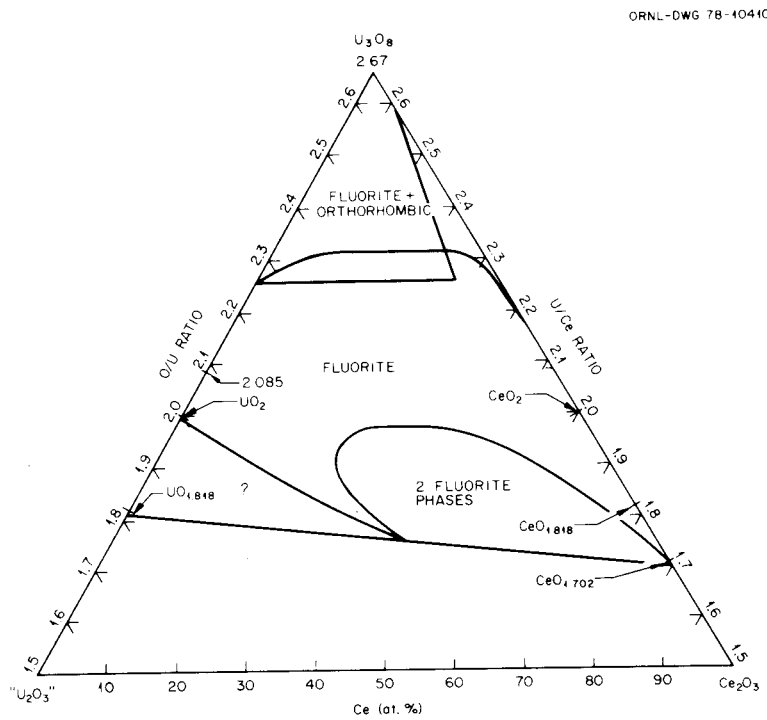


Fig. A24. The  $\text{CeO}_{1.5}\text{-}\text{UO}_{1.5}\text{-}\text{U}_3\text{O}_8$  System at  $900^\circ\text{C}$ . Based on Hoch and Furman.<sup>72</sup>

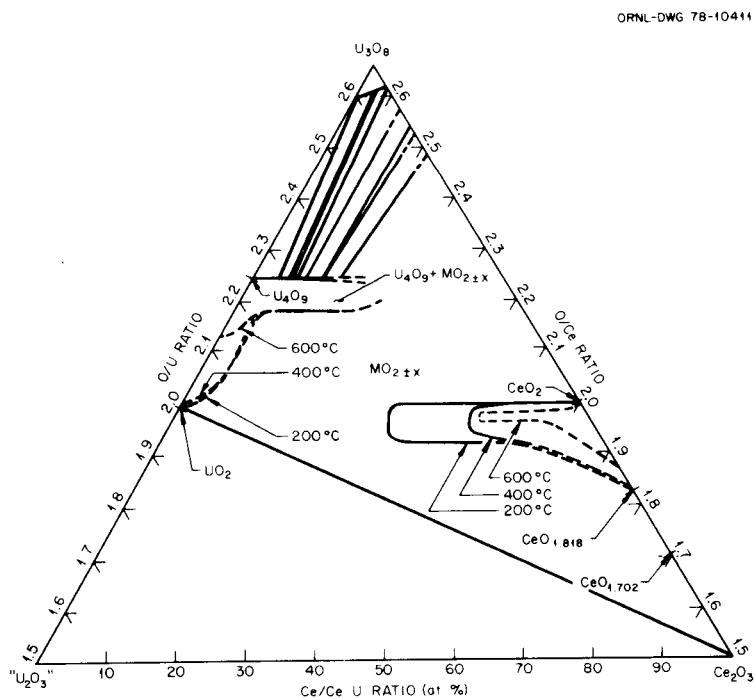


Fig. A25. The  $\text{CeO}_{1.5}\text{-}\text{UO}_{1.5}\text{-}\text{U}_3\text{O}_8$  System at 200, 400, and  $600^\circ\text{C}$ . Based on Markin et al.<sup>71</sup>

presence of the miscibility gap of two fluorite phases. Both diagrams are somewhat lacking in experimental verification. Neither work was sufficient to establish the limit of solid solubility between CeO<sub>2</sub> and U<sub>3</sub>O<sub>8</sub>.

#### Co-U-O System

The compound CoU<sub>2</sub>O<sub>6</sub> has been identified by Kemmler-Sack and Rüdorff.<sup>73</sup> It has a hexagonal structure with  $a = 0.9095$  nm and  $c = 0.4990$  nm. No data were found on the solubility of cobalt in UO<sub>2</sub>, but in view of the large difference in the size of the cations (~41%), the solubility should be very low.

#### Nd-Th-O System

In the Nd<sub>0.5</sub>-ThO<sub>2</sub> system, Keller et al.<sup>74</sup> found extensive solubility of Nd<sub>0.5</sub> in ThO<sub>2</sub> and two intermediate compounds, ThO<sub>2</sub>·3Nd<sub>0.5</sub> and ThO<sub>2</sub>·11Nd<sub>0.5</sub>, which are unstable below 1800 and 1500°C, respectively. Similarly, Sibieude and Foex<sup>75</sup> found the solubility of Nd<sub>0.5</sub> in ThO<sub>2</sub> to be about 35 mol % at 1400°C and less than 40 mol % at 2200°C. The Nd<sub>2</sub>O<sub>3</sub>-ThO<sub>2</sub> diagram according to Sibieude and Foex<sup>75</sup> in Fig. A26 shows five intermediate compounds along with some solubility of ThO<sub>2</sub> in Nd<sub>2</sub>O<sub>3</sub>.

#### Nd-U-O System

A large region of solid solubility of Nd<sub>0.5</sub> in UO<sub>2+x</sub> exists,<sup>76-78</sup> with the fcc fluorite phase extending over a large region. The UO<sub>2</sub>-UO<sub>3</sub>-Nd<sub>0.5</sub> ternary system<sup>76</sup> at 1250°C is given in Fig. A27. The work of Wadier et al.<sup>78</sup> is in basic agreement with Fig. A27, with minor displacements of some of the phase field boundaries.

Four single-phase fields exist in this system, and crystallographic data for these phases are summarized in Table A7. With the exception of UO<sub>2</sub>, the solubility of Nd<sub>0.5</sub> in these phases is negligible. There is no solubility of uranium in Nd<sub>0.5</sub>. A rhombohedral phase exists

ORNL-DWG 78-10412

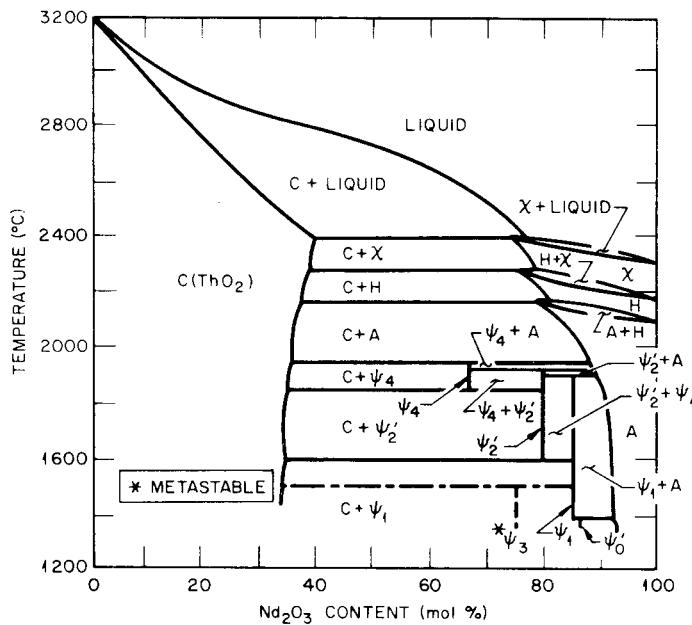


Fig. A26. Tentative Phase Diagram for the ThO<sub>2</sub>-Nd<sub>2</sub>O<sub>3</sub> System According to Sibieude and Foex.<sup>75</sup>

ORNL-DWG 78-10413

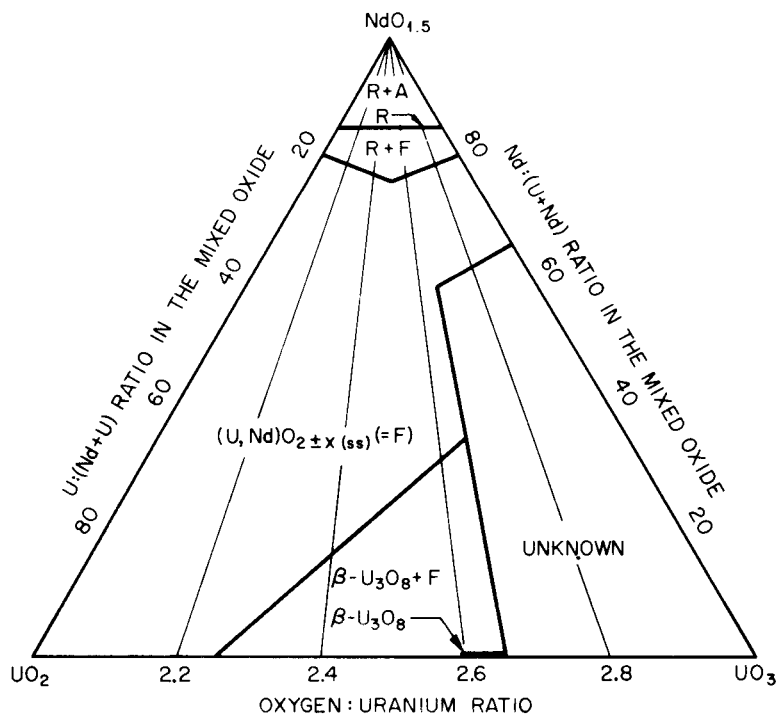


Fig. A27. The Ternary System UO<sub>2</sub>-UO<sub>3</sub>-NdO<sub>1.5</sub> at 1250°C, Based on Boroujerdi.<sup>76</sup>

Table A7. Crystallographic Data for Compounds in  
the UO<sub>2</sub>-UO<sub>3</sub>-NdO<sub>1.5</sub> System

Phase	Structure	Lattice Parameters, nm			Remarks
		<i>a</i>	<i>b</i>	<i>c</i>	
β-U <sub>3</sub> O <sub>8</sub>	Orthorhombic	0.6725	0.3967	0.4145	<i>T</i> = 1250°C
UO <sub>2</sub>	Cubic (Fluorite)	0.5470			
UO <sub>3</sub> •6NdO <sub>1.5</sub>	Rhombohedral	0.6743 1.0254 <sup>α</sup>		0.9760 <sup>α</sup>	<i>α</i> = 98.75°C
NdO <sub>1.5</sub>	Hexagonal	0.3823		0.5996	<i>T</i> = 1100°C

<sup>α</sup>Indexed as hexagonal.

between UO<sub>2</sub>•6NdO<sub>1.5</sub> and UO<sub>3</sub>•6NdO<sub>1.5</sub> with no range of solubility of neodymium. No other phases, such as the ordered phases found in analogous systems with lanthanide oxides, could be found. Rudorff et al.<sup>79</sup> claim to have found a compound with the fluorite structure, NdUO<sub>4</sub>, with a lattice parameter of 0.5445 nm. However, it appears that this phase is not a separate compound, but is merely a single-phase solid solution of the type (U,Nd)O<sub>2+x</sub>.

#### Ni-U-O System

Two compounds have been identified in this system: NiU<sub>2</sub>O<sub>6</sub> has a hexagonal structure<sup>73</sup> with *a* = 0.901 nm and *c* = 0.501 nm and NiU<sub>3</sub>O<sub>10</sub>.<sup>80</sup> No solubility or melting point data were found.

#### Pr-Th-O System

The only information found for this system indicates complete solid solubility between ThO<sub>2</sub> and both PrO<sub>1.83</sub> and PrO<sub>2</sub>, as indicated by

the x-ray data<sup>81</sup> of Fig. A28. A very tentative phase diagram<sup>81</sup> for the ThO<sub>2</sub>-PrO<sub>2</sub>-PrO<sub>1.5</sub> system in Fig. A29 suggests a very large single-phase region. The solid solution would have the fcc fluorite structure. The limit of the miscibility gap in the PrO<sub>2</sub>-PrO<sub>1.5</sub> system is only conjectural.

#### Sc-Pu-O System

Only one reference to this system was found.<sup>82</sup> The solubility of ScO<sub>1.5</sub> in PuO<sub>2</sub> is relatively small, although it is slightly greater in the substoichiometric oxide than in the stoichiometric oxide. Table A8 summarizes the available data. No data are available on the solubility of PuO<sub>2</sub> in ScO<sub>1.5</sub>. No intermediate compounds are reported, although information is sketchy.

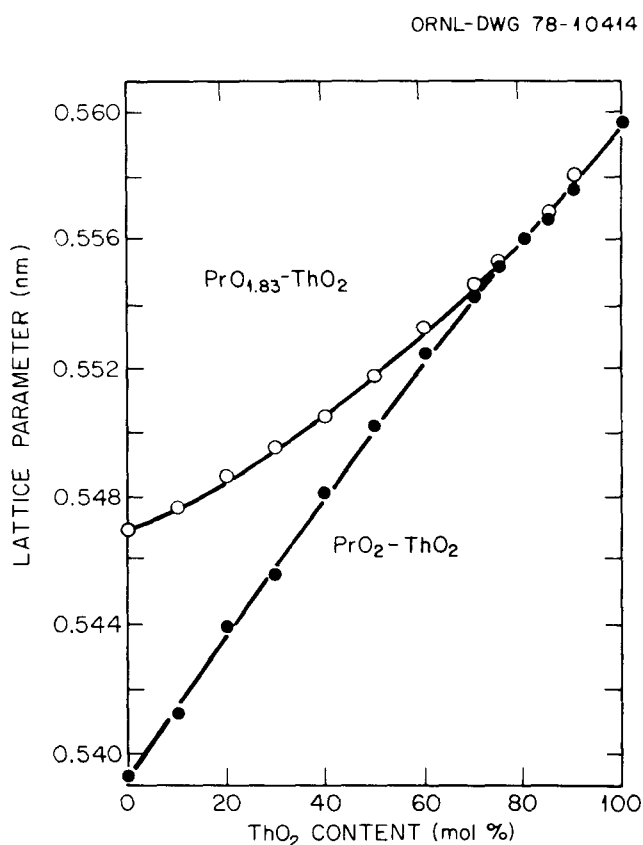


Fig. A28. Lattice Parameters in the PrO<sub>2</sub>-ThO<sub>2</sub> and PrO<sub>1.83</sub>-ThO<sub>2</sub> Systems, Based on Brauer and Willaredt.<sup>81</sup>

ORNL-DWG 78-10415

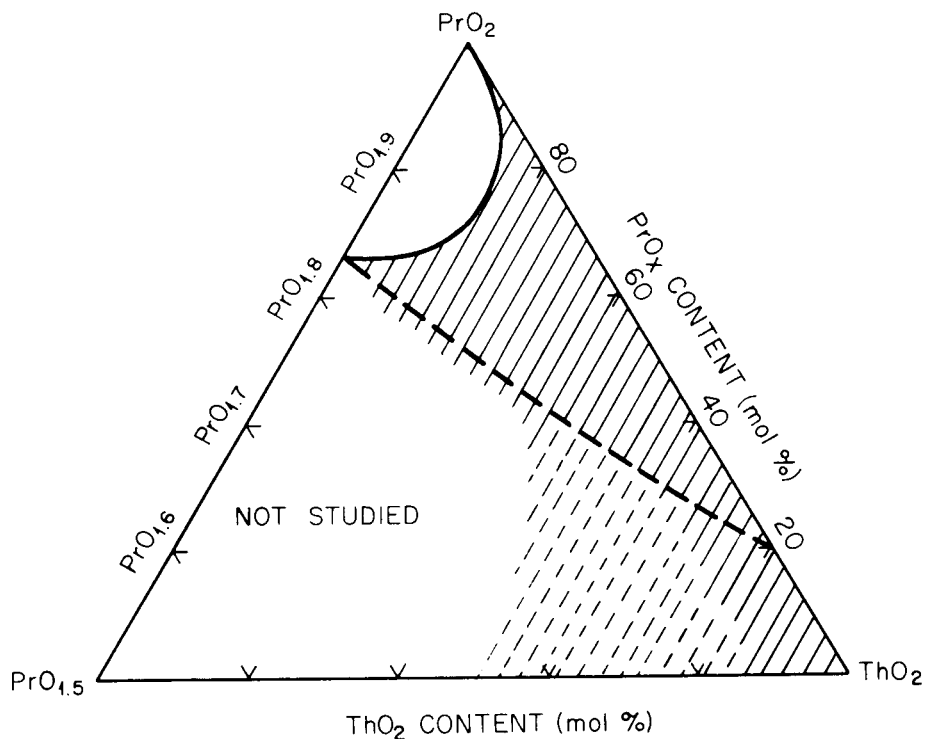


Fig. A29. Tentative Phase Diagram of the Ternary System  $\text{ThO}_2\text{-}\text{PrO}_2\text{-}\text{PrO}_{1.5}$ , Based on Brauer and Willaredt.<sup>81</sup>

Table A8. Solubility of  $\text{ScO}_{1.5}$  in Actinide Oxides

Temperature (°C)	Solubility (mol % $\pm$ 0.1–0.2)			
	$\text{PuO}_{2.0}$	$\text{PuO}_{2-x}$	$\text{ThO}_2$	$\text{UO}_2$
1100	0.5	0.8	0.4	1.6
1250	1.2	1.0		1.8
1400	1.4	1.8		2.1
1500			0.6	
1550	2.4	4.2		2.9
1750			0.9	
1900			1.2	
2100			1.5	

Sc-Th-O System

Data for this system are limited,<sup>82</sup> but the solubility of Sc<sub>0.5</sub> in ThO<sub>2</sub> is known to be low, as summarized in Table A8, and a partial phase diagram is given in Fig. A30. There appears to be no solubility of ThO<sub>2</sub> in Sc<sub>0.5</sub> and no intermediate compounds in the system. No liquidus or solidus data are available.

Sc-U-O System

Phase relationships for the UO<sub>2</sub>-UO<sub>2.67</sub>-Sc<sub>0.5</sub> system are given in Fig. A31, which is taken from the work of Keller et al.<sup>82</sup> The solubility of Sc<sub>0.5</sub> in stoichiometric UO<sub>2</sub> is given in Table A8 and is seen to be low. However, as indicated in Fig. A31, the solubility in hyper-stoichiometric UO<sub>2+x</sub> increases considerably. This result is also confirmed by Trzebiatowski and Roman.<sup>83</sup> No solubility of Sc<sub>0.5</sub> was found in β-U<sub>3</sub>O<sub>8</sub>, nor was any solubility of UO<sub>2</sub> in Sc<sub>0.5</sub> found, within the limits of detection (0.1 mol %).

The partial quasi-binary system UO<sub>2.67</sub>-Sc<sub>0.5</sub> system is shown in Fig. A32 for P<sub>O<sub>2</sub></sub> = 0.10 MPa (1 atm) and 21 kPa (0.21 atm) (air). Under air, the single-phase field for the fluorite structure is displaced toward the UO<sub>2.67</sub> end of the diagram, compared with the case for an oxygen atmosphere, although the width of the phase field changes only slightly.

Rüdorff et al.<sup>79</sup> report the successful preparation of a compound with the fluorite structure, ScUO<sub>4</sub>, but this "compound" is probably actually (U,Sc)<sub>0.2+x</sub> and not a separate compound. No other intermediate compounds were found in this system.

Ti-Pu-O System

Very little work has been done on this system. An unsuccessful attempt was made<sup>84</sup> to produce the compound PuTi<sub>2</sub>O<sub>6</sub>. X-ray patterns revealed lines for cubic PuO<sub>2</sub>. It is unclear whether any lattice parameter change occurred to suggest solubility of TiO<sub>2</sub> in PuO<sub>2</sub>.

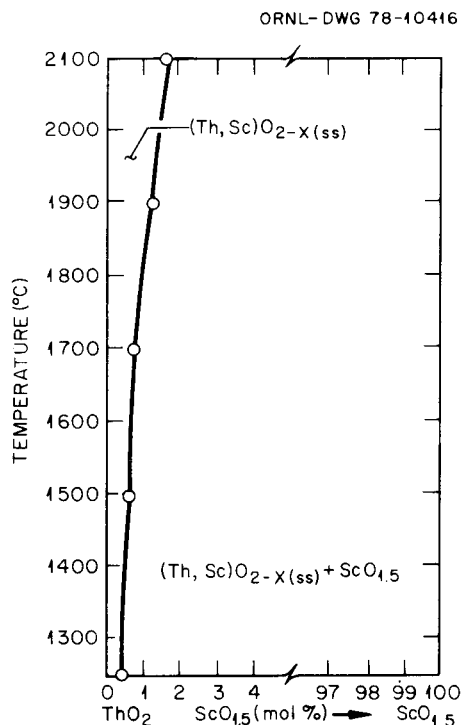


Fig. A30. Partial Phase Diagram of the  $\text{ScO}_{1.5}$ - $\text{ThO}_2$  System Between 1250 and 2100°C. Based on Keller et al.<sup>82</sup>

ORNL-DWG 78-10417

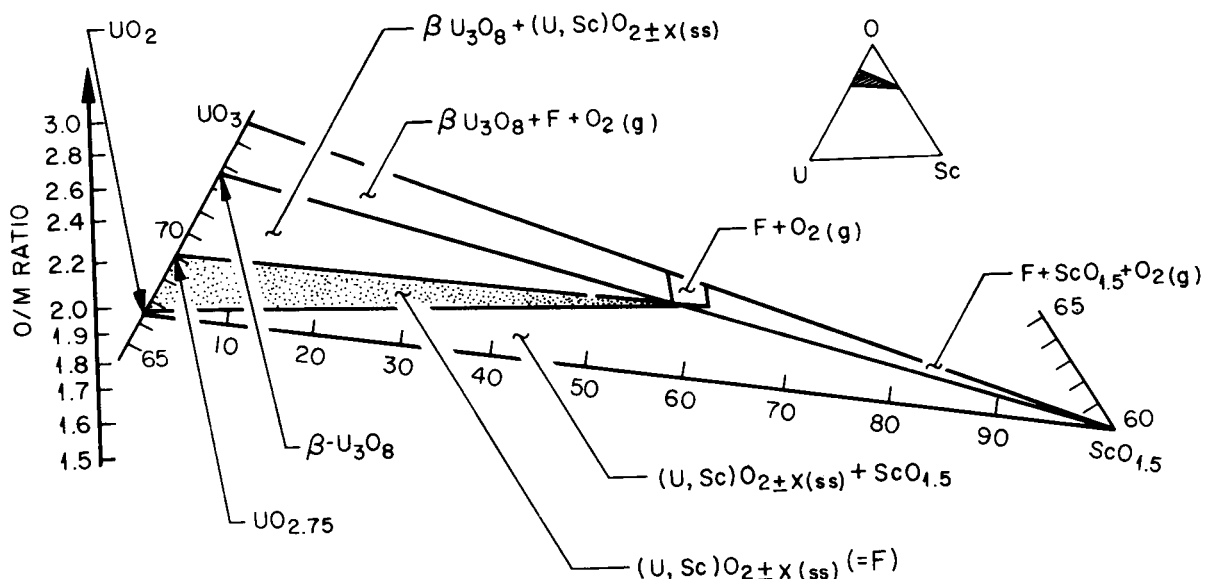


Fig. A31. The Ternary System  $\text{ScO}_{1.5}$ - $\text{UO}_2$ - $\text{UO}_3$  at 1250°C. According to Keller et al.<sup>82</sup>

ORNL-DWG 78-10418

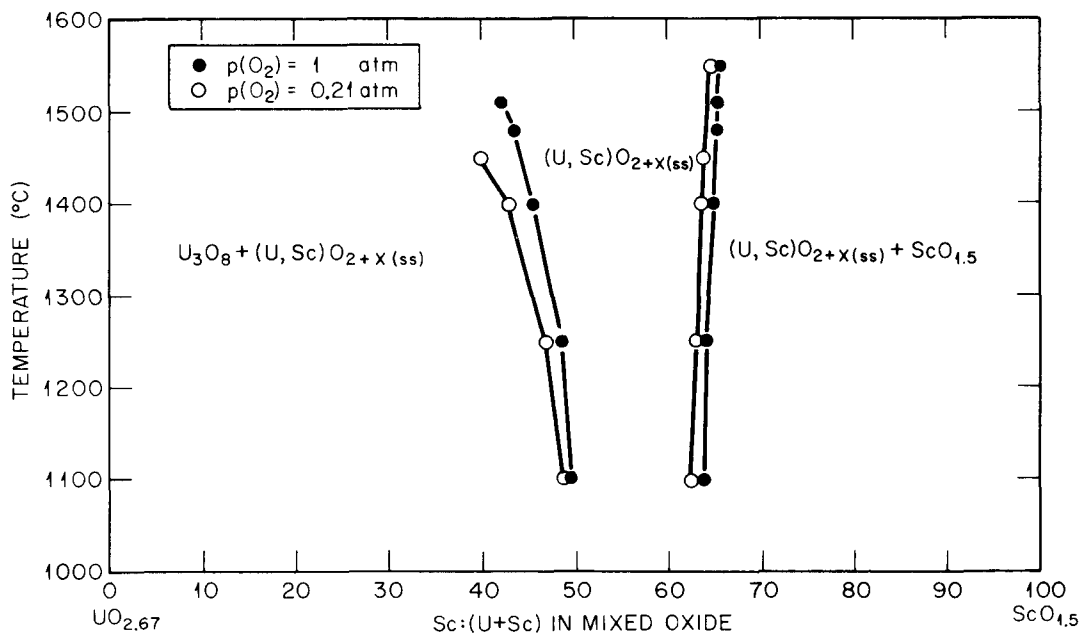


Fig. A32. The Quasi-Binary System Sc<sub>0.1.5</sub>-UO<sub>2.67</sub> at  $P(O_2) = 0.10$  MPa and 21 kPa [1.0 and 0.21 atm. (air)].

#### Ti-Th-O System

The compound ThTi<sub>2</sub>O<sub>6</sub> was found to have two modifications.<sup>85</sup> The  $\alpha$  phase is stable below 1300°C and is orthorhombic with lattice parameters  $a = 1.67$  nm,  $b = 1.495$  nm,  $c = 0.41$  nm. The beta phase is stable above 1300°C, with a tetragonal structure and lattice parameters  $a = 0.758$  nm; and  $c = 1.045$  nm. However, Radzewitz<sup>84</sup> suggests a lower symmetry for  $\beta$ -ThTi<sub>2</sub>O<sub>6</sub> and classifies it as monoclinic, isostructural with UTi<sub>2</sub>O<sub>6</sub>. Lattice parameters are:  $a = 0.989$  nm;  $b = 0.383$  nm;  $c = 0.710$  nm; and  $\beta = 119^\circ 30'$ .

#### Ti-U-O System

At least three compounds are known in this system. Several investigators<sup>80,86</sup> have reported the existence of UTi<sub>5</sub>. This compound appears to have a close structural relationship with  $\alpha$ -Nb<sub>2</sub>O<sub>5</sub>. It has a monoclinic structure (pseudo-hexagonal) with pseudo cell dimensions of  $a = 0.370$  nm and  $c = 0.390$  nm. Marshall and Hoekstra<sup>86</sup>

found that  $UTi_3O_8$  has also been reported.<sup>87</sup> The third compound,<sup>84</sup>  $UTi_2O_6$ , has a monoclinic structure with  $a = 0.979$  nm;  $b = 0.377$  nm;  $c = 0.691$  nm, and  $\beta = 118^\circ 50'$ . A reference was found<sup>86</sup> that indicates that  $TiO_2$  (or lower oxide) is soluble in  $UO_2$ , but no limits were specified.

#### REFERENCES

1. M. H. Rand et al., "The Plutonium-Oxygen and Uranium-Plutonium-Oxygen Systems: A Thermochemical Assessment," *Report of a Panel on Thermo-dynamics of Plutonium Oxides* (held in Vienna, 24-28, October 1966) IAEA Technical Reports Series 79, International Atomic Energy Agency, Vienna, 1967.
2. E. R. Gardner, T. L. Markin, and R. S. Street, "The Plutonium-Oxygen Phase Diagram," *J. Inorg. Nucl. Chem.* 27: 541-51 (1965).
3. H. Blank, *A Comparison of the Pu-O System with the Rare Earth Oxide Systems Ce-O, Pr-O and Tb-O*, EUR-3563 (1967).
4. C. Sari, U. Benedict, and H. Blank, *A Metallographic and X-ray Investigation of Plutonium Oxides at Room Temperature*, EUR-3564 (1967).
5. T. D. Chikalla, C. E. McNeilly, and R. E. Skavdahl, "The Plutonium-Oxygen System," *J. Nucl. Mater.* 12(2): 131-41 (1964).
6. R.N.R. Mulford, F. H. Ellinger, and K. A. Johnson, "The Plutonium-Oxygen System," *J. Nucl. Mater.* 17: 324-29 (1965).
7. F. Anselin et al., "On the System (UPu) (CNO) as Applied to Sintered Carbides Carbonitrides and Oxycarbides," pp. 113-61 in *Carbides in Nuclear Energy*, ed. by L. E. Russell et al., London, 1964.
8. R. Benz, "Thorium-Thorium Dioxide Phase Equilibria," *J. Nucl. Mater.* 29: 43-49 (1969).
9. W. H. Zachariason, "Crystal Chemical Studies of the 5f-Series of Elements. XVI. Identification and Crystal Structure of Protactinium Monoxide," *Acta Crystallogr.* 5: 9-11 (1952).
10. R. E. Rundle, "A New Interpretation of Interstitial Compounds - Metallic Carbides, Nitrides and Oxides of Composition MX," *Acta Crystallogr.* 1: 180-87 (1948).

11. R. J. Ackerman et al., "A Thermodynamic Study of the Thorium-Oxygen System at High Temperatures," *J. Phys. Chem.* 67: 762-69 (1963).
12. H. E. Swanson and E. Tatge, *Standard X-ray Diffraction Powder Patterns*, Natl. Bur. Stand. (U.S.) Circ. 539 1: 57-58 (1953).
13. S. Abramowitz, *The Thermodynamics of the Thorium-Oxygen and Uranium-Oxygen Systems - Final Report*, 14 June 1973-30 June 1974 AD/A-008438 (1974).
14. L. Brewer, "The Thermodynamic Properties of the Oxides and Their Vaporization Processes," *Chem. Rev.* 52: 1-75 (1953).
15. L. Eyring, "Lanthanide and Actinide Oxides: A Case Study in Solid State Chemistry," pp. 565-634 in *Solid State Chemistry*, ed. by C.N.R. Rao, Marcel Dekker, New York, 1974.
16. R. E. Latta and R. E. Fryxell, "Determination of Solidus-Liquidus Temperatures in the  $UO_2+x$  System ( $-0.50 < x < 0.20$ )," *J. Nucl. Mater.* 35: 195-210 (1970).
17. R. K. Edwards and A. E. Martin, "Phase Relations in the Uranium-Uranium Dioxide System at High Temperatures," pp. 423-29 in *Thermodynamics - Proceedings of the Symposium on Thermodynamics with Emphasis on Nuclear Materials and Atomic Transport in Solids*, Vol. 2, International Atomic Energy Agency, Vienna, 1966.
18. L.E.J. Roberts and A. J. Walter, "Equilibrium Pressures and Phase Relations in the Uranium Oxide System," *J. Inorg. Nucl. Chem.* 22: 213-29 (1961).
19. A. Kotlar, P. Gerdanian, and M. Dode, "Determination des Limites de Phases du Systeme U-O Par 'Transfert L'Oxygene.' — Diagramme de Phase Pour la Region  $2.19 < O/U < 2.63$  et  $1080 < \theta^\circ C < 1200^\circ C$ ," *J. Chim. Phys.* 64: 687-91 (1968).
20. H. R. Hoekstra, S. Siegel, and F. X. Gallagher, "The Uranium-Oxygen System at High Pressure," *J. Inorg. Nucl. Chem.* 32: 3237-48 (1970).
21. M. H. Rand and L.E.J. Roberts, "Thermochemistry and Nuclear Engineering," pp. 3-31 in *Thermodynamics - Proceedings of the Symposium on Thermodynamics with Emphasis on Nuclear Materials and Atomic Transport in Solids* Vol. 1, International Atomic Energy Agency, Vienna, 1966.

22. J. J. Kozhina and L. V. Shiryaeva, "Phase Diagram of Uranium-Oxygen in the Region of Compositions from  $UO_2.25$  to  $UO_2.67$ ," *Radiokhimiya* 16: 360-63 (1974).
23. M. D. Freshly and H. M. Mattys, "Properties of Sintered  $ThO_2-PuO_2$ ," *Ceramics Research and Development Operation Quarterly Report October-December 1962*, HW-76559, pp. 11.6-11.9.
24. R. N. R. Mulford and F. H. Ellinger, "Th<sub>2</sub>O<sub>3</sub>-PuO<sub>2</sub> and Ce<sub>2</sub>O<sub>3</sub>-PuO<sub>2</sub> Solid Solutions," *J. Phys. Chem.* 62: 1466-67 (1958).
25. W. L. Lyon and W. E. Baily, "The Solid-Liquid Phase Diagram for the UO<sub>2</sub>-PuO<sub>2</sub> System," *J. Nucl. Mater.* 22: 332-39 (1967).
26. T. L. Markin and R. S. Street, "The Uranium-Plutonium-Oxygen Ternary Phase Diagram," *J. Inorg. Nucl. Chem.* 29: 2265-80 (1967).
27. T. D. Chikalla, "Melting Behavior in the System UO<sub>2</sub>-PuO<sub>2</sub>," *J. Am. Ceram. Soc.* 46(7): 323-28 (1963).
28. C. Sari, U. Benedict, and H. Blank, "A Study of the Ternary System UO<sub>2</sub>-PuO<sub>2</sub>-Pu<sub>2</sub>O<sub>3</sub>," *J. Nucl. Mater.* 35: 267-77 (1970).
29. M. Koizumi and Y. Nakamura, "Phase Studies and Fuel Performance in the System Pu-U-O," *Tokai Works Semiannual Progress Report, July-December 1969* NP-18353 (April 1970), pp. 10-16.
30. Y. Nakayama, "A Phase Study on the Line of U<sub>3</sub>O<sub>7</sub>-PuO<sub>2</sub>," *J. Inorg. Nucl. Chem.* 33: 4077-84 (1971).
31. G. Dean et al., "Contribution to the Study of the U-Pu-O System," pp. 753-61 in *Proceedings 4th Conf. Plutonium and Other Actinides*, American Institute of Mining, Metallurgical, and Petroleum Engineering, New York, 1970.
32. S. Fukushima et al., "Three Phase Region in Ternary System UO<sub>2</sub>-PuO<sub>2</sub>-Pu<sub>2</sub>O<sub>3</sub>," *J. Nucl. Sci. Technol.*, 8(9): 534-35 (1971).
33. W. A. Lambertson, M. H. Mueller, and F. H. Gunzel, Jr., "Uranium Oxide Phase Equilibrium Systems: IV, UO<sub>2</sub>," *J. Am. Ceram. Soc.* 36(12): 397-99 (1953).
34. F. A. Mumpton and R. Roy, "Low-Temperature Equilibria among ZrO<sub>2</sub>, ThO<sub>2</sub>, and Zr<sub>2</sub>O<sub>3</sub>," *J. Am. Ceram. Soc.*, 43(5): 234-40 (1960).
35. J. A. Christensen, "UO<sub>2</sub>-ThO<sub>2</sub> Phase Studies," *Ceramics Research and Development Operation Quarterly Report October-December 1962*, HW-76559, (December 1962) pp. 11.5-11.6.

36. E. Slowinski and N. Elliott, "Lattice Constants and Magnetic Susceptibilities of Solid Solutions of Uranium and Thorium Dioxide," *Acta Crystallogr.*, 5: 768-70 (1952).
37. R. E. Latta, E. C. Duderstadt, and R. E. Fryxell, "Solidus and Liquidus Temperatures in the  $UO_2$ - $ThO_2$  System," *J. Nucl. Mater.* 35: 347-49 (1970).
38. R. Paul, *Phase Equilibria in the Systems  $ThO_2$ - $UO_2$ ,  $CeO_2$ - $UO_{2+x}$  and  $NpO_2$ - $UO_2$* , KFK-1297 (October 1970); translation available as ORNL/tr-2483.
39. R. Paul and C. Keller, "Phasengleichgewichte in den Systemen  $UO_2$ - $UO_{2.67}$ - $ThO_2$  und  $UO_{2+}$ - $NpO_2$ ," *J. Nucl. Mater.* 41: 133-42 (1971).
40. I. Cohen and R. M. Berman, "A Metallographic and X-Ray Study of the Limits of Oxygen Solubility in the  $UO_2$ - $ThO_2$  System," *J. Nucl. Mater.* 18: 77-107 (1966).
41. H. A. Friedman and R. E. Thoma, "Phase Equilibrium Studies in the System  $UO_2$ - $ThO_2$ - $O_2$ ," *Reactor Chemistry Division Annu. Prog. Rep. Jan. 31, 1963*, ORNL-3417, pp. 130-34.
42. V. V. Rachev et al., "A New Compound  $Th_2U_2O_9$ ," *Izv. Akad. Nauk SSSR Neorg. Mater.* 4(3): 475-76 (1968); *Inorg. Mater. (Engl. Trans.)* 4: 408-09 (1968).
43. E. D. Lynch, *Studies of Stoichiometric and Hyperstoichiometric Solid Solutions in the Thoria-Urania System*, ANL-6894 (December 1965).
44. R. Braun, S. Kemmler-Sack, and W. Rüdorff, "Spectroscopic Studies of the  $(U_{0.5}Th_{0.5})O_{2.25}$ - $ThO_2$  and  $UO_{2.25}$ - $ThO_2$  Systems," *Z. Naturforsch.* 25b: 424-26 (1970).
45. K. D. Reeve, *The Stability of Fissile-Fertile Oxide Solid Solutions in Air*, AAEC/TM-352 (October 1966).
46. D.J.M. Bevan and J. Kordis, "Mixed Oxides of the Type  $MO_2$  (Fluorite)- $M_2O_3$ -I. Oxygen Dissociation Pressures and Phase Relationships in the System  $CeO_2$ - $Ce_2O_3$  at High Temperatures," *J. Inorg. Nucl. Chem.* 26: 1509-23 (1964).
47. S. P. Ray and D. E. Cox, "Neutron Diffraction Determination of the Crystal Structure of  $Ce_7O_{12}$ ," *J. Solid State Chem.* 15: 333-43 (1975).

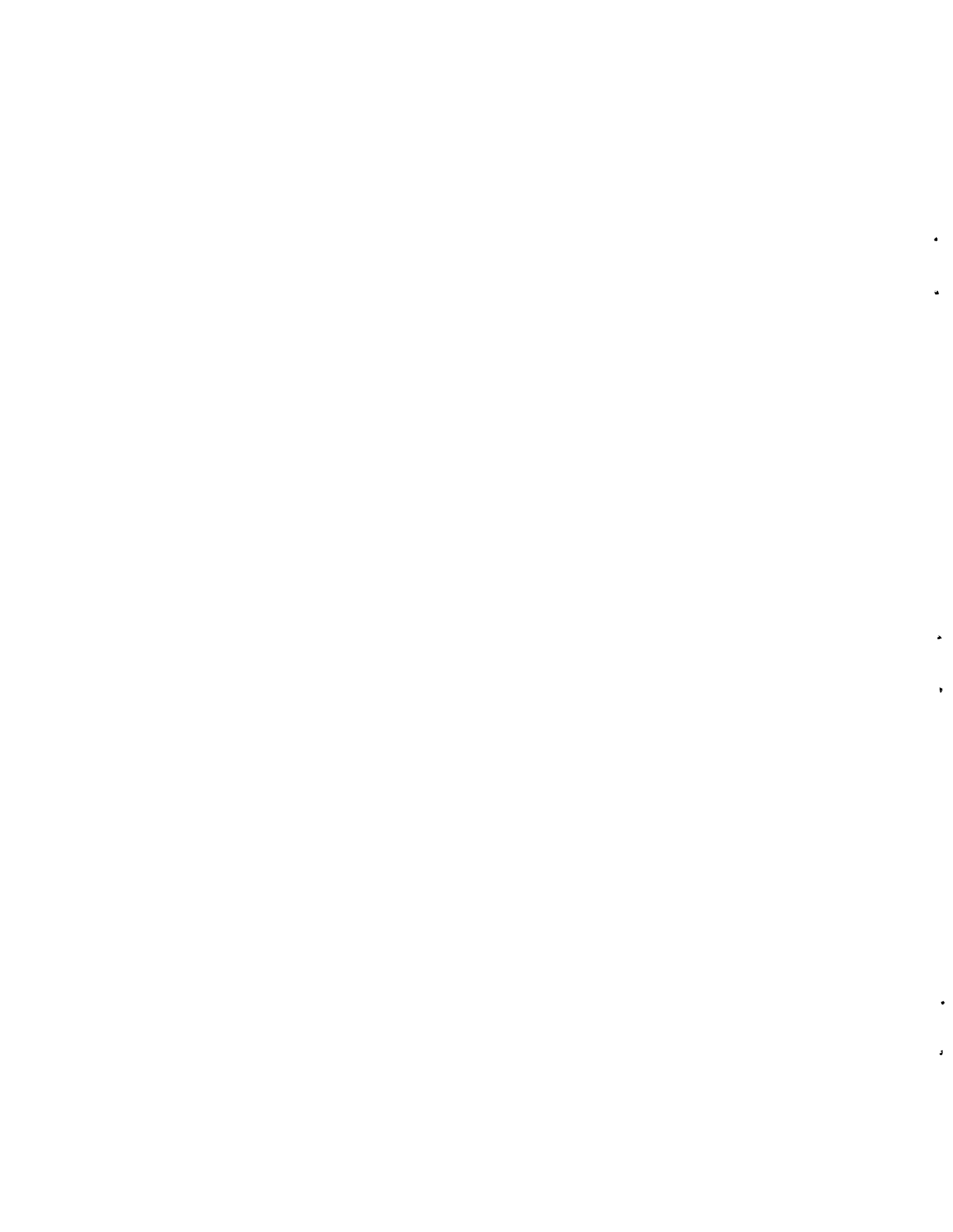
48. S. P. Ray, A. S. Nowick, and D. E. Cox, "X-Ray and Neutron Diffraction Study of Intermediate Phases in Nonstoichiometric Cerium Dioxide," *J. Solid State Chem.* 15: 344-51 (1975).
49. D.J.M. Bevan, "Ordered Intermediate Phases in the System CeO<sub>2</sub>-Ce<sub>2</sub>O<sub>3</sub>," *J. Inorg. Nucl. Chem.* 1: 49-59 (1955).
50. G. Brauer and K. A. Gingerich, "Uber die Oxyd des Cers - V. Hochtemperatur-Rontgenuntersuchungen an Ceroxyden," *J. Inorg. Nucl. Chem.* 16: 87-99 (1960).
51. R. J. Panlener, R. N Blumenthal, and J. E. Garner, "A Thermodynamic Study of Nonstoichiometric Cerium Dioxide," *J. Phys. Chem. Solids* 36: 1213-22 (1975).
52. G. Brauer and K. Gingerich, "The Influence of Temperature on the Cerium Oxide System, CeO<sub>2</sub>-Ce<sub>2</sub>O<sub>3</sub>," pp. 96-104 in *Rare Earth Research*, ed. by E. V. Kleber, Macmillan, New York, 1961.
53. B. G. Hyde and L. Eyring, "On Phase Equilibria and Phase Reactions in TbO-O<sub>2</sub> and Related Systems," pp. 623-64, in *Proceedings of the Fourth Conference on Rare Earth Research*, ed by L. Eyring, Gordon and Breach, New York, 1965.
54. R. J. Ackerman and E. G. Rauh, "A High Temperature Study of the Stoichiometry, Phase Behavior, Vaporization Characteristics, and Thermodynamic Properties of the Cerium + Oxygen System," *J. Chem. Thermodyn.* 3: 609-24 (1971).
55. L. Eyring, "Lanthanide and Actinide Oxides: A Case Study in Solid State Chemistry," pp. 565-634 in *Solid State Chemistry*, ed. by C.N.R. Rao, Marcel Dekker, New York, 1974.
56. B. Love, "An Investigation of Neodymium Oxides by Electron Diffraction," *Properties of Yttrium and the Rare Earth Metals Oxygen and Alloy Systems*, WADD-TR-61-123 (1961), pp. 34-40.
57. M. S. Beletskii and M. I. Erusalimski, *Dokl. Akad. Nauk SSSR* 133: 355-58 (1960); *Dokl. Chem. (Engl. Transl.)* 133: 771-75 (1960).
58. F. A. Shunk, *Constitution of Binary Alloys - Second Supplement*, McGraw Hill, New York, 1969.
59. B. G. Hyde, D.J.M. Bevan, and L. Eyring, private communication 1965, referenced in: E. M. Levin, C. R. Robbins, and H. F.

- McMurdie Phase Diagram for Ceramists - 1969 Supplement, American Ceramic Society, Columbus, Ohio, 1969.
60. I. S. Kuprashvili, O. P. Naumkin, and E. M. Savitskii, "The Scandium-Oxygen Phase Diagram," *Izv. Akad. Nauk SSSR Neorg. Mater.* 5: 2123-27 (December 1969).
  61. H. E. Swanson, R. K. Fuyat, and G. M. Ugrinic, *Standard X-ray Diffraction Powder Patterns, Natl. Bur. Std. (U.S.) Circ.* 539, 3: 27 (1954).
  62. S. G. Tresvyatskii, L. M. Lopato, and Z. A. Yaremenko, "The Phase Diagram of the System  $\text{Sc}_2\text{O}_3-\text{MgO}$ ," *Poroshk. Metall.* 4(1): 29-33 (1964); *Sov. Powder Metall. Met. Ceram. (Engl. Transl.)*, 1964 (1), 22-25.
  63. V. N. Fedosov, V. A. Liopo, and A. P. Nadolskii, "Studying Scandium Oxide Structure at Different Temperatures," *Izv. Vyssh. Uchebn. Zaved. Tsvetn. Metall.*, 7(3) 131-32 (1964).
  64. N. A. Toropov and V. A. Vasileva, "Synthetic Scandium Silicates," *Kristallografiya*, 6: 968-72 (1961); *Soviet Phys.-Crystallogr.* 6: 779-83 (1962).
  65. P. G. Wahlbeck and P. W. Gilles, "Reinvestigation of the Phase Diagram for the System Titanium-Oxygen," *J. Am. Ceram. Soc.* 49(4): 180-83 (1966).
  66. M. Hoch and H. S. Yoon, "Non-Stoichiometry in  $\text{CeO}_{2-x}$ " pp. 665-75, in *Proceedings of the Fourth Conference on Rare Earth Research*, ed. by L. Eyring, Gordon and Breach, New York, 1965.
  67. M. Murabayashi, "Thermal Conductivity of Ceramic Solid Solutions," *J. Nucl. Sci. Technol.* 7(11): 559-63 (1970).
  68. H. J. Whitfield, D. Roman, and A. R. Palmer, "X-Ray Study of the System  $\text{ThO}_2-\text{CeO}_2-\text{Ce}_2\text{O}_3$ ," *J. Inorg. Nucl. Chem.* 28: 2817-25 (1966).
  69. W. Rüdorff and G. Valet, "Über das Ceruranblau und Mischkristalle in System  $\text{CeO}_2-\text{UO}_2-\text{U}_3\text{O}_8$ ," *Z. Anorg. Allg. Chem.* 271: 257-72 (1953).
  70. A. Magneli and L. Kihlborg, "On the Cerium Dioxide-Uranium Dioxide System and 'Uranium Cerium Blue,'" *Acta Chem. Scand.* 5: 578-80 (1951).

71. T. L. Markin, R. S. Street, and E. C. Crouch, "The Uranium-Cerium-Oxygen Ternary Phase Diagram," *J. Inorg. Nucl. Chem.* 32: 59-75 (1970).
72. M. Hoch and F. J. Furman, "Non-Stoichiometry of  $UO_2$ -CeO<sub>2</sub>; The System  $UO_2$ -CeO<sub>2</sub>-CeO<sub>1.5</sub> at 900 to 1200 °C," pp. 517-32 in *Thermodynamics - Proceedings of the Symposium on Thermodynamics with Emphasis on Nuclear Materials and Atomic Transport in Solids*, Vol 2 International Atomic Energy Agency, Vienna, 1966.
73. S. Kemmler-Sack and W. Rüdorff, "Ternary Oxides. VII - Ternary Uranium(V) Oxides with Single and Divalent Cations," *Z. Anorg. Allg. Chem.* 354: 255-72 (1967).
74. C. Keller et al., "Phase Equilibria in the Systems Thorium Oxide-Lanthanum Oxide," *J. Solid State Chem.* 4: 453-65 (1972).
75. F. Sibieude and M. Foex, "Phases and Phase Transitions at High Temperature Observed in the  $ThO_2$ -Ln<sub>2</sub>O<sub>3</sub> (Ln = lanthanide and yttrium) Systems," *J. Nucl. Mater.* 56(2): 229-38 (May 1975).
76. A. Boroujerdi, *Phase Equilibria in the Systems  $UO_2$ - $UO_3$ -NdO<sub>1.5</sub> and  $NpO_{2+x}$ -NdO<sub>1.5</sub>*, KFK-1330 (January 1971).
77. C. Keller and A. Boroujerdi, "Phase Equilibria in the Systems  $UO_2$ - $UO_3$ -NdO<sub>1.5</sub> and  $NpO_{2+x}$ -NdO<sub>1.5</sub>," *J. Inorg. Nucl. Chem.* 34: 1187-93 (1972).
78. J. F. Wadier, J. P. Marcon, and O. Pesme, *Thermodynamic Properties and Diagram of the System U-Nd-O* (from Panel on the Behavior and Chemical State of Fission Products in Irradiated Fuel, Vienna 7-11 August 1972) ANL-trans-925.
79. W. Rüdorff, H. Erfurth, and S. Kemmler-Sack, "Ternary Oxides. VIII - Ternary Uranium(V) Oxides with Trivalent Cations," *Z. Anorg. Allg. Chem.* 354: 273-86 (1967).
80. L. M. Kovba et al., "Studies of Binary Uranium Oxides," *Vestn. Mosk. Univ. Khim.* No. 6, 29-32 (November-December 1966).
81. G. Brauer and B. Willaredt, "Mixed Crystal Phases in the System  $ThO_2$ -PrO<sub>x</sub>," *J. Less-Common Met.* 24: 311-16 (1971).
82. C. Keller et al., "Phase Equilibria in the Systems Scandium Oxide-Actinide Oxides (Th-Am)," *J. Nucl. Mater.* 42: 23-31 (1972).

83. W. Trzebiatowski and R. Horyn, "Regular Solid Solution of  $UO_{2+x}$ - $Sc_2O_3$  Compounds," *Roczn. Chem.* 41: 1711-20 (1967).
84. H. Radzewitz, *Solid State Chemistry Investigation of the System  $SeO_{1.5}-ZrO_2(HfO_2)$ ,  $AmO_{1.5}-ZrO_2(HfO_2, ThO_2)-O_2$  and  $TiO_2-NpO_2(PuO_2)$* , KFK-433 (July 1966).
85. M. Perez y Jorba, H. Mondage, and R. Collonques, "On the Compounds Formed by Thoria with Oxides of Tetravalent Metals," *Bull. Soc. Chim. Fr.* 1961, 79-81.
86. R. H. Marshall and H. R. Hoekstra, "The Preparation and Properties of  $TiUO_5$ ," *J. Inorg. Nucl. Chem.* 27: 1947-50 (September 1965).
87. L. M. Manojlavic, M. M. Ristic, and S. S. Malcic, "A High Temperature Reaction in the  $UO_2-TiO_2$  System," pp. 245-51 in *Conference on New Nuclear Materials Technology Including Non-Metallic Fuel Elements* (held in Prague 1963), International Atomic Energy Agency, Vienna, 1963.
88. K. Suzuki, K. Maruya, and T. Kubota, "Activated Sintering of Uranium Dioxide Fuel III. Measurement of Lattice Constant by X-Ray," *Nippon Genshiryoku Gakkaishi* 5: 587-92 (1963).

**APPENDIX B**  
**FISSION PRODUCT INTERACTIONS**



## FISSION PRODUCT INTERACTIONS

An understanding of the distribution and effects of fission products may lead directly to predictions on the distribution of spikants within the fuel, and of possible spikant-cladding interactions. Therefore, the purpose of this appendix is to summarize the information available on the subject into a coherent concept of the factors involved and extend these principles to the potential spikants listed in Table 1.

## Fission Product Distribution

In the course of reactor operation a number of fission products that are formed can have a profound effect on fuel element performance. In order to understand these effects we first need to determine what fission products are produced and the chemical and physical state of these elements.

Fission product yields for the various fissionable isotopes are summarized in Fig. B1. The general shape of these curves is similar, although displaced slightly to the right or left for the heavy or light fissionable isotopes respectively. These curves show that elements such as Kr, Rb, Sr, Y, Zr, Nb, Mo, Tc, Ru, Pd, Ag, Te, I, Xe, Cs, Ba, La, Ce, Pr, Nd, Pm, and Sm may be present in appreciable amounts (>0.5%) and thus should be considered in an analysis of fission product distribution.

The chemical form and physical state of the fission products are important for this analysis. The chemical form can be predicted with the aid of thermodynamics. In oxide fuels the oxygen potential of the fuel and the free energy of formation of the various oxides are the important considerations. Figure B2 shows that the oxygen potential of the fuel varies with both temperature and stoichiometry. When the free energy of formation of an oxide is more negative than the oxygen potential of the fuel, the oxide is stable with respect to the fuel. Conversely, when the free energy of formation is more positive than the oxygen potential of the fuel the oxide is unstable in the presence of

ORNL-DWG 78-10419

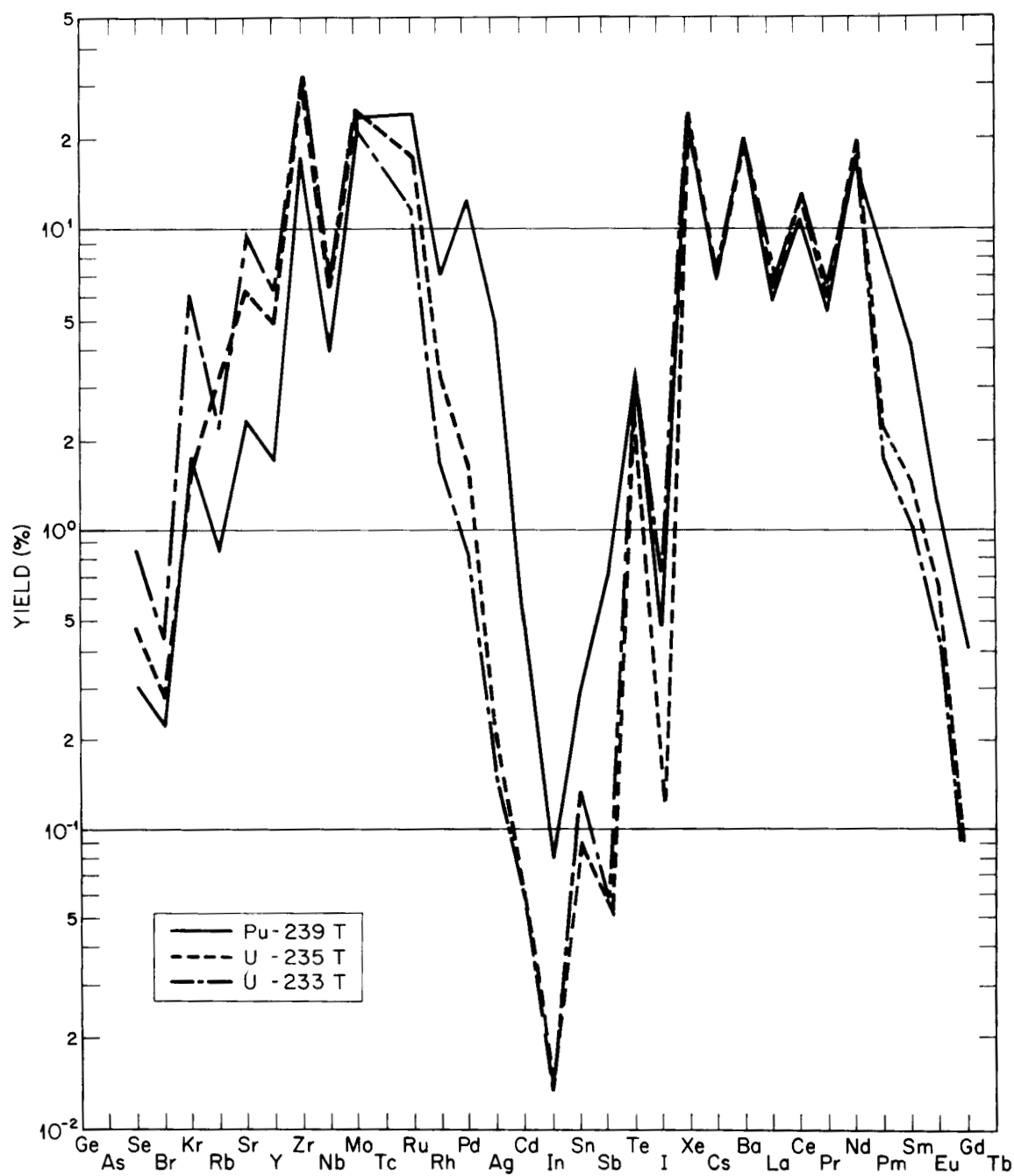


Fig. B1. Fission Product Yields for  $^{233}\text{U}$ ,  $^{235}\text{U}$ , and  $^{239}\text{Pu}$  with Thermal Neutrons.<sup>1</sup>

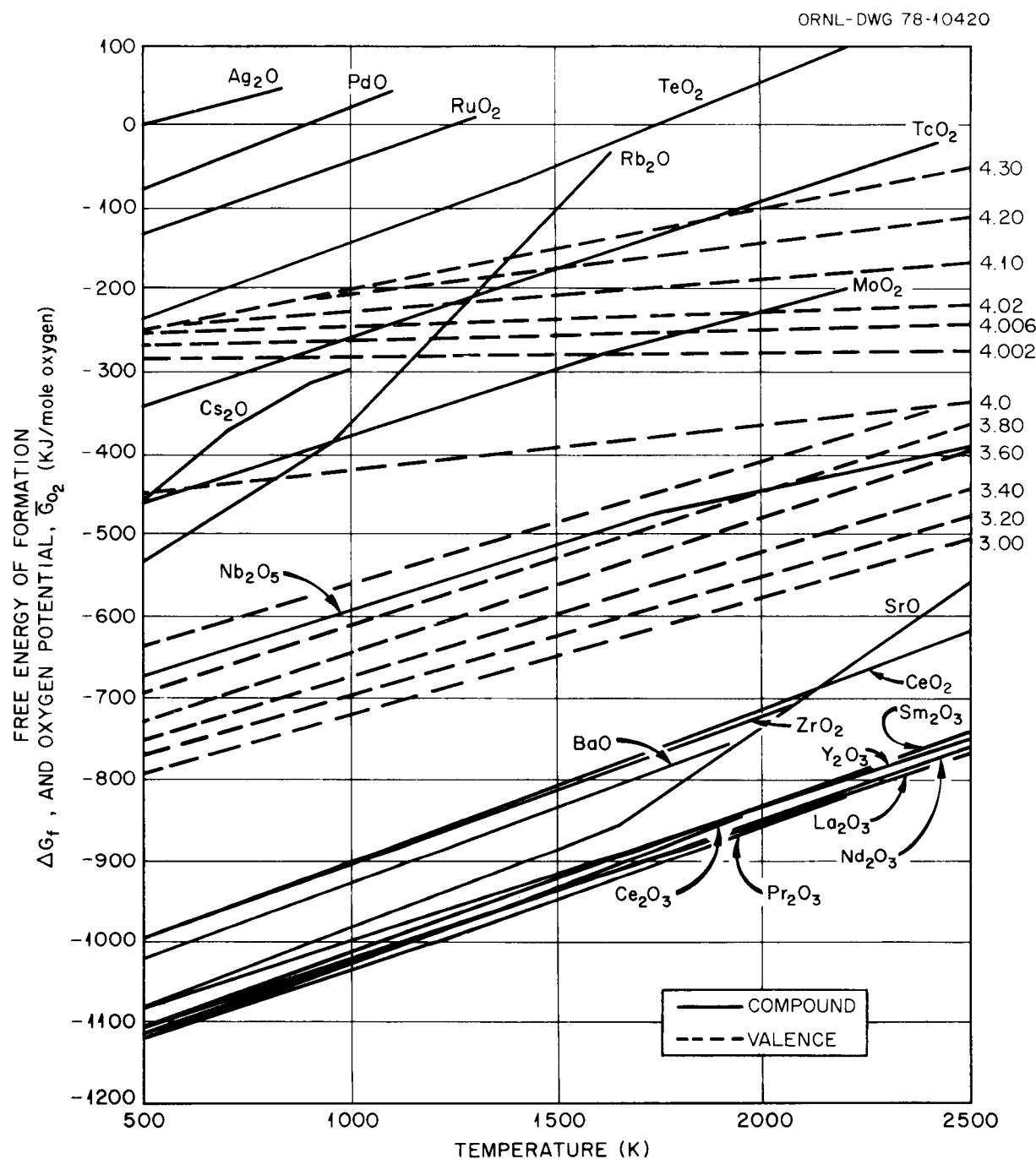


Fig. B2. Thermodynamic Data for Fission Products and Fuel.

the fuel and the fission product can be expected to be present in the elemental form. Once the chemical state has been determined, the physical state in various parts of the fuel element can be predicted from an analysis of the melting and boiling points of the species of concern. Following this procedure, we constructed Table B1, which summarizes information<sup>2,3</sup> on the various species possible within the system. The physical states listed in this summary agree well with experimental observations.

In general, solid fission products are distributed in various phases in the fuel as follows:

1. The oxide matrix of the original fuel — These elements are present as oxides in solid solution in the fuel matrix and include yttrium, the rare earths, niobium, some of the zirconium, and some of the molybdenum.
2. Separate oxide phase — This phase contains those fission products whose oxides are insoluble in the fuel matrix, such as barium, strontium, and some zirconium.
3. Metallic inclusions — This phase occurs in the grain boundaries of the columnar grain region or within the large central void and is a homogeneous alloy of Ru, Tc, Rh, Pd, and Mo.
4. Other — Xenon and krypton fill the void spaces within the fuel. Intermetallic compounds of the type  $MN_3$  may form, where M denotes uranium or plutonium and N denotes rhodium or palladium. Cesium and molybdenum are found in the grain boundaries of the cladding.

The temperature gradient in the fuel is rather steep, and some fission products move up the gradient while others move down. Much depends on the chemical form of the fission product, but this migration affects the oxygen potential of the fuel, swelling, mechanical properties, thermal conductivity, and ultimately the temperature profile.

Zirconium, niobium, yttrium, and the rare earths form oxides that are soluble in the fluorite structure of the fuel, and these elements, with the possible exception of cerium,<sup>4</sup> do not migrate in the temperature gradient. A small amount of cerium migration has been observed in out-of-reactor tests.<sup>5</sup> Similarly, Bates<sup>6,7</sup> has found a very

Table B1. States of Fission Products

	Melting Point (°C)	Boiling Point (°C)	Physical State
<u>Stable Elements</u>			
Kr	-157.2	-152	Elemental vapor
Rb	38.9	688	Elemental vapor
Mo	2010	5560	Metallic Inclusions
Tc			Metallic inclusions
Ru	2500	4900	Metallic inclusions
Rh	1966	4500	Metallic inclusions
Pd	1552	3980	Metallic inclusions
Ag <sup>a</sup>	960.8	2210	Metallic inclusions
Te	449.5	989.8	Elemental vapor
I	113.7	183	Elemental vapor
Xe	-111.9	-108	Elemental vapor
Cs	28.7	690	Elemental vapor
<u>Stable Oxides</u>			
SrO	2420	3000	Alkaline earth oxide phase, SrZrO <sub>3</sub>
Y <sub>2</sub> O <sub>3</sub>	2410		Soluble oxide
ZrO <sub>2</sub>	2700	(5000)	Soluble oxide and alkaline earth oxide phase
Nb <sub>2</sub> O <sub>5</sub>	1485		Soluble oxide
MoO <sub>3</sub>	795	subl.	Soluble oxide
BaO	1918	(2000)	Alkaline earth oxide phase BaZrO <sub>3</sub>
La <sub>2</sub> O <sub>3</sub>	2307	4200	Soluble oxide
CeO <sub>2</sub>	(2727)		Soluble oxide
Pr <sub>2</sub> O <sub>3</sub>	(1927)		Soluble oxide
Nd <sub>2</sub> O <sub>3</sub>	2272		Soluble oxide
Sm <sub>2</sub> O <sub>3</sub>			Soluble oxide
Pm <sub>2</sub> O <sub>3</sub>			Soluble oxide

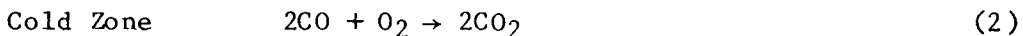
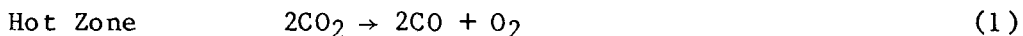
<sup>a</sup>Of concern only in plutonium fuels.

small amount of cerium migration in irradiated uranium dioxide fuel elements. Considerable migration of ruthenium up the temperature gradient was also observed.

#### Oxygen Redistribution

The presence of a temperature gradient complicates the elemental distribution within the fuel considerably. Considerable redistribution of fuel components, including oxygen, has been observed experimentally. This redistribution is due directly to the presence of the temperature gradient. The problem of determining the mechanism of this redistribution becomes one of combining a model of the transport mechanism with thermodynamic analysis. A knowledge of the extent of oxygen distribution is important because many properties of the fuel are functions of the O/M ratio. Among the properties affected by the O/M ratio are: thermal conductivity, oxygen potential, creep, and diffusion coefficients of various species in the solid.

Several models have been proposed to explain the oxygen redistribution observed in reactor fuels. For hyperstoichiometric fuels the model proposed by Markin, Rand, and Roberts<sup>8,9</sup> has explained the observed results rather well. This model is based on transport in the gas phase. All nuclear fuel contains several parts per million of carbon as an impurity. This carbon can be oxidized to CO<sub>2</sub> and CO, which in turn fill all the cracks and interconnected pores as well as the plenum above the fuel. Under these conditions oxygen can be transported by means of the reactions:



Thus, CO<sub>2</sub> diffuses up the temperature gradient, where it decomposes according to reaction (1), thereby depositing oxygen. The CO then diffuses down the temperature gradient, where reaction (2) occurs. No net

transport of carbon takes place, although there is an increase in oxygen in the hot zone. This agrees with experiment.<sup>10-17</sup> Table B2 summarizes some experimental observations and shows that in hyperstoichiometric fuels the O/M ratio increases in the hot zone.

Limitations of this model occur with substoichiometric fuel or systems containing free carbon. Under these conditions the oxygen potential is low so that the maximum CO<sub>2</sub> pressure is also low. At lower temperatures the extent of oxygen redistribution may also be limited by the presence of volatile oxides (MoO<sub>2</sub>, Cs<sub>2</sub>O or Cs<sub>2</sub>MoO<sub>4</sub>), which may transport oxygen down the temperature gradient.<sup>9</sup> However, the stability of Cs<sub>2</sub>MoO<sub>4</sub> in substoichiometric fuel is not known. Above about 2000°C gaseous oxides of uranium and plutonium may transport oxygen as they diffuse down the temperature gradient. Solid-state diffusion of oxygen down the temperature gradient may also reduce oxygen redistribution.

Table B2. Summary of Oxygen Redistribution Experiments

Investigator	Material	Geometry	Redistribution
Christensen <sup>10</sup>	UO <sub>2+x</sub>	Radial	O/U highest at hot zone
Fryxell and Aitken <sup>11</sup>	UO <sub>2-x</sub>	Axial	O/U highest at cold end; no redistribution in UO <sub>2.000</sub>
Evans, Aitken, and Craig <sup>12</sup>	(U,Pu)O <sub>2-x</sub>	Axial	O/M highest at cold end
Jeffs <sup>13</sup>	(U,Pu)O <sub>2+x</sub>	Radial	O/M highest at hot zone; no redistribution in UO <sub>2.000</sub>
Adamson <sup>14</sup>	UO <sub>2+x</sub>	Axial	O/U highest at hot end
Adamson and Carney <sup>15</sup>	(U,Pu)O <sub>2</sub>	Axial	O/M highest at hot end
Adamson et al. <sup>16</sup>	UO <sub>2</sub> , UO <sub>2+x</sub> (U,Pu)O <sub>1.955</sub>		O/M highest at centerline O/M highest at cold zone
Sari and Schumacher <sup>17</sup>	(U,Pu)O <sub>2+x</sub>	Axial Radial	O/M highest at cold end O/M highest at cold zone

For hypostoichiometric fuels, the above mechanism is invalid for the reasons outlined. This has led Aitken<sup>18</sup> to propose that the stoichiometry parameter  $x$  in  $(U, Pu)O_{2-x}$  should vary with temperature according to the relationship:

$$nx = \frac{Q^+}{RT} + \text{const} \quad (3)$$

where  $Q^+$  is called a "characteristic heat of transport," which represents the combined effect of solid-state diffusion and the vapor migration of all oxygen-bearing species contained in the gas phase filling the cracks and fissures in the fuel. The value of  $Q^+$  depends on the mechanism responsible for the oxygen migration. By means of curve-fitting techniques, stoichiometry profiles can be calculated.

For fully dense fuel, oxygen also redistributes in hypostoichiometric fuels, even though  $CO_2$ -CO gas phase redistribution is impossible. Bober and Schumacher<sup>19</sup> propose that solid-state diffusion is responsible for oxygen redistribution.

#### Fuel-Cladding Reactions

Thermodynamic relationships between  $(U, Pu)O_{2+x}$  fuel and austenitic stainless steel are summarized in Fig. B3. This figure shows that reactions between the fuel and cladding should not proceed until the O/M ratio exceeds 1.998. Early out-of-reactor tests verified this relationship. As the results of in-reactor tests became available, reactions were obviously occurring between the fuel and the cladding. Cesium and tellurium, both fission products, were identified as participants in the reaction. This apparent conflict between theory and experiment is explained by the initiation and control of cladding attack by the oxidizing potential of the fuel and the temperature of the fuel-cladding interface.<sup>20</sup> This is shown in Fig. B3. Factors that control the oxidizing potential of a given fuel are: the initial O/M ratio, the amount of fuel burnup, temperature, thermal conductivity, and the oxidation states of the uranium and plutonium. Various studies have shown that fuel

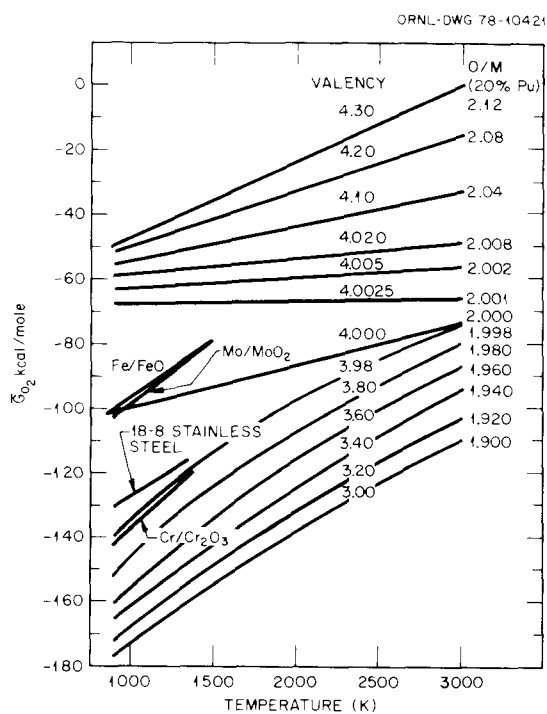


Fig. B3. Equilibrium Oxygen Potentials of  $(Pu,U)O_{2+x}$  Fuel and Cladding Components.

does not react with the cladding except when it is hyperstoichiometric<sup>21-24</sup> (i.e., O/M > 2.0). The effect of an increase in oxygen potential is to allow oxidation of alloy constituents, notably chromium. Most of the recent work on the fuel-cladding reactions has been done with out-of-reactor tests using fuel compositions designed to simulate given burnup levels.

At least one reference<sup>25</sup> concludes that neutron energy does not influence the chemistry of the system, although the thickness of reaction layers is greater with fast neutrons.

#### Types of Reaction

In general, three types of reaction have been observed as the result of interaction of fuel, fission products, and cladding:

1. intergranular (grain boundary) cladding attack,
2. matrix attack, usually characterized by a continuous layer at the fuel-cladding interface,

3. "rivers" of metallic material along cracks in the fuel.

Intergranular attack is the more serious mode of attack since the penetration occurs through a greater proportion of the cladding thickness and therefore weakens the cladding more.

#### Cesium

Cesium, a secondary spikant, has been found to have the most adverse effect on austenitic stainless steel of any fission product.<sup>22</sup> A number of proposed mechanisms will be described in a later section. Oxygen-free cesium has been described as compatible with stainless steel up to 3000 h at 1000°C.<sup>24</sup> Cesium, when present as the element, is usually found in the grain boundary reaction product. This intergranular corrosion product has been identified as cesium plus: Mo and O<sup>20</sup>,<sup>21</sup> and Cr.<sup>24</sup> Several investigators claim stability for certain Cs-O-U or Cs-O-Mo compounds under certain conditions.<sup>22,26</sup> The threshold for attack by Cs-O appears to occur at a higher oxygen potential than that required for reaction of stainless steel.<sup>26</sup> In hyperstoichiometric fuel cesium uranate vapor forms at high temperatures. Movement of the cesium uranate down the temperature gradient leads to preferential movement of uranium from the fuel at high temperature and subsequent deposition at low temperature.<sup>26</sup>

Even though the interpretations of the data differ, most investigators agree that the presence of oxygen is necessary for intergranular reaction to occur. The presence of oxygen is usually indicated by hyperstoichiometric fuel, and in all cases where reactions were found oxygen was present.

#### Iodine

In general, iodine does not seem to present any problems because it is usually combined with cesium as CsI. No attack was observed at any Cs/I ratios in the absence of oxygen.<sup>26</sup> A combination of CsI + UO<sub>2.08</sub> gave marked reaction, while UO<sub>2.08</sub> or CsI alone did not.<sup>24</sup> French

workers, on the other hand, conclude that iodine is important in producing Mn, Cr, and Fe iodides, which then migrate to cold portions of the system. The metals deposit and the iodine is released and is then available for further transport of stainless steel constituents. This mechanism will be discussed in more detail in a later section.

#### Molybdenum

Molybdenum has been found in an intergranular corrosion product along with cesium and oxygen,<sup>20,21</sup> but in general is not considered a reactive fission product.<sup>24</sup> In another series of out-of-reactor tests with molybdenum no attack was observed.<sup>26</sup>

#### Oxygen

Oxygen is usually found in intergranular reaction products<sup>20,26</sup> and seems to be necessary for the promotion of intergranular corrosion. It is also present in the matrix reaction product.

#### Tellurium

Some intergranular penetration of tellurium was found<sup>21,23</sup> when Cs/Te ratios were less than 2. Reaction with tellurium is claimed to be unrelated to oxygen.<sup>24</sup> However, in another test, intergranular attack was found with stoichiometric fuel, while none was found with hypo-stoichiometric fuel.

#### Selenium

Severe reactions with selenium were found and were claimed not to depend upon oxygen.<sup>24</sup> While selenium is much more reactive than tellurium, it is present in such small quantities as to be unimportant as a corrodant.<sup>26</sup>

Iron-Chromium-Nickel

These elements are usually found in the matrix reaction zone.<sup>21,22</sup>

Antimony and Cadmium

These elements react preferentially with chromium.<sup>24</sup>

Indium and Tin

These elements react preferentially with nickel.<sup>24</sup>

Corrosion Mechanisms

One possible mechanism for these observations has been presented by Ohse and Schlechter.<sup>27</sup> Three types of attack are considered by the authors:

1. formation of a layered structure in the case of initially nearly stoichiometric fuels,
2. dissolution of passivating layers and the subsequent surface ablation of the steel in the presence of a liquid phase,
3. the intergranular attack of sensitized steel within the grain boundaries.

Passivating oxide layers are probably formed before an appreciable amount of fission products reach the fuel-cladding interface. Surface ablation is observed on the nonprotected steel surface after a thin protective oxide film has been dissolved in the liquid phase. Intergranular attack is observed especially in sensitized steels, where Cr<sub>23</sub>C<sub>6</sub> precipitate along the grain boundaries is oxidized. The general features observed<sup>27</sup> are summarized in Fig. B4.

Phase relationships of the Cs-O system,<sup>28</sup> given in Fig. B5, show that cesium oxide in any form is not to be expected at the temperatures and oxygen potentials involved. Rather, a thin layer of liquid cesium containing oxygen and the more volatile fission products such as tellurium, selenium, and rubidium is to be expected. In hypostoichiometric

ORNL-DWG 78-14180

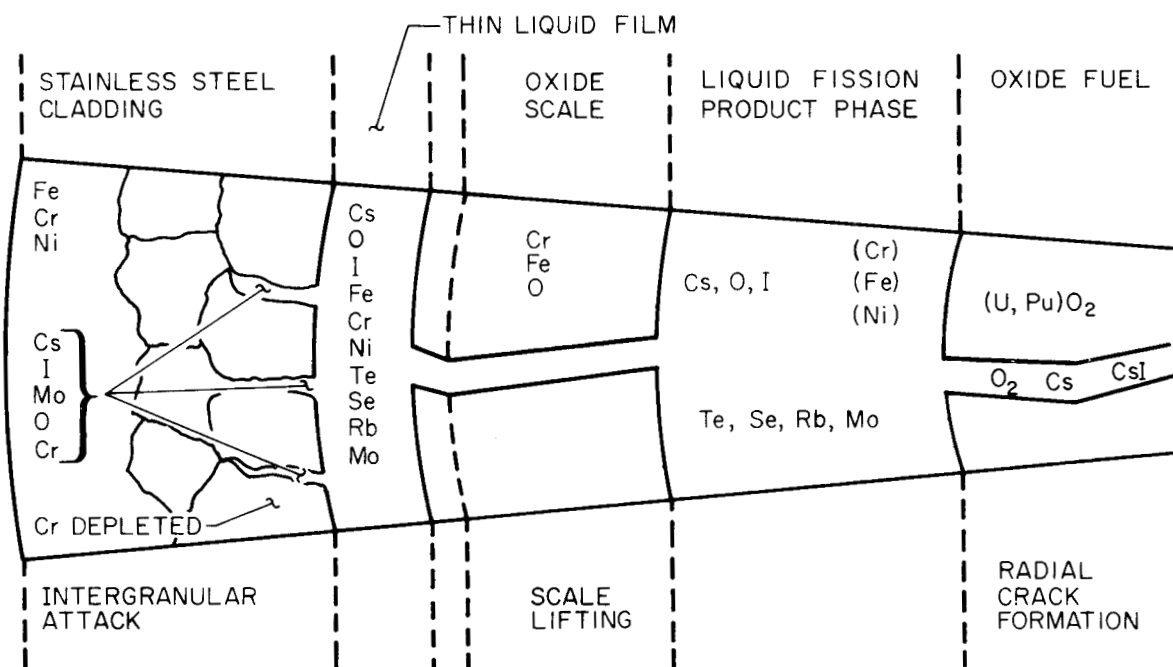


Fig. B4. Schematic Summary of Fission Products Analyzed Within the Layered Structure at the Fuel/Cladding Interface After High Burnup.  
Based on Ohse and Schlechter.<sup>27</sup>

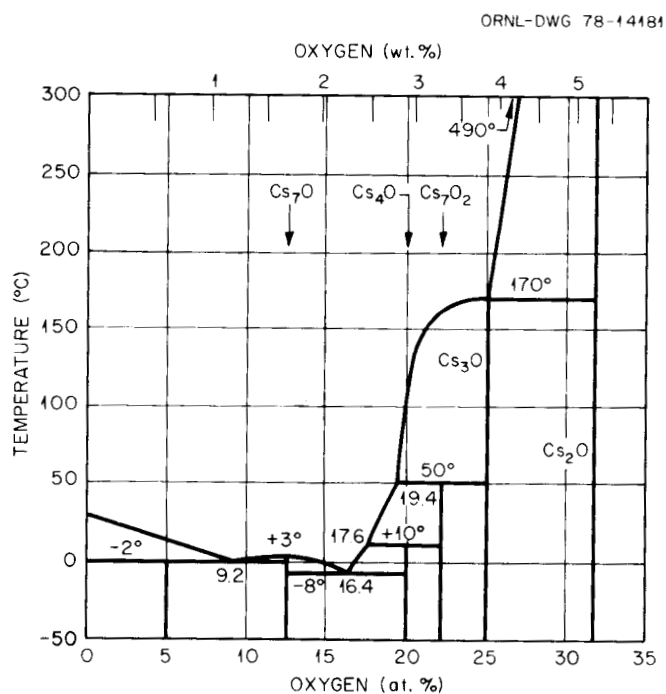


Fig. B5. The Cs-Cs<sub>2</sub>O System. Adapted from Rengade.<sup>28</sup>

fuels, cesium migrates toward the cladding, while in hyperstoichiometric fuels cesium tends to form stable compounds.

A schematic of possible reaction mechanisms at the fuel-cladding interface<sup>27</sup> is given in Fig. B6. Important features of this schematic are: (1) solution of  $\text{Cr}_2\text{O}_3$  in cesium and, (2) precipitation of  $\text{CsCrO}_2$  at the high-temperature side of the liquid multicomponent layer. Precipitation of  $\text{CsFeO}_2$  can be expected only at the chromium-depleted iron-rich surface of the oxide layer at an oxygen potential of hyperstoichiometric fuel. Selective dissolution of the  $\text{M}_2\text{O}_3$  layer will disturb the defect concentration balance and increase the rate of chromium diffusion to the Cs-O liquid phase. The resulting chromium depletion leads to the formation of an intermediate layer of spinel-type oxide. Stress developments can lead to cracks within the oxide layer and lifting of the oxide scale. Penetration of the liquid between the oxide layer and the metal would then give rise to ablation of the oxide scale and further chromium removal as described above.

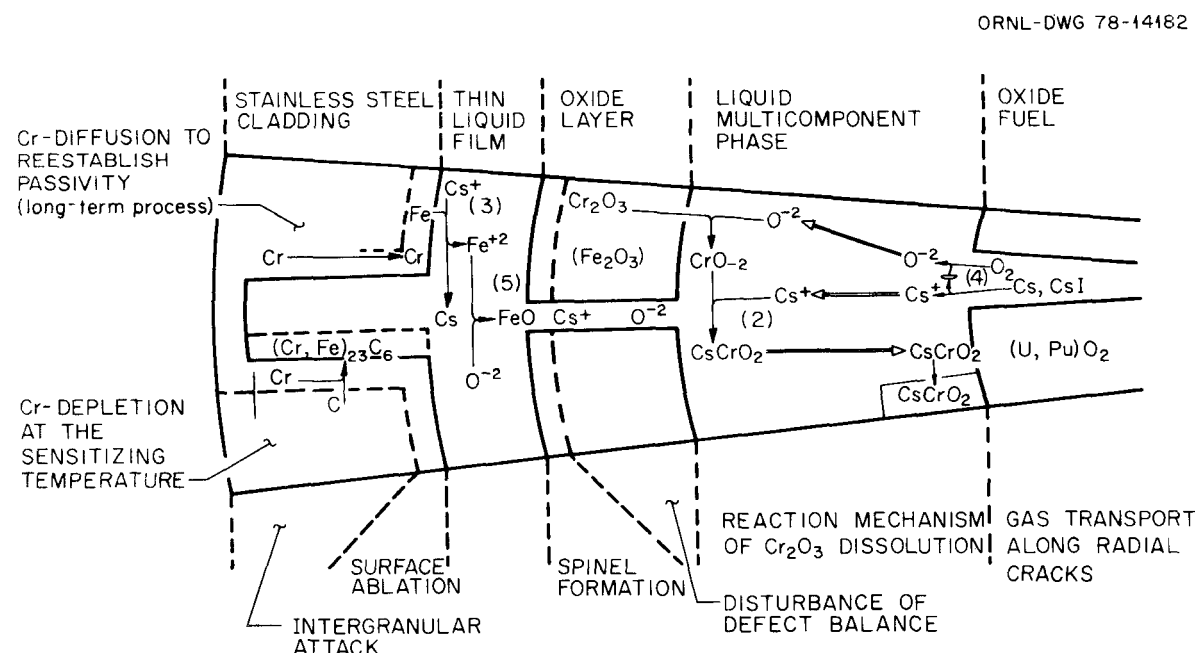


Fig. B6. Schematic Display of Possible Reaction Mechanism of Chemical Interaction in Oxide Fuels at the Fuel-Cladding Interface. Adapted from Ohse and Schlechter.<sup>27</sup>

Another proposed mechanism involves transport in the vapor phase by means of a van Arkel-de Boer mechanism.<sup>29</sup> In this mechanism CsI reacts with Mn, Cr, and Fe of the stainless steel where fuel  $(U, Pu)O_{2+x}$  is present to form the iodides  $MnI_2$ ,  $CrI_2$ , and  $FeI_2$  and  $Cs_2(U, Pu)O_4$ . The iodides decompose in the hot zones at the fuel surface, precipitating Mn, Cr, and Fe and releasing the iodine for further reaction as CsI. Obviously this mechanism depends on the formation of cesium compounds more stable than CsI. Unless the iodine potential is vanishingly small, this is unlikely.<sup>30</sup> However, that iodine has been found in areas of intergranular attack<sup>31</sup> lends support to this hypothesis.

#### REFERENCES

1. M. E. Meek and B. F. Rider, *Compilation of Fission Product Yields* *Vallecitos Nuclear Center 1974*, NEDO-12154-1 (January 1974).
2. *Metals Handbook*, 8th ed., Vol. 1, American Society for Metals, Metals Park, Ohio, 1961.
3. *Handbook of Chemistry and Physics* 58th ed., CRC Press, Cleveland, 1977.
4. T. A. Lauritzen, P. E. Novak, and J. H. Davies, *Experimental Studies of Plutonium and Fission Product Redistribution in Fast Reactor Fuels*, GEAP-4466 (March 1966).
5. A. A. Bauer et al., *Microanalytical Studies of Micro- and Macro-Segregation in Oxide Fuels*, ANL-7120 (1965).
6. J. L. Bates, *Fission Product Distribution in Irradiated  $UO_2$* , BNWL-58 (March 1965).
7. J. L. Bates, "Fission Product Distribution in Irradiated  $UO_2$ ," *Trans. Am. Nucl. Soc.* 7: 389-90 (November 1964).
8. M. H. Rand and T. L. Markin, "Some Thermodynamic Aspects of  $(U, Pu)O_2$  Solid Solutions and Their Use as Nuclear Fuels," pp. 637-50 in *Thermodynamics of Nuclear Materials*, 1967 (Symposium Proceedings) International Atomic Energy Agency, Vienna, 1968.
9. M. H. Rand and L.E.J. Roberts, "Thermochemistry and Nuclear Engineering," pp. 3-31 in *Thermodynamics - Proceedings of the Symposium on Thermodynamics with Emphasis on Nuclear Materials and*

*Atomic Transport in Solids Vol. 1, International Atomic Energy Agency, Vienna, 1966.*

10. J. A. Christensen, *High Temperature Studies of Urania in a Thermal Gradient BNWL-536* (December 1967).
11. R. E. Fryxell and E. A. Aitken, *J. Nucl. Mater.* 30: 50-56 (1969).
12. S. K. Evans, E. A. Aitken, and C. N. Craig, "Effects of a Temperature Gradient on the Stoichiometry of Urania-Plutonia Fuel," *J. Nucl. Mater.* 30: 57-61 (1969).
13. A. J. Jeffs, *Oxygen: Metal Ratio Effects in  $(U,Pu)O_2$  Fuels*, AECL-3690 (August 1970).
14. M. G. Adamson, "Thermal Diffusion of Oxygen in Hyperstoichiometric Urania with Very Low Carbon Content," *J. Nucl. Mater.* 38: 213-16 (1971).
15. M. G. Adamson and R.F.A. Carney, *Thermal Diffusion Phenomena in Non-Stoichiometric Oxide Fuels. Part I. Evidence of Gas Phase Oxygen Transport in  $UO_{2+x}$  from Axial and Radial Temperature Gradient Experiments*, AERE-R-6830 (October 1972); *ibid. Part II. Oxygen Redistribution in Hyperstoichiometric Urani-Plutonia. Results of Axial Temperature-Gradient Experiments*, AERE-R-6831 (October 1972).
16. M. G. Adamson et al., "Oxygen Redistribution and its Measurement in Irradiated Oxide Fuels," pp. 59-71 in *Thermodynamics of Nuclear Materials 1974*, Vol. I, International Atomic Energy Agency, Vienna, 1975.
17. C. Sari and G. Schumacher, "Radial Transport of Oxygen in Mixed-Oxide Fuel Pins," pp. 73-82 in *Thermodynamics of Nuclear Materials 1974*, Vol. I, International Atomic Energy Agency, Vienna, 1975.
18. E. A. Aitken, "Thermal Diffusion in Closed Oxide Fuel Systems," *J. Nucl. Mater.* 30: 62-73 (1969).
19. M. Bober and G. Schumacher, "Material Transport in the Temperature Gradient of Fast Reactor Fuels," *Adv. Nucl. Sci. Technol.* 7: 121-79 (1973).
20. C. E. Johnson, I. Johnson, and C. E. Crouthamel, "Fuel Cladding Chemical Interactions in  $UO_2$ -20 wt %  $PuO_2$  Fast Reactor Fuel Clad

- with Stainless Steel," pp. 393-410 in *Proceedings of the Conference on Fast Reactor Fuel Element Technology*, April 13-15, 1971, New Orleans, American Nuclear Society, Hinsdale, Ill., 1971.
21. K. J. Perry et al., "Fuel Cladding Reactions Observed in Stainless Steel-Clad Mixed-Oxide Fuel Pin Irradiation," pp. 411-29 in *Proceedings of the Conference on Fast Reactor Fuel Element Technology*, April 13-15, 1971, New Orleans, American Nuclear Society, Hinsdale, Ill., 1971.
  22. R. B. Fitts, E. L. Long, Jr., and J. M. Leitnaker, "Observations of Fuel-Cladding Chemical Interactions as Applied to GCBR Fuel Rods," pp. 431-53 in *Proceedings of the Conference on Fast Reactor Fuel Element Technology*, April 13-15, 1971, New Orleans, American Nuclear Society, Hinsdale, Ill., 1971.
  23. E. A. Aitken et al., "Fission Product Reactions and Thermomigration in Breeder Reactor Oxide Fuel Systems," pp. 187-203 in *Thermodynamics of Nuclear Materials 1974*, Vol. I, International Atomic Energy Agency, Vienna, 1975.
  24. P. Hoffman and O. Gotzmann, "Chemical Interactions of Fission Products with Stainless Steel Claddings," pp. 237-54 in *Behavior and Chemical State of Irradiated Ceramic Fuels*, International Atomic Energy Agency, Vienna, 1974.
  25. D. Calais et al., "Reactions at the Clad (Stainless Steel)/Fuel [Mixed Oxide  $(U,Pu)O_{2+x}$ ] Interface in Fuel Elements Irradiated with Fast Neutrons," pp. 287-97 in *Behavior and Chemical State of Irradiated Ceramic Fuels*, International Atomic Energy Agency, Vienna, 1974.
  26. E. A. Aitken, S. K. Evans, and B. F. Rubin, "Out of Pile Investigation of Fission Product-Cladding Reactions in Fast Reactor Fuel Pins," pp. 269-85 in *Behavior and Chemical State of Irradiated Ceramic Fuels*, International Atomic Energy Agency, Vienna, 1974.
  27. R. W. Ohse and M. Schlechter, "The Role of Cesium in Chemical Interaction of Austenitic Stainless Steels with Uranium Plutonium Oxide Fuels," pp. 299-314 in *Behavior and Chemical State of*

*Irradiated Ceramic Fuels*, International Atomic Energy Agency,  
Vienna, 1974.

28. M. E. Rengade, "Sur les Sous-Oxydes de Caesium," *C. R. Hebd. Seances Acad. Sci.* 148: 1199-1202 (1909).
29. D. Calais et al., "The Role of Cesium Iodide in the Development of Reactions at the Interfaces Between  $(U,Pu)O_2$  Fuels and Austenitic Stainless Steel Cladding," pp. 207-15 in *Thermodynamics of Nuclear Materials 1974*, Vol. I, International Atomic Energy Agency, Vienna, 1975.
30. T. M. Besmann and T. B. Lindemer, *Chemical Thermodynamics of the System Cs-U-Zr-H-I-O in the LWR Fuel-Clad Gap*, ORNL/TM-6130 (January 1978).
31. C. E. Johnson and C. E. Crouthamel, "Cladding Interactions in Mixed Oxide Irradiated Fuels," *J. Nucl. Mater.* 34: 101-04 (1970).

## APPENDIX C

CALCULATION OF THE FUEL SPIKANT CONCENTRATION  
REQUIRED FOR A DOSE RATE OF 27,000 R/H



CALCULATION OF THE FUEL SPIKANT CONCENTRATION  
REQUIRED FOR A DOSE RATE OF 27,000 R/H

Calculations presented here refer to a fuel assembly 16 cm on a side by 366 cm (12 ft) long. Assuming a cylindrical shape and an effective distance from the fuel assembly of 37 cm, the calculations are based on the radiation dose at the surface of a cylinder with a radius of 37 cm and a length of 366 cm (12 ft). This yields an area ( $A$ ) of  $8.49 \times 10^4 \text{ cm}^2$ . End effects were neglected.

The weight of fuel was determined by assuming a pellet diameter of 0.94 cm (0.37 in.). For a rod 366 cm (12 ft) long the volume of the fuel is  $256 \text{ cm}^3$ . Assuming a density of  $10.2 \text{ g/cm}^3$  yields  $2.6 \times 10^3$  grams of fuel per rod. If a fuel assembly contains 204 rods the total fuel weight ( $W$ ) is 533 kg.

Other required parameters are the decay constant  $\lambda = (\ln 2)(t_{1/2})$  and  $e^{-\lambda t}$  at  $t = 2$  years, which is the intensity of the  $\gamma$  radiation after 2 years.

A sample calculation is made for  $^{65}\text{Zn}$  with a half-life of 245 days. This yields:

$$\lambda = (\ln 2)/(245 \text{ d} \times 86,400 \text{ s/d}) = 3.274 \times 10^{-8}/\text{s}$$

$$e^{-\lambda t} = \exp[-(\ln 2) \times 2 \times 365/245] = 0.127 \text{ after 2 years.}$$

For  $^{65}\text{Zn}$  there are 2 gamma rays:

$\gamma$ Energy	Intensity	Flux to give 1 R/h
0.511 MeV	3.4%	$1.0 \times 10^6 \text{ cm}^2/\text{s}$
1.1 MeV	49%	$4.9 \times 10^5 \text{ cm}^2/\text{s}$

The last column is the gamma flux equivalent to 1 R/h and is obtained from Fig. C1, which given the gamma flux as a function of gamma energy.

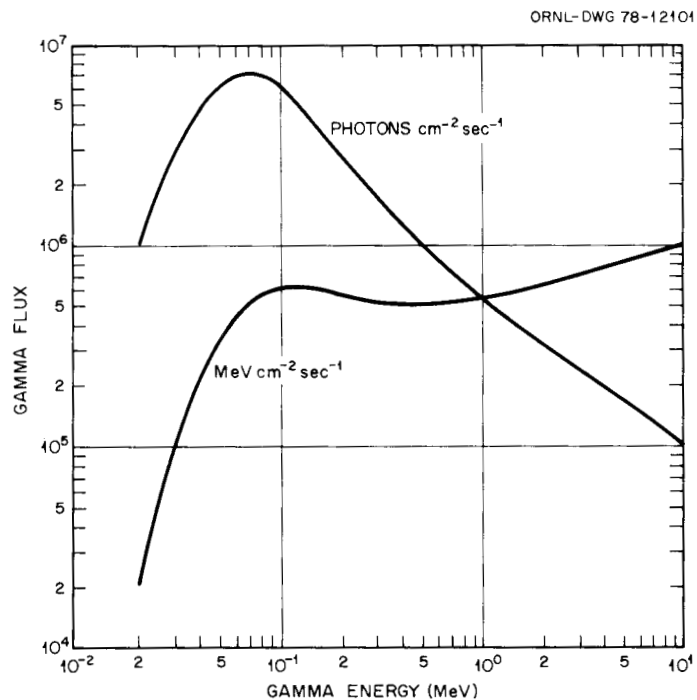


Fig. C1. Gamma Flux Equivalent to 1 R/h as a Function of Gamma Energy. From U.S. Department of Health, Education, and Welfare, *Radiological Health Handbook*, revised ed., September 1960, p. 140.

With this information we can use the relationship:

$$\frac{A}{1.0 \times 10^6} + \frac{B}{4.9 \times 10^5} = 27,000 \text{ R/hr} , \quad (1)$$

where 27,000 R/hr is the desired dose after 2 years;  $A$  is the flux of 0.511-MeV  $\gamma$ s and  $B$  is the flux of 1.1-MeV  $\gamma$ s. Normalizing with respect to  $B$ :

$$A = 0.034B/0.49 = 0.069B .$$

Equation (1) then becomes

$$\frac{0.069B}{1.0 \times 10^6} + \frac{B}{4.9 \times 10^5} = 27,000 ,$$

so  $B = 1.279 \times 10^{10}$ , which is the flux of 1.1-MeV  $\gamma$ s in photons/cm<sup>2</sup>s and is called the number of reference  $\gamma$ s ( $P$ ).

The total number of 1.1 MeV  $\gamma$ s per second =  $P \times \alpha$  where  $\alpha$  is the area of the reference cylinder, or  $8.49 \times 10^4 P = 1.086 \times 10^{15}$  (the number of 1.1-MeV  $\gamma$ s per second).

Since this particular  $\gamma$  occurs in 49% of the decays, the fraction of reference  $\gamma$ s,  $f$ , = 0.49, and the number of decays per second is:

$$\frac{1.086 \times 10^{15}}{0.49} = 2.217 \times 10^{15} \text{ } {}^{65}\text{Zn decays/s} .$$

The activity =  $\lambda N_0$ , where  $N_0$  is the number of  ${}^{65}\text{Zn}$  atoms at time 0.

$$\lambda N_0 e^{-\lambda t} = 2.217 \times 10^{15} \text{ decays/s}$$

and

$$N_0 = \frac{2.217 \times 10^{15}}{3.27 \times 10^{-8} \times 0.127} = 5.332 \times 10^{23} \text{ atoms} .$$

The mass of  $5.332 \times 10^{23}$  atoms is:

$$M = \frac{N_0 A}{N_A} = \frac{5.332 \times 10^{23} \times 65}{6.023 \times 10^{23}} = 57.54 \text{ g} ,$$

where  $A$  is the atomic weight and  $N_A$  is Avogadro's number. The concentration of  ${}^{65}\text{Zn}$  required in the fuel is then

$$M \times 10^6 = \frac{57.5 \times 10^6}{533000} = 108 \text{ ppm by weight} .$$

The actual dose rate required of a spikant has not been identified. For dose rates different from 27,000 R/hr the required concentrations will change proportionally. For a dose rate of 1000 R/hr 4 ppm of  ${}^{65}\text{Zn}$  would be required.

Combining these calculations, the following equation can be used:

$$C(\text{ppm}) = \frac{PaA \times 10^6}{f\lambda e^{-\lambda t} N_A W} . \quad (2)$$

where  $P$  = number of reference  $\gamma$ s [from Fig. C1 and Eq. (1)],

$\alpha$  = area of reference cylinder =  $8.49 \times 10^4 \text{ cm}^2$ ,

$f$  = fraction of decays in reference,

$\lambda$  = decay constant =  $(\ln 2)/t_{1/2}$ ,

$e^{-\lambda t}$  = intensity after time  $t$  (2 years),

$A$  = atomic weight of nuclide ,

$N_A$  = Avogadro's number =  $6.023 \times 10^{23}$  atoms/mol ,

$W$  = weight of fuel = 533,000 g.

After substituting for the constants this equation becomes:

$$C = 2.646 \times 10^{-19} PA/f\lambda e^{-\lambda t} . \quad (3)$$

Considering the approximations used and the fact that effects such as self-shielding and cladding shielding have been neglected, we estimate that the concentrations listed in Table 1 are accurate within a factor of 2.

ORNL/TM-6412  
 Distribution Categories  
 UC-77, UC-79-b,  
 -c, -d, -e, UC-83

## INTERNAL DISTRIBUTION

1-2.	Central Research Library	50.	E. J. Lawrence
3.	Document Reference Section	51.	D. A. Lee
4-6.	Laboratory Records Department	52.	R. E. Leuze
7.	Laboratory Records, ORNL RC	53.	K. H. Lin
8.	ORNL Patent Office	54.	R. B. Lindauer
9.	E. J. Allen	55.	T. B. Lindemer
10.	W. J. Armento	56.	E. L. Long, Jr.
11.	D. E. Bartine	57.	A. L. Lotts
12.	R. L. Beatty	58.	J. E. Mack
13.	B. J. Bolfing	59.	A. P. Malinauskas
14.	E. S. Bomar	60.	S. R. McNeany
15.	R. A. Bradley	61.	R. K. Nanstad
16.	R. E. Brooksbank	62.	K. J. Notz
17.	W. D. Burch	63.	A. R. Olsen
18.	D. O. Campbell	64.	J. R. Parrott
19.	A. J. Caputo	65.	A. E. Pasto
20.	J. A. Carpenter, Jr.	66.	P. Patriarca
21.	W. L. Carter	67.	R. L. Pearson
22.	G. L. Copeland	68.	H. Postma
23.	D. A. Costanzo	69.	G. A. Potter
24.	D. J. Crouse	70.	J. P. Renier
25.	R. G. Donnelly	71.	D. L. Selby
26.	W. P. Eatherly	72-76.	J. E. Selle
27.	R. B. Fitts	77.	R. L. Senn
28.	G. F. Flanagan	78.	R. D. Spence
29.	J. C. Griess	79.	I. Spiewak
30.	M. L. Grossbeck	80.	P. E. Stein
31.	P. A. Haas	81.	D. P. Stinton
32.	W. O. Harms	82.	R. R. Suchomel
33.	F. E. Harrington	83.	S. M. Tiegs
34.	R. E. Helms	84.	T. N. Tiegs
35-37.	M. R. Hill	85.	V. J. Tennery
38.	J. A. Horak	86.	D. B. Trauger
39.	J. R. Horton	87.	V.C.A. Vaughn
40.	J. D. Jenkins	88.	B. L. Vondra
41.	D. R. Johnson	89.	D. R. Vondy
42.	R. R. Judkins	90.	L. C. Williams
43-44.	P. R. Kasten	91.	R. G. Wymer
45.	J. R. Keiser	92.	R. W. Balluffi (Consultant)
46.	H. T. Kerr	93.	P. M. Brister (Consultant)
47.	F. G. Kitts	94.	W. R. Hibbard, Jr. (Consultant)
48.	J. J. Kurtz	95.	M. J. Mayfield (Consultant)
49.	W. J. Lackey	96.	N. E. Promisel (Consultant)
		97.	J. T. Stringer (Consultant)

## EXTERNAL DISTRIBUTION

- 98-99. DOE DIVISION OF REACTOR RESEARCH AND TECHNOLOGY, Washington, DC 20545  
Director
- 100-101. DOE DIVISION OF NUCLEAR POWER DEVELOPMENT, Washington, DC 20545  
Director
102. DOE IDAHO OPERATIONS OFFICE, P.O. Box 2108, Idaho Falls, ID 83401  
Barry Smith
103. SAN-DEVELOPMENT, San Diego Area Office, P.O. Box 81325,  
San Diego, CA 92138  
Senior Program Coordinator
104. DOE OAK RIDGE OPERATIONS OFFICE, P.O. Box E, Oak Ridge, TN 37830  
Director, Research and Technical Support Division
- 105-445. DOE TECHNICAL INFORMATION CENTER, P.O. Box 62, Oak Ridge, TN 37830  
For distribution as shown in TID-4500 Distribution Category  
UC-77 (Gas-Cooled Reactor Technology)  
UC-79b (Fuels and Materials Engineering Development)  
-79c (Fuel Recycle)  
-79d (Physics)  
-79e (Reactor Core Systems)  
UC-83 (Nuclear Converter Reactor Fuel Cycle Technology)